SANDIA REPORT
SAND2007-6547
Unlimited Release
Printed October 2007

Tools for Characterizing Biomembranes: Final LDRD Report

Todd M. Alam, Greg P. Holland, Alison Costello, Sarah K. McIntyre, and Mark Stevens

Prepared by
Sandia National Laboratories
Albuquerque, New Mexico 87185 and Livermore, California 94550

Sandia is a multiprogram laboratory operated by Sandia Corporation,
a Lockheed Martin Company, for the United States Department of Energy's
National Nuclear Security Administration under Contract DE-AC04-94AL85000.

Issued by Sandia National Laboratories, operated for the United States Department of Energy by Sandia Corporation.

Available to DOE and DOE contractors from

U.S. Department of Energy
Office of Scientific and Technical Information
P.O. Box 62
Oak Ridge, TN 37831

Telephone: (865) 576-8401
Facsimile: (865) 576-5728
E-Mail: reports@adonis.osti.gov
Online ordering: http://www.osti.gov/bridge

Available to the public from

U.S. Department of Commerce
National Technical Information Service
5285 Port Royal Rd.
Springfield, VA 22161

Telephone: (800) 553-6847
Facsimile: (703) 605-6900
E-Mail: orders@ntis.fedworld.gov
Online order: http://www.ntis.gov/help/ordermethods.asp?loc=7-4-0#online

SAND2007-6547
Unlimited Release
Printed October 2007

Tools for Characterizing Biomembranes: Final LDRD Report

Todd M. Alam[*a], Greg P. Holland[†], Alison Costello[‡],
Sarah K. McIntyre[a], and Mark Stevens[b]

[a] Department of Electronic and Nanostructured Materials,
[b] Department of Biomolecular Analysis and Imaging

Sandia National Laboratories
P. O. Box 5800
Albuquerque, NM 87185

Abstract

A suite of experimental nuclear magnetic resonance (NMR) spectroscopy tools were developed to investigate lipid structure and dynamics in model membrane systems. By utilizing both multinuclear and multidimensional NMR experiments a range of different intra- and inter-molecular contacts were probed within the membranes. Examples on pure single component lipid membranes and on the canonical raft forming mixture of DOPC/SM/Chol are presented. A unique gel phase pretransition in SM was also identified and characterized using these NMR techniques. In addition molecular dynamics into the hydrogen bonding network unique to sphingomyelin containing membranes were evaluated as a function of temperature, and are discussed.

[*] Author to whom correspondence should be addressed: tmalam@sandia.gov
[†] Present address: Department of Chemistry and Biochemistry, Magnetic Resonance Research Center, Arizona State University, Tempe, AZ 85287-1604, USA.
[‡] Present address: Los Alamos National Laboratories.

Acknowledgements

The authors would like to acknowledge Ryan S. Berry and Mark E. Stavig for performing the differential scanning calorimetry measurements. Sandia is multiprogram laboratory operated by Sandia Corporation, a Lockheed Martin Company, for the United Stated Department of Energy's National Nuclear Security Administration under Contract DE-AC04-94AL85000. This work was supported under the Sandia LDRD program (Project 79746).

Definitions

1D – one dimensional

2D – two dimensional

Chol - cholesterol

CPMAS – cross polarization magic angle spinning

CSA - chemical shift anisotropy

DMPC – 1,2- dimyristoyl-*sn*-glycero-3-phosphocholine

DOPC - 1,2-dioleoyl-*sn*-glycero-3-phosphocholine

DPPC - 1,2-dipalmitoyl-*sn*-glycero-3-phosphocholine

DSC - differential scanning calorimetry

FSLG – frequency switched Lee-Goldburg

FWHM - full width at half maximum

HETCOR – heteronuclear correlation

HOESY – heteronuclear NOE spectroscopy

INEPT - insensitive nuclear enhancement polarization transfer

L_α – liquid crystalline phase

L_β - gel phase

l_d – liquid disordered

l_o – liquid ordered

NMR – Nuclear Magnetic Resonance

MAS NMR - magic-angle spinning nuclear magnetic resonance

MD – molecular dynamics

NOE – nuclear Overhauser effect

NOESY – NOE spectroscopy

PC – phosphatidylcholine

PFG – pulsed field gradient

RDF – Radial Distribution Function

RFDR – radio frequency dipolar recoupling

SM - sphingomyelin

s_o – solid ordered phase

T_2 – spin-spin relaxation time

T_m – phase transition temperature

Table of Contents

Table of Contents (Continued)

List of Figures

List of Figures (Continued)

List of Tables

Chapter 1

Tool for Characterizing Biomembranes: Final LDRD Report

Executive Summary

The simplistic picture proposed in the Singer-Nicholson “Fluid Mosaic Model” in which membrane proteins are imbedded and diffuse freely in a fluid lipid bilayer is both simplistic and naïve. Instead it is now argued that biomembranes are composed of domains that are heterogeneous in both their physical and biochemical properties. These micro-domains or “membrane rafts” are complex and are argued to play a pivotal role in the bioactivity of membranes, including transport, cell signaling, cell fusion and toxin interactions. In this LDRD novel NMR experiments for experimentally measuring the size and chemical composition of membrane rafts were developed. In addition, NMR experiments that allow specific molecular contacts to be probe on the atomic levels are presented. By utilizing multi-frequency and multi-dimensional NMR techniques in combination with multi-pulse sequences, a range of different interactions and dynamics within the biomembranes were realized. Finally molecular dynamics simulations that investigate the role of unique hydrogen bond motifs within the sphingomyelin lipid bilayer are presented.

1.1 Lipid Domains and Raft Formation

The viewpoint that cellular membranes exist in a continuous fluid mosaic model [1] has evolved considerably in the last three and a half decades, and continues to rapidly change with the development of improved tools for characterizing membrane systems. It is now generally accepted that membranes can form heterogeneous domains with unique biochemical compositions. Of particular interest are domains composed of sphingolipids and cholesterol and are called “membrane rafts” or “lipid rafts” [2-4]. The formation and detection of lipid rafts in biomembranes has attracted much attention in recent years due to their potential role in cell signaling, signal transduction, cholesterol shuttling and protein sorting [5-11]. Lipid rafts are thought to be involved in the trafficking and formation of proteins associated with prion and Alzheimer’s diseases [12, 13], and as potential sites for toxin interactions and entryways for pathogens [14, 15]. For

example, it has become widely accepted that lipid rafts play a key role in how HIV-1 fuses to cell membranes [16-18]. A schematic of the various biological mechanism that have been associated with lipid rafts is shown in **Figure 1.1**. Although their biological relevance and importance is apparent, the way in which lipid rafts self assemble and organize on a molecular to nanometer scale is still far from understood.

Recent studies strongly suggest that the presence of cholesterol can cause lipids with high liquid crystalline (L_α) phase transition temperatures (T_m), to form liquid ordered (l_o) phases in biological membranes [10, 19]. The l_o phase differs from the L_α liquid crystalline phase in that it exhibits a higher degree of acyl chain order [20]. It has been shown in a number of model ternary systems that these l_o phases, rich in cholesterol and high T_m saturated chain lipids, will phase separate in the presence of low T_m unsaturated lipids [21-28]. Lipid rafts are l_o domains rich in saturated lipids and cholesterol floating in a sea of liquid disordered (l_d) phospholipids that are cholesterol-poor. The first evidence for the existence of lipid rafts was the detection of detergent resistant membranes that were insoluble in Triton X-100 [19]. These insoluble phases were composed primarily of sphingolipids and cholesterol. The raft phase is believed to be in a l_o state while the more fluid phase has a high content of unsaturated phospholipids and exists in the l_d state. **Figure 1.2** shows a representation of these different phases used in describing the lipid raft model. While domains have been readily observed in model lipid systems, in cells lipid domains have been elusive [29]. Presently, it is not clear what the lipid organization exists within cells. There are a variety of conflicting hypotheses. Understanding how domains form based on the molecular interactions will help resolve many aspects of domain formation and its biological significance.

Sphingomyelin (SM) is one of the primary saturated lipids that comprise mammalian cells [30, 31] and has been indicated in the formation of l_o domains or rafts in cellular membranes [6, 10, 19, 32]. Until recently much more attention has been given to the role of glycerolipids within biomembranes, but the discovery of membrane rafts and the role of SM in these domains have brought new interest in studying the nature of SM bilayers [5, 21, 29]. Convincing evidence exists that cholesterol prefers to pack with saturated lipids over unsaturated lipids and further, that cholesterol favors sphingolipids over glycerophospholipids [33]. Although surmounting evidence supports the existence of cholesterol rich l_o domains of SM in cellular and model membranes systems, the specific molecular contacts that mediate this sphingolipid-cholesterol interaction are still far from understood.

Although there have been various lipid raft systems studied, the two most common models appear to be the 1,2-dioleoyl-*sn*-glycero-3-phosphocholine/1,2-dipalmitoyl-*sn*-glycero-3-phosphocholine/Cholesterol (DOPC/DPPC/Chol) and 1,2-dioleoyl-*sn*-glycero-3-phosphocholine/Sphingomyelin/Cholesterol (DOPC/SM/Chol) systems. Raft formation has been observed experimentally in both of these model membrane systems with various techniques, including fluorescence microscopy [21-24, 26, 34], ^{2}H NMR [24], pulsed field gradient (PFG) NMR [35], electron spin resonance (ESR) [36], atomic force microscopy (AFM) [28, 33], X-ray diffraction (XRD) [37], and neutron scattering [27]. Phase diagrams have been constructed for both DPPC [22] and SM [23, 25] ternary systems containing DOPC and Chol. Some of these phase diagrams have led to a thermodynamic model involving condensed complexes [38]. In these systems DPPC or SM forms the raft phase by incorporating Chol that preferentially packs with the saturated chains, while the unsaturated chains of DOPC comprise the "disordered sea" in which the lipid rafts are dispersed. The phase diagram for the canonical raft forming DOPC/SM/Chol system is shown in **Figure 1.3**.

The primary goal of this LDRD was to developed spectroscopic tools that allow these specific molecular contacts within raft systems to be probed. In particular the use of nuclear magnetic resonance (NMR) spectroscopy to look for specific molecular contacts and at the local structure and molecular dynamics of the DOPC/SM/Chol raft forming membrane mixture.

1.1 Development of NMR Tools

In the individual chapters of this LDRD final SAND report we describe the progress made in the development of new NMR spectroscopy techniques to probe raft forming membrane systems, and some of the insights gained into specific SM containing model membranes.

In **Chapter 2**, two-dimensional (2D) ^{1}H-^{13}C insensitive nuclear enhancement polarization transfer (INEPT) magic angle spinning (MAS) NMR experiments utilizing a ^{1}H-^{1}H magnetization exchange mixing period are presented for characterization of lipid systems. The introduction of the exchange period allows for structural information to be obtained via ^{1}H-^{1}H dipolar couplings but with ^{13}C chemical shift resolution. It is shown that utilizing a radio frequency dipolar recoupling (RFDR) pulse sequence with short mixing times in place of the more standard nuclear Overhauser Effect (NOE) cross-

relaxation for magnetization exchange during the mixing period allowed for the identification and separation of close ^{1}H-^{1}H dipolar contacts versus longer-range inter-molecular ^{1}H-^{1}H dipolar cross-relaxation. These 2D INEPT MAS NMR experiments were used to address different both intra- and inter-molecular contacts in lipid and lipid/cholesterol mixtures.

In **Chapter 3**, ^{13}C cross polarization magic angle spinning (CP-MAS) and ^{1}H MAS NMR spectra were collected on egg sphingomyelin (SM) bilayers containing cholesterol above and below the liquid crystalline phase transition temperature (T_m). Two-dimensional dipolar heteronuclear correlation (HETCOR) spectra were obtained on SM bilayers in the liquid crystalline (L_α) state for the first time and display improved resolution and chemical shift dispersion compared to the individual ^{1}H and ^{13}C spectra and significantly aid in spectral assignment. In the gel (L_β) state, the ^{1}H dimension suffers from line broadening due to the ^{1}H-^{1}H homonuclear dipolar coupling that is not completely averaged by the combination of lipid mobility and MAS. This line broadening is significantly suppressed by implementing frequency switched Lee-Goldburg (FSLG) homonuclear ^{1}H decoupling during the evolution period. In the liquid crystalline (L_α) phase, no improvement in line width is observed when FSLG is employed. All of the observed resonances are assignable to cholesterol and SM environments. This study demonstrates the ability to obtain 2D heteronuclear correlation experiments in the gel state for biomembranes, expands on previous SM assignments, and presents a comprehensive ^{1}H/^{13}C NMR assignment of SM bilayers containing cholesterol. Comparisons are made to a previous report on cholesterol chemical shifts in dimyristoylphosphatidylcholine (DMPC) bilayers. A number of similarities and some differences are observed and discussed.

In **Chapter 4**, a model membrane system composed of egg sphingomyelin (SM), 1,2-dioleoyl-*sn*-glycero-3-phosphocholine (DOPC), and cholesterol was studied with static MAS ^{31}P NMR spectroscopy. This model membrane system is of significant biological relevance since it is known to form lipid rafts. ^{31}P NMR under MAS conditions resolves the SM and DOPC headgroup resonances allowing for extraction of the ^{31}P NMR parameters for the individual lipid components. The isotropic chemical shift, chemical shift anisotropy (CSA), and asymmetry parameter can be extracted from the spinning side band manifold of the individual components that form liquid ordered and liquid disordered domains. The magnitude of the ^{31}P CSA and the line width is used to determine headgroup mobility and monitor the gel to gel and gel to liquid crystalline

phase transitions of SM as a function of temperature in these mixtures. Spin-spin (T_2) relaxation measurements are in agreement with the line width results reflecting mobility differences and some membrane heterogeneity. It will be shown that the presence of DOPC and/or cholesterol greatly impacts the headgroup mobility of SM both above and below the liquid crystalline phase transition temperature (T_m), while DOPC displays only minor variations in these lipid mixtures.

In **Chapter 5**, this SM gel phase pretransition was further investigated. The impact of low cholesterol concentrations on an egg sphingomyelin bilayer is investigated using ^{31}P MAS NMR spectroscopy. The magnitude of the isotropic ^{31}P MAS NMR line width is used to monitor the main gel to liquid crystalline phase transition, along with a unique gel phase pretransition. In addition, the ^{31}P CSA and spin-spin relaxation times (T_2), along with the effects of spinning speed, proton decoupling and magnetic field strength, are reported. The variation of this unique gel phase thermal pretransition with the inclusion of 5 through 21 mol% cholesterol are presented and discussed.

In **Chapter 6**, 2D ^{1}H/^{31}P dipolar HETCOR MAS NMR is used to investigate the correlation of the lipid headgroup with various intra- and intermolecular proton environments. CPMAS NMR techniques involving ^{31}P have not been previously pursued to a great extent in lipid bilayers due to the long ^{1}H-^{31}P distances and high degree of headgroup mobility that averages the dipolar coupling in the liquid crystalline phase. The results presented herein show that this approach is very promising and yields information not readily available with other experimental methods. Of particular interest is the detection of a unique lipid backbone-water intermolecular interaction in egg SM that is not observed in lipids with glycerol backbones like phosphatidylcholines (PC). This backbone-water interaction in SM is probed when a mixing period allowing magnetization exchange between different ^{1}H environments via the NOE is included in the NMR pulse sequence. The molecular information provided by these ^{1}H/^{31}P dipolar HETCOR experiments with NOE mixing differ from those previously obtained by conventional NOE spectroscopy (NOESY) and heteronuclear NOE (HOESY) NMR experiments. In addition, 2D ^{1}H/^{13}C INEPT HETCOR MAS NMR experiments with NOE mixing support the ^{1}H/^{31}P dipolar HETCOR results and confirm that a H_2O environment with non-vanishing dipolar interactions with the SM backbone is present. This unique lipid backbone-water interaction is attributed to intermolecular hydrogen-bonding motifs that are formed between the sphingosine backbone of SM and water.

In **Chapter 7**, molecular dynamic (MD) simulations of SM bilayers as a function of temperature are presented. Of particular interest will be the development of the SM force fields and the use of these simulations to characterize the hydrogen bonding present in this lipid system, including insight into the role of water hydrogen bonding networks at the sphinospine backbone.

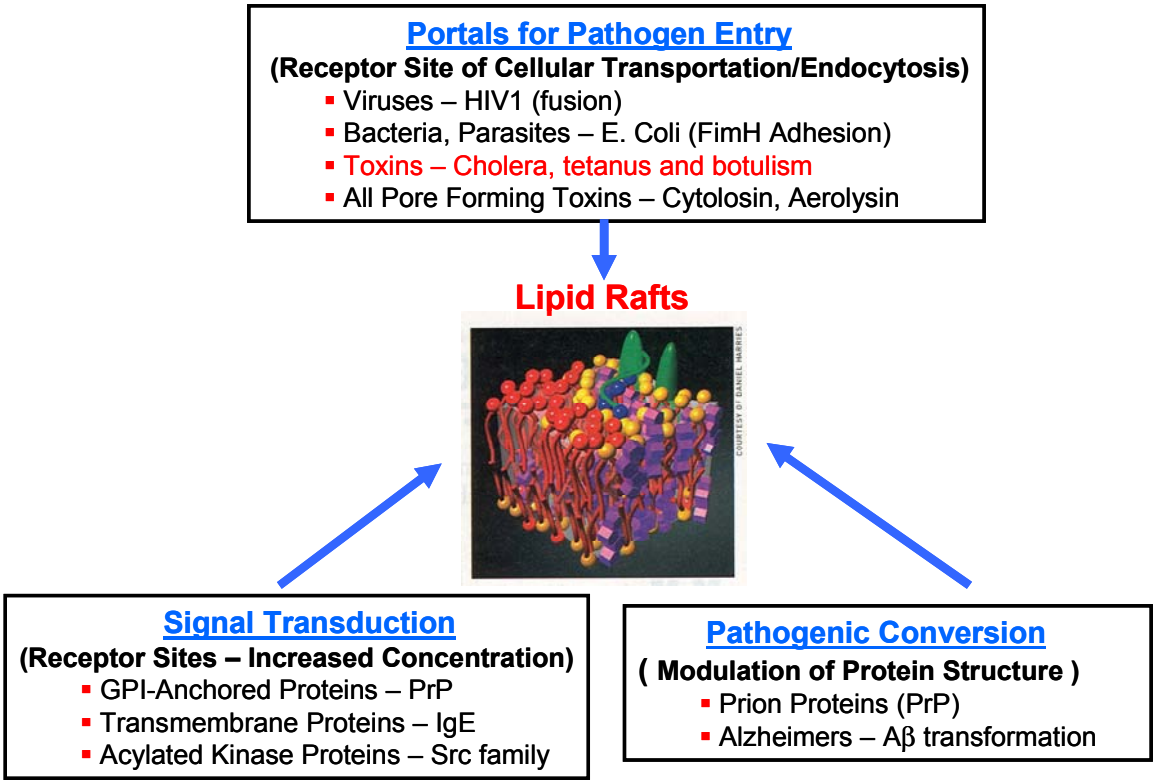

Figure 1.1 Biological significance and impact of membrane rafts.

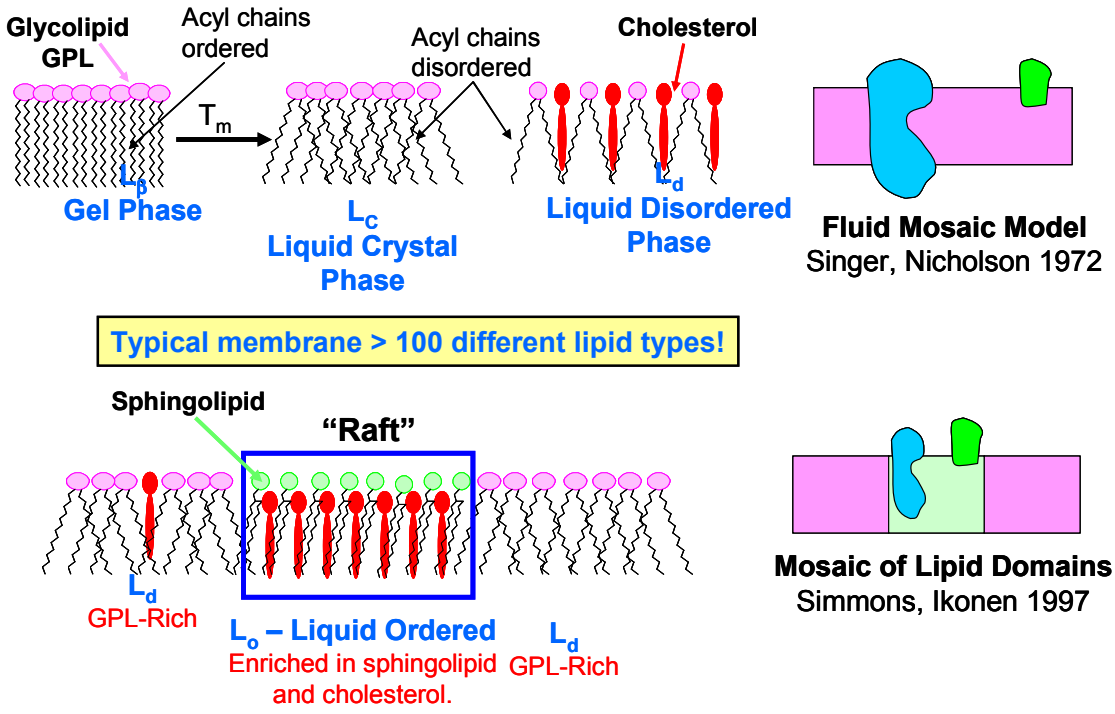

Figure 1.2 Representation of the different phases with membrane rafts. These domains lead to the current Mosaic of Lipid Domain model to describe biomembranes.

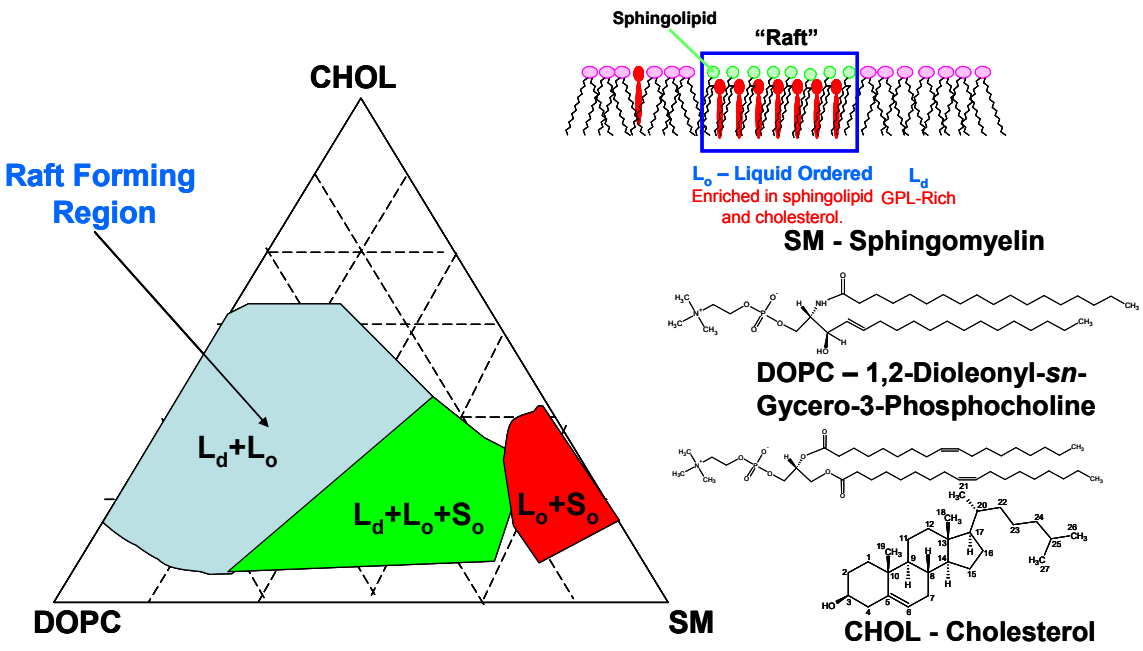

Figure 1.3 The phase diagram for SM/DOPC/Chol mixtures.

This Page Left Intentionally Blank

Chapter 2

^{1}H-^{13}C INEPT MAS NMR Correlation Experiments With ^{1}H-^{1}H Mediated Magnetization Exchange to Probe Organization in Lipid Biomembranes

2.1. MAS NMR in Biomembranes

Magic angle spinning (MAS) NMR continues to be an important and versatile tool for the investigation of lipids and biological membranes. Investigations using ^{1}H, ^{13}C, ^{31}P and ^{14}N MAS NMR on a variety of different lipid and membrane systems has been reported [39-46]. Due to the high sensitivity ^{1}H was one of the first nuclei pursued using modern MAS NMR techniques [47, 48]. It has been found that the rapid axial rotation, fast lateral diffusion and *trans-gauche* isomerizations of the lipids in the liquid crystalline (L_{α}) phase significantly averages the ^{1}H-^{1}H dipolar coupling transforming the interaction from homogeneous to inhomogeneous such that modest spinning speeds can produce well resolved ^{1}H MAS spectra [48-50]. These observations prompted a series of two-dimensional (2D) ^{1}H NOESY MAS NMR experiments that allowed molecular contacts between different lipid regions, as well as between lipids and other constituents within the membrane to be determined [51-56]. The observation of contacts between the methyl protons in lipid headgroup and the protons of the terminal methyl in the alkyl chain lead to extensive discussion into the relative impact of spin diffusion and intermolecular dipolar interactions resulting from lipid disorder on the observed cross-relaxation in ^{1}H NOESY MAS NMR experiments [51, 52, 55, 57, 58]. More recently, the selectivity and sensitivity of ^{1}H MAS NMR has been improved by use of pulsed field gradients (PFG) [40]. The use of gradients and ^{1}H MAS NMR has also allowed the measurement of diffusion rates in lipid and biomembranes systems [59-61], while ^{1}H saturation transfer experiments probing specific lipid-protein interactions have been recently reported [62]. A common limitation or difficulty encountered in many of these ^{1}H MAS NMR studies is the severe spectral overlap between different lipids and sterol constituents in complex membrane systems.

To improve the spectral resolution 2D ^{1}H-^{13}C MAS NMR correlation experiments have also been developed for lipid systems, including ^{1}H-presaturation cross polarization

(CP) transfer experiments and CP based heteronuclear correlation (HETCOR) experiments [45, 46, 63-65]. The effectiveness and variation of the CP transfer was used to estimate ^{13}C-^{1}H, ^{31}P-^{1}H, and ^{31}P-^{13}C dipolar couplings as a basis for structural input. 2D ^{1}H-^{13}C dipolar recoupling experiments have also been developed to directly measure CH dipolar order parameters [66, 67], or inter-proton dipolar pair order parameters [68]. For lipid systems higher MAS frequencies can effectively reduce residual ^{1}H-^{1}H dipolar interactions such that J-coupling polarization transfer experiments become feasible. It has been shown that the ^{1}H-^{13}C INEPT (Insensitive Nuclei Enhancement by Polarization Transfer) experiment under MAS is well suited for lipid systems in the L_{α} phase [44]. The INEPT experiment has the advantage that the ^{1}H-^{13}C polarization transfer occurs directly through the CH bond via J-coupling such that non-bonding correlations are not observed, and is independent of the CH bond orientation. The efficiency of the ^{1}H-^{13}C INEPT transfer has also been shown to be sensitive to the motional dynamics of the different ^{1}H environments, and can be used as a probe of different lipid phases [50]. The INEPT experiment is easily incorporated into 2D ^{1}H-^{13}C HETCOR experiments and has been reported for uniformly labeled lipid dispersions [69] and lipid-cholesterol mixtures [45, 70, 71]. 2D gradient enhanced ^{1}H-^{13}C HSQC (Heteronuclear Single Quantum Coherence) MAS NMR experiments have also been reported for dimyristoylphosphatidylcholine (DMPC)/Cholesterol mixtures allowing for the complete assignment of cholesterol in the lipid L_{α} phase [70, 71].

In this chapter we extend these 2D ^{1}H-^{13}C INEPT MAS NMR correlation experiments by introducing a mixing period for ^{1}H spin exchange to probe intra- and inter-molecular ^{1}H-^{1}H contacts within model lipid systems. This type of experiment was originally demonstrated by Alonoso and Massiot for mesostructured materials at very high spinning speeds [72]. Two different schemes for ^{1}H-^{1}H dipolar magnetization exchange where investigated. The first scheme used a mixing period with no ^{1}H irradiation during the mixing period corresponding to standard incoherent dipolar NOESY cross-relaxation, and a second scheme used a radiofrequency dipolar recoupling (RFDR) pulse sequence during the mixing period to coherently drive the ^{1}H-^{1}H magnetization exchange. Examples of the 2D ^{1}H-^{13}C INEPT MAS correlation experiment on pure DMPC and DMPC/Cholesterol mixture are presented and discussed.

2.2 INEPT MAS Experimental Details

Unlabelled 1,2-dimyristoyl-*sn*-glycero-3-phosphocholine (DMPC), [1,2-$^{2}H_{54}$]-dimyristoyl-*sn*-glycero-3-phosphocholine (DMPC-d_{54}) and unlabelled cholesterol (CHOL) were purchased from Avanti Polar Lipids (Alabaster, AL). Multilamellar vesicles (MLV) were prepared by dissolving a 1:1 mol% mixture of lipid and cholesterol in chloroform/methanol (3:1 v/v). Samples were then dried overnight under vacuum, and suspended in de-ionized water to produce a 28 wt% DMPC concentration. This mixture was then freeze-thawed-centrifuged 5 times. The lipid samples were transferred to 4 mm zirconia MAS rotors and sealed with kel-F inserts and caps. No dehydration effects were observed. The typical volume of MLV sample for NMR analysis was 50-100 μL corresponding to 25-50 mg of phospholipid. The samples were stored in a -20 ºC freezer when NMR experiments were not being performed.

All NMR experiments were performed on a Bruker Avance 600 spectrometer at an observe frequency of 600.14 and 150.92 MHz for ^{1}H and ^{13}C respectively. The 1D ^{1}H MAS NMR spectra were obtained using 8K points with a 30 kHz spectral width. The 1D ^{13}C CPMAS and ^{1}H-^{13}C INEPT spectra were obtained using 4K points with a 42 kHz spectral width. All ^{13}C and ^{1}H chemical shifts were referenced to the C-14 (δ = +14.0 ppm) and H-14 (δ = +0.9 ppm) resonances of DMPC [73]. The experiments utilized a 4 mm broadband MAS NMR probe with sample temperatures maintained at ± 0.2 K through the regulation of the bearing N_2 temperature. Heating effects due to frictional heating during sample spinning and due to rf irradiation during ^{1}H decoupling have previously been discussed [73]. These heating effects at moderate spinning speeds and high decoupling powers are not negligible, but can be compensated for appropriate choice of decoupling powers, spinning speed and “set” temperatures. In the present study actual sample temperatures were calibrated using the ^{1}H chemical shift difference ($\Delta\delta$) between the H-14 and H_2O resonances as detailed by Dvinskikh and co-workers [73]. A 2K increase in the lipid sample temperature was observed for a 5 kHz spinning speed, while a 10 kHz spinning speed produced a 10K increase in sample temperature, versus non-spinning conditions. All temperatures reported in the text are the actual sample temperature determined by this calibration method.

The ^{1}H-^{13}C INEPT MAS NMR correlation experiment [45] modified for ^{1}H-^{1}H mediated magnetization exchange is shown in **Figure 2.1**. The phase cycle for this modified sequence has previously been described [72]. Phase sensitive detection in t_1

was obtained using the States method [74]. All inter-pulse delays (t_1, τ_m, Δ_1 and Δ_2) were rotor synchronized. The delays Δ_1 and Δ_2 were optimized as detailed in the results section. For the ^{1}H-^{13}C correlation experiments presented in this paper, two different methods for ^{1}H-^{1}H magnetization exchange during the mixing time (τ_m) were investigated. In one set of experiments no additional ^{1}H rf pulses were introduced during τ_m such that the observed ^{1}H-^{1}H magnetization exchange occurs via NOE type dipolar relaxation analogous with the ^{1}H NOESY MAS NMR experiments previously reported [51, 52, 55, 57, 58]. In the second set of experiments the ^{1}H-^{1}H magnetization exchange occur via scaled ^{1}H-^{1}H dipolar interactions reintroduced using the radio-frequency dipolar recoupling (RFDR) pulse sequence on the ^{1}H channel during τ_m. This sequence consists of rotor-synchronized π pulses with the XY-8 phase cycle to reduce the impact of resonance offsets and pulse errors [75-77]. A 25 kHz TPPM ^{1}H decoupling with a 15^o phase shift was used during acquisition [78]. Typical acquisition parameters for the ^{1}H-^{13}C INEPT MAS NMR correlation experiments were 256 scans, 2s recycle delay, 4k t_2 points using a 42 kHz spectral width, 64-128 t_1 increments with a 15 kHz spectra width, with spinning speeds ranging from 5 kHz to 10 kHz.

2.3 2D INEPT Results and Discussion

The ^{1}H-^{13}C INEPT polarization transfer sequence for lipid biomembranes has been demonstrated by a number of groups [44, 45, 50, 67, 69-71]. These examples have utilized the INEPT sequence for obtaining 1D ^{13}C MAS NMR spectra, or have utilized the INEPT building block in more complicated pulse sequences. The ^{1}H-^{13}C INEPT MAS NMR spectra for the different DMPC and DMPC/CHOL mixtures in the present study are shown in **Figure 2.2**. The ^{13}C NMR resonance assignments for DMPC and cholesterol were based on previous studies (correcting for differences in referencing) [45, 65, 70, 71, 73], the sign of the INEPT signal modulation, direct polarization ^{13}C MAS NMR spectra and ^{1}H-^{13}C chemical shift correlations (see below). The assignment of DMPC is given in **Figure 2.2a**, with select cholesterol resonances being shown in **Figures 2.2b** and **2.2c**. With the addition of 50% cholesterol, the DMPC ^{13}C NMR resonances were not observed to shift significantly (± 0.1 ppm) except for the C4-C11 resonance envelope which shifts downfield and narrows slightly (**Figure 2.2b**), consistent with previous investigations [48, 79]. The C1 carbonyl resonance has been reported to vary with cholesterol concentration, but that ^{13}C NMR resonance (δ = 173.5

ppm) is not observed in the ^{1}H-^{13}C INEPT experiments since there is no one bond CH J-coupling present for that resonance, as well as the C5 and C13 carbons of cholesterol.

Figure 2.2 also shows that there are differences in the relative intensities between different DMPC carbon environments in the ^{1}H-^{13}C INEPT MAS NMR spectra that depend on the choice of the inter-pulse delays Δ_1 and Δ_2. For example, compare the C3 and C13 resonances of the alkyl chain, or the α and β headgroup resonances of DMPC in **Figures 2.2a** and **2.2b**. The majority of these intensity variations result from different J_{CH} coupling values making the optimization of the INEPT delays resonance specific (see below). More striking is the reduction in the cholesterol resonance intensity in comparison to the phospholipid signal intensity for the ^{1}H-^{13}C INEPT spectra shown in **Figure 2.2b**. This intensity discrepancy is not simply due to differences in the magnitude of J_{CH} couplings; the C18-CHOL and C14 DMPC methyl groups have almost identical J_{CH} but reveal large differences in signal intensity (**Figure 2.2b**). Rather these intensity changes are a function of molecular motions and the degree of ^{1}H-^{1}H dipolar coupling averaging. The impact of this averaging can be seen in **Figure 2.2c** where the increased spinning speed (and slightly higher temperature) increases the observed intensity of the cholesterol resonances. It is known that saturated phosphatidylcholines (such as DMPC) and cholesterol form a liquid ordered (l_o) phase at higher cholesterol concentrations [20, 80]. The addition of cholesterol to DMPC has also been shown to increase the axial rotation rate for the phospholipid, while the rotation of the cholesterol remains significantly slower than that of the lipid [81]. Discussion about the INEPT MAS sequence performance and the impact of differential motional dynamics of lipids and lipid constituents in membrane systems has been limited, except for the recent work by Warschawski and Devaux [50] using INEPT/NOE ratios as a tool to probe different lipid domains. A brief discussion of the optimization of the INEPT sequence for membrane systems is therefore warranted.

2.3.1 Optimization of the INEPT Sequence

In solution the optimization of the INEPT sequence is realized by matching of the Δ_1 and Δ_2 inter-pulse delays (**Figure 2.1**) to coherence evolution under specific values of the J_{CH} coupling. These inter-pulse delays are typically on the order of 1-2 ms. However for rigid solids this can be significantly longer than the ^{1}H transverse relaxation times (T_2^H). For short T_2^H values, the optimal signal intensity observed using the INEPT

sequence may no longer correspond to the simple $1/J_{CH}$ relationship. Recent ^{1}H-^{13}C INEPT MAS NMR experiments in mesostructured materials demonstrate that the contributions from T_2^H relaxation need to be directly considered [72]. Assuming that the ^{1}H relaxation (T_2^H) dominates relaxation effects from the ^{13}C (T_2^C), the signal intensity $S(\Delta_1, \Delta_2)$ during the ^{1}H-^{13}C INEPT experiment is given by [72, 82]

$$
\begin{aligned}
&S(\Delta_1, \Delta_2) \sim F_1(\Delta_1, T_2^H) F_2(\Delta_2, T_2^H) \\
&F_1 = \sin\left(2\pi J_{CH}\Delta_1\right)\exp\left[-2\Delta_1 / T_2^H\right] \\
&F_2 = \sin\left(2\pi J_{CH}\Delta_2\right)\exp\left[-2\Delta_2 / T_2^H\right], \quad \mathrm{AX} \\
&F_2 = \sin(4\pi J_{CH}\Delta_2)\exp\left[-2\Delta_2 / T_2^H\right], \quad \mathrm{AX_2} \\
&F_2 = \frac{3}{4}\left\{\sin\left(2\pi J_{CH}\Delta_2\right) + \sin\left(6\pi J_{CH}\Delta_2\right)\right\}\exp\left[-2\Delta_2 / T_2^H\right], \quad \mathrm{AX_3}
\end{aligned}
\tag{2.1}
$$

where the delays Δ_1 and Δ_2 are defined in **Figure 2.1**. The optimal signal intensity is observed at $\Delta_1 \sim 1/4J_{CH}$ and $\Delta_2 \sim 1/4J_{CH}$ for CH, $1/8J_{CH}$ for CH_2 and $\sim 0.098/J_{CH}$ for CH_3.

The question arises are there situations in membrane systems where short T_2^H make a significant impact on the performance of the ^{1}H-^{13}C INEPT sequence? **Figure 2.3** shows the signal variation of the ^{1}H-^{13}C INEPT MAS NMR sequence as a function of the inter-pulse delays Δ_1 and Δ_2 for select carbon resonances in DMPC at 313K, ν_R = 10 kHz. The dashed and solid lines were obtained by fitting the experimental results to **Eqn 2.1**. The J_{CH} values ranged from 110 to 150 Hz, with the T_2^H values ranging from 15 to 100 ms, consistent with independent T_2 values observed from rotor-synchronized ^{1}H Hahn echo experiments (data not shown). Similar INEPT response curves were observed for the cholesterol resonance, but at a significantly lower relative intensity (see additional discussion below). The long T_2^H values means that the maximum of the signal intensity is not shifted considerably away from the simple theoretical predictions, yet there is a noticeable loss of signal intensity for the longer Δ durations, in particular for Δ_2 values >2 ms, as might be used in experiments to distinguish CH_2 from CH or CH_3 carbon environments. For the CH_2 carbons this loss is on the order of 50% and can be related to the shorter T_2^H values observed for the methylene protons. This difficulty in T_2^H related signal loss during long Δ values was

noted in the reduced signal noise of methylene carbon resonances in previous studies of DMPC/Chol [71].

These relatively long T_2^H values and well behaved INEPT signal response agree with the small spinning sideband pattern observed in the ^{1}H MAS NMR spectra of DMPC and DMPC/CHOL shown in **Figure 2.4**, which give a measure of the residual ^{1}H-^{1}H dipolar coupling present. In the ^{1}H MAS NMR spectra of these lipid samples (**Figure 2.4a**) the headgroup resonances of DMPC shows very small ±1 spinning sidebands (relative intensity ~2% of the central isotropic intensity), and almost no higher-order spinning sidebands. The large methylene proton resonance (δ = +1.3 ppm, H4-H13) showing both ±1 and ±2 spinning sidebands, but the +1 sideband constitutes only ~9% of the central intensity at ν_R = 7.5 kHz. Similar results are observed for lipid resonances in the DMPC/Chol mixture. This observation is consistent with previous studies that reveal that for DMPC in the L_α phase the molecular dynamics are significant, reducing the ^{1}H-^{1}H homonuclear dipolar coupling so that it becomes effectively inhomogeneous in nature [47, 48, 50]. With this motional averaging the T_2^H values become sufficiently long as to not greatly impact the optimization of the INEPT sequence.

Figures 2.4b and **2.4d** shows the ^{1}H MAS NMR spectra of the DMPC-d_{54}/Chol sample in which many of the cholesterol ^{1}H resonances are now clearly visible. The cholesterol ^{1}H resonances (specifically between δ = +0.5 and + 2.5 ppm) have a significantly larger spinning sideband manifold, with the intensity of the +1 sideband being ~14%, the +2 sideband 6%, and the +3 sideband 1%, of the central intensity, implying a larger residual ^{1}H-^{1}H dipolar coupling due to the reduced motion of this cholesterol within the membrane. The relative ratio of the spinning sidebands also decreases with increased spinning from I_{+1}/I_0 ~ 14 % at ν_R = 7.5 kHz to I_{+1}/I_0 ~ 3% at ν_R = 12.5 kHz. Analysis of ^{1}H-^{1}H double quantum (DQ) MAS NMR sideband patterns have revealed residual ^{1}H-^{1}H dipolar couplings (under MAS) between 1 and 4 kHz in related lipid/Chol mixtures (Alam, personal communication, Rocky Mountain Conference 2005). The apparent proton T_2 as measured from rotor-synchronized Hahn-echo experiments (data not shown) also increases with higher spinning speed suggesting that the INEPT performance should be spinning speed dependent. This is confirmed in **Figure 2.4e** which shows the signal intensity for the ^{1}H-^{13}C INEPT MAS NMR experiment for the C26/C27 methyl resonances (δ = +22.6 ppm) and the C6 methine (δ = +120.4 ppm) carbon resonances of cholesterol. The most important observation was the dramatic

increase in the overall signal intensity with increasing spinning speed, especially for the C6 resonance. For these experiments the set temperature was adjusted such that the true sample temperature was the same (308 K) for all the different spinning speeds investigated. For the methyl C26/C27 carbon resonance there was a small ~ 10% increase in the signal intensity by increasing the spinning speed from 5 kHz to 10 kHz. The T_2^H values obtained from fitting **Eqn 2.1** were ~ 50 ms. The rapid internal motion of the methyl group still produces significant averaging of the ^{1}H-^{1}H dipolar coupling that the spinning speed variation is minor. For the cholesterol C6 methine carbon environment increasing the spinning speed from 5 and 10 kHz produced an >25% increase in the overall signal intensity. The corresponding T_2^H values was found to be ~ 10 ms. For the less mobile sterol component the efficiency of the INEPT sequence is dramatically reduced by the increased ^{1}H-^{1}H dipolar coupling, but a portion of this impact can be reduced by increases in the spinning rate. This is also consistent with the slower axial rotation observed for cholesterol in comparison to DMPC based on ^{2}H NMR relaxation studies [81]. Unfortunately, ultra-high spinning speeds (> 20 kHz) readily applied to other materials are not applicable to membrane systems due to the segregation/centrifugation of the water from the lipid mixture. These results presented above can now be used for the optimization of the 2D ^{1}H-^{13}C INEPT MAS NMR correlation experiments described below.

2.3.2 Two-dimensional ^{1}H-^{13}C Heteronuclear Correlation

The 2D ^{1}H-^{13}C INEPT MAS NMR heteronuclear correlation spectrum for DMPC at a short mixing time (τ_{mix} = 1 ms) is shown in **Figure 2.5** (total experiment time ~ 4.5 hrs), while the 2D correlation spectrum for DMPC-d_{54}/Cholesterol is shown in **Figure 2.6**. These results show that these heteronuclear correlation experiments at natural ^{13}C abundance can readily be performed. The benefit of the INEPT experiment is that the correlations arise from direct bonding interactions through the J_{CH} coupling polarization transfer, and do not contain cross peaks due to long range interactions as well as being independent of the CH bond orientation. The C1 carbonyl region, $\delta(^{13}C)$ = +173.5 ppm, is not shown since no cross peaks will be observed in the INEPT experiments for quaternary carbon environments. These 2D spectra allow confirmation of ^{1}H and ^{13}C resonance assignments and are consistent with previous investigations [51, 71, 73]. The 2D ^{1}H-^{13}C INEPT MAS NMR correlation spectrum for the DMPC/Chol mixture (data not

shown) is similar to **Figure 2.5** and shows significant overlap between many of the DMPC and cholesterol resonances even in the 2D experiment, but also reveals several distinct cholesterol resonances including the C6 methine at $\delta(^{13}C)$ = +120.4 ppm, the C3 methine at $\delta(^{13}C)$ = +70.7 ppm, the C14,C17 methines at $\delta(^{13}C)$ = +57.2 ppm, the C9 methine at $\delta(^{13}C)$ = +50.9 ppm, and the C19 methyl at $\delta(^{13}C)$ = +12.9 ppm. By using DMPC-d_{54}/ CHOL mixtures, it is possible to observe and identify all proton containing cholesterol carbon resonances as shown in **Figure 2.6**. Again the lipid carbonyl region and the cholesterol C5 quaternary, $\delta(^{13}C)$ = +142 ppm, spectral region is not shown since the INEPT experiment does not produce cross peaks for these carbon environments. ^{1}H-^{13}C HETCOR correlation experiments have been reported that utilized ^{13}C-C3,C4 labeled cholesterol in order to emphasize and clearly identify cholesterol cross peaks [45]. The 2D INEPT reported here demonstrate that ^{13}C labeling is not required to obtain correlation experiments in cholesterol containing membrane mixtures. The one draw back of these 2D INEPT experiments is the relatively low ^{1}H resolution afforded by the direct ^{13}C detection. This reduced ^{1}H resolution is clearly seen in the 2D spectra shown **Figures 2.5** and **2.6** (compared to the 1D ^{1}H MAS projections) where a very limited number of t_1 increments were used to help reduce overall experimental time. There is also a slight increase in the ^{13}C line width versus the 1D projection as a result of doubling the exponential line broadening for the 2D spectra. More recently, ^{1}H-^{13}C HMQC experiments have been reported for DMPC/CHOL mixtures that overcome this limitation [70, 71].

2.3.3 ^{1}H-^{1}H Dipolar Cross-Relaxation

To explore through space connectivities and interactions the 2D ^{1}H-^{13}C INEPT MAS NMR correlation experiments were expanded (**Figure 2.1**) to include a mixing time (τ_{mix}). During this period no additional *rf* pulses are applied to either channel such that ^{1}H-^{1}H magnetization exchange occurs via dipolar cross-relaxation. These types of experiments are analogous to ^{1}H-^{1}H MAS NOESY experiments,[51-56, 83] but now include the improved resolution afforded by ^{13}C detection. Similar to the ^{1}H NOESY experiments, ^{1}H-^{1}H correlations only become significant for τ_{mix} > 100 ms. **Figure 2.7** shows the 2D ^{1}H-^{13}C INEPT MAS NMR correlation spectra at τ_{mix} = 300 ms for DMPC. Numerous cross-peaks are observed (compared to **Figure 2.5**) correlating different ^{1}H environments to a single carbon environments as a result of ^{1}H-^{1}H dipolar cross-

relaxation. These include the short range through-space ^{1}H-^{1}H dipolar interactions between g_1 and g_2, g_1 and α, along with g_1 and γ within the DMPC head group, plus the C2-C3 interaction within the alkyl chain. In addition, long range inter-molecular correlations are observed including the dipolar cross-relaxation between γ and 4-11 carbons, γ to the C14 methyl and α to the C14 methyl. These interactions have previously been noted and discussed in the 2D ^{1}H-^{1}H NOESY investigations [51, 52, 54, 83], and demonstrate the dynamical disorder of the lipid present within the L_α phase. The scaled S/N of this 2D spectrum (scaled for the increased number of acquisitions) is ~ 30% of that observed in **Figure 2.5**. This S/N merit was estimated from the area of the intense γ resonance, with some loss expected due to relaxation during the 300 ms mixing period, but also reflects some loss of signal due to magnetization exchange with other coupled protons.

Similarly the 2D ^{1}H-^{13}C INEPT MAS NMR correlation spectrum for the DMPC-d54/CHOL mixture using τ_{mix} = 250 ms is shown in **Figure 2.8**. Again cross peaks between the different carbon resonances are observed (compared to **Figure 2.6**), including dipolar interactions within cholesterol (C6 to C7) as well as lipid-cholesterol interactions including: β, g_1, g_2 contacts to cholesterol, γ to cholesterol and γ to the C26,C27 methyl carbons of cholesterol. The low ^{1}H dispersion of the cholesterol resonances in the $\delta(^1H)$ = +0.5 to 1.5 ppm region make the assignment of these lipid-cholesterol contacts to specific cholesterol environments difficult, so we have simply denoted them as cholesterol contacts. From the 1D ^{1}H MAS NMR experiments along with the 1D ^{1}H-^{13}C INEPT (including phase variation with Δ_2, see section of INEPT optimization) we know that there is not a significant contribution from residual non-deuterated lipid in the $\delta(^1H)$ = +0.5 to 1.5 ppm region, supporting our arguments that the observed contacts are between the lipid and cholesterol. Also the strong ^{1}H-^{13}C cross-peak observed at $\delta(^{13}C)$ = +33.9 ppm, $\delta(^1H)$ = +2.4 ppm in **Figure 2.6** is assigned to the C8 of cholesterol since the signal modulation observed in 2D INEPT spectra for long Δ_2 values (data not shown) is consistent with a CH or CH_3 carbon environment, and not with a CH_2 species. There is a small contribution from residual non-deuterated C4-C11 methylene CH_2 carbons of the DMPC observed at $\delta(^{13}C)$ = +34.1 ppm and $\delta(^1H)$ = +1.3 ppm, but it is not visible in **Figure 2.6**. It should also be noted that the intensity of cross peaks between the lipid head group resonances in the DMPC-d_{54}/Chol mixture are lower than observed in pure DMPC (**Figure 2.7**) or DMPC/Chol mixtures. This reduction is

consistent with previous studies that have shown the cross-relaxation occurs via inter-molecular contacts and that the presence of deuterated alkyl chains will slow this process [51, 52, 83]. These 2D results show that the INEPT correlation experiments can be used to observe inter-molecular contacts between different constituents within membrane mixtures. Again, both **Figures 2.7** and **2.8** show a reduced ^{1}H (F1) resolution as a result of the limited number of t_1 increment utilized. The S/N of this 2D spectrum was ~ 35% of that observed in **Figure 2.6**.

2.3.4 ^{1}H-^{1}H RFDR Correlation

As discussed above, rapid lateral diffusion in the L_α lipid phase averages intermolecular ^{1}H-^{1}H dipolar interactions, while rapid axial rotation and molecular motions reduces the intra-molecular ^{1}H-^{1}H dipolar interactions within biomembranes. Early observations that MAS (even at slow spinning speeds) significantly improved the resolution of ^{1}H NMR spectra of membranes showed that residual ^{1}H-^{1}H dipolar couplings were present in these systems. For example, in DMPC (36 ^{o}C) and DPPC (50 ^{o}C) the dipolar order parameter S_{dip} was measured to be ~ 0.17 and 0.18, respectively [48]. These MAS-removed ^{1}H-^{1}H dipolar couplings can be reintroduced (scaled) through the use of different multiple pulse dipolar recoupling sequences during the τ_{mix} period (**Figure 2.1**). In the present study we have utilized the rotor-synchronized radio frequency dipolar recoupling (RFDR) sequence [75-77, 84] to re-introduce residual ^{1}H-^{1}H dipolar coupling via zero-quantum coherences as a means of magnetization transfer [85]. ^{1}H-^{1}H RFDR correlation experiments were recently demonstrated for swollen protein resins [86] and are similar to proton-mediated rare spin correlation experiments developed for protein structure determination in the solid state [87-90]. **Figure 2.9a** shows the 2D ^{1}H-^{13}C INEPT MAS NMR correlation spectrum for DMPC utilizing a τ_{mix} = 53.3 ms RFDR recoupling sequence. This period corresponds to 50 cycles of the XY-8 phase cycle. Even for this relatively short mixing time multiple cross peaks were observed arising from ^{1}H-^{1}H magnetization exchange within the membrane, with the spectrum being very similar to the 300 ms NOESY exchange spectra (**Figure 2.7**). The appearance of ^{1}H-^{1}H correlations at short mixing times distinguishes the RFDR based experiment from the cross-relaxation (NOE) based experiment (section 2.3.4) where no significant ^{1}H-^{1}H exchange cross-peaks were observed at τ_{mix} = 50 ms. Using the RFDR significant ^{1}H-^{1}H magnetization exchange was observed for τ_{mix} as short as ~10 ms. For τ_{mix} < 50 ms the appearance of new cross-peaks in the 2D ^{1}H-^{13}C INEPT exchange

experiments arise from the coherent reintroduction of dipolar couplings under the RFDR sequence, while for $\tau_{mix} \geq 100$ ms ^{1}H-^{1}H magnetization exchange cross-peaks can derive from both the coherent RFDR recoupling and the incoherent (diffusive like) dipolar cross-relaxation. More importantly, the long range inter-molecular dipolar contacts between the headgroup and the alkyl chain are not observed for these short mixing time RFDR type experiments (compare **Figure 2.7** and **Figure 2.9a**, in particular the C14 methyl contacts). The S/N for this 2D spectrum was ~ 40% of that observed in **Figure 2.5**, but is slightly improved over the S/N obtained from the 300 ms spin exchange experiment shown in **Figure 2.7**. Similar results are observed in the 2D ^{1}H-^{13}C INEPT MAS NMR correlation spectrum for DMPC-d_{54}/Chol utilizing a τ_{mix} = 26.7 ms RFDR recoupling shown in **Figure 2.9b**, where many of the cholesterol/lipid contacts are not observed due to the reduced magnitude of the inter-molecular dipolar coupling. The one notable exception to this is the cross peak at $\delta(^{13}C)$ = +33.9 ppm and $\delta(^1H)$ = +4.3 ppm (**Figure 2.9b**), which results from contact between the protons of the C8 methine carbon in cholesterol and either the protons of the g_1 or α carbons of the DMPC. As noted above this +33.9 ppm ^{13}C chemical shift originates from a CH or CH_3 carbon species based on INEPT modulation with Δ_2, and is therefore not the residual non-deuterated CH_2 carbons of DMPC. The origin of this strong inter-molecular contact between DMPC and cholesterol will be explored in future work. The S/N of this 2D RFDR spectrum is ~ 35% of that shown in **Figure 2.6**.

The difference in the behavior of the ^{1}H-^{1}H magnetization exchange under the cross-relaxation (NOE exchange) or the RFDR type mixing periods is more easily understood by measuring the evolution of the ^{1}H-^{1}H exchange as a function of τ_{mix}. To perform multiple ^{1}H-^{13}C INEPT experiments at different τ_{mix} would prove to be extremely time restrictive, but this information can be obtained by using a standard 2D ^{1}H NOESY MAS NMR correlation experiments [51, 52, 83, 86]. From NOESY exchange experiments the individual ^{1}H-^{1}H cross-relaxation rates can be directly measured as shown in **Figure 2.10** for select protons in the DMPC sample. The results are shown for experiments in which the τ_{mix} contain no rf pulses (standard NOE cross-relaxation) or the dipolar coupling was reintroduced incorporating a ^{1}H RFDR sequence. For protons that are expected to be spatially close the ^{1}H-^{1}H exchange under RFDR is observed to build up very rapidly, reaching a maximum between 10 and 25 ms, followed by a rapid decay away. For example, the exchange between the g_2 and the α protons is extremely rapid, reaching a maximum near 10 ms. The diagonal intensity under the RFDR sequence is

also observed to decay much more rapidly than the NOE type cross-relaxation. This decay results from the distribution of the magnetization under RFDR via the recoupled dipolar interactions, but also can be ascribed to a non-recoverable loss of magnetization due to pulse error and timing errors in the multiple-π RFDR pulse train. The performance of the RFDR sequence may be improved by incorporation of improved RFDR phase cycling, [91] or the introduction of compensated RFDR sequences [92]. For the NOE based cross-relaxation the buildup rates of the ^{1}H-^{1}H exchange is generally slower (**Figure 2.10**), usually reaching a maximum between 150 ms and 500ms as previously noted [51, 52, 83]. This magnetization exchange occurs through incoherent cross-relaxation which is dependent on both the residual dipolar coupling and the motional correlation time, and scales as r_{ij}^{-6} (where r_{ij} is the ^{1}H-^{1}H distance). The application of the RFDR sequence allows for the recovery (amplification) of dipolar couplings that are averaged by MAS, and not completely averaged by molecular motions. The sequence allows for exchange via a coherent process that is dependent on the reintroduced dipolar coupling independent of the correlation time and will scale as r_{ij}^{-3}. By using short mixing time in the RFDR sequence only protons with a larger (closer) ^{1}H-^{1}H dipolar coupling will give rise to exchange, while protons with smaller ^{1}H-^{1}H dipolar couplings do not have enough time to buildup and do not exchange. The larger dipolar interactions recoupled under RFDR most likely represent residual intra-molecular ^{1}H-^{1}H dipolar coupling, since the rapid axial diffusion of the lipids within the membrane are expected to produce a second averaging of dipolar inter-molecular contacts (making them smaller) such that they are not re-introduced by RFDR for short mixing times. By comparing the results of these two exchange experiments it is possible to assign strongly and weakly dipolar coupled protons contacts within membrane systems.

Interestingly for longer range ^{1}H-^{1}H contacts, such as the g_2 proton to the methyl C14 protons (**Figure 2.10**), the magnetization exchange is very similar for the RFDR and the NOE cross-relaxation based experiments. During the RFDR sequence it is known that magnetization transfer can occur both through recoupling and through NOE cross relaxation [86]. It has also been observed that the RFDR sequence may actually accelerate the incoherent NOE cross-relaxation by a process that has been called rotor-driven or RF-driven spin diffusion [93, 94]. This type of acceleration of the ^{1}H-^{1}H NOE cross-relaxation was not observed for the membrane systems investigated. Further

analysis of the individual ^{1}H-^{1}H exchange patterns within the complete lipid spin system will be explored in a later manuscript.

It should be noted that the RFDR sequence is not the only dipolar recoupling sequence (or perhaps even the most suitable) that could be utilized during the mixing period of the INEPT sequence shown in **Figure 2.1**. We have also explored the use of the symmetry based double quantum sequence recently described by Levitt and co-workers [95]. For example we have performed ^{1}H-^{13}C INEPT exchange experiments using the $C7_2^1$ recoupling sequence, and combined $C7_2^1$-$C9_3^1$ schemes,[96, 97] on a lower magnetic field strength instrument observing very similar results (albeit lower resolution) with the nearest neighbor dipolar contacts dominating. Unfortunately the performance of these windowless CN_n^ν-type decoupling sequences [95] on our higher field 600 MHz NMR instrument was rather poor due to hardware limitations and were not pursued further.

2.4 INEPT MAS Conclusions

In conclusion, we have demonstrated a 2D ^{1}H-^{13}C INEPT correlation experiment for membrane systems. By incorporating a mixing period for ^{1}H-^{1}H magnetization exchange structural information can be obtained through the ^{13}C detection of ^{1}H-^{1}H contacts. A comparison of the ^{1}H-^{1}H correlations observed under a mixing period incorporating NOE cross-relaxation versus correlations observed under the RFDR sequence makes it is possible to identify close intra-molecular ^{1}H-^{1}H contacts (or very strong inter-molecular contacts), versus long-range inter-molecular contacts within the membrane constituents. These types of correlation experiments should prove valuable for future investigations of complex biomembrane systems.

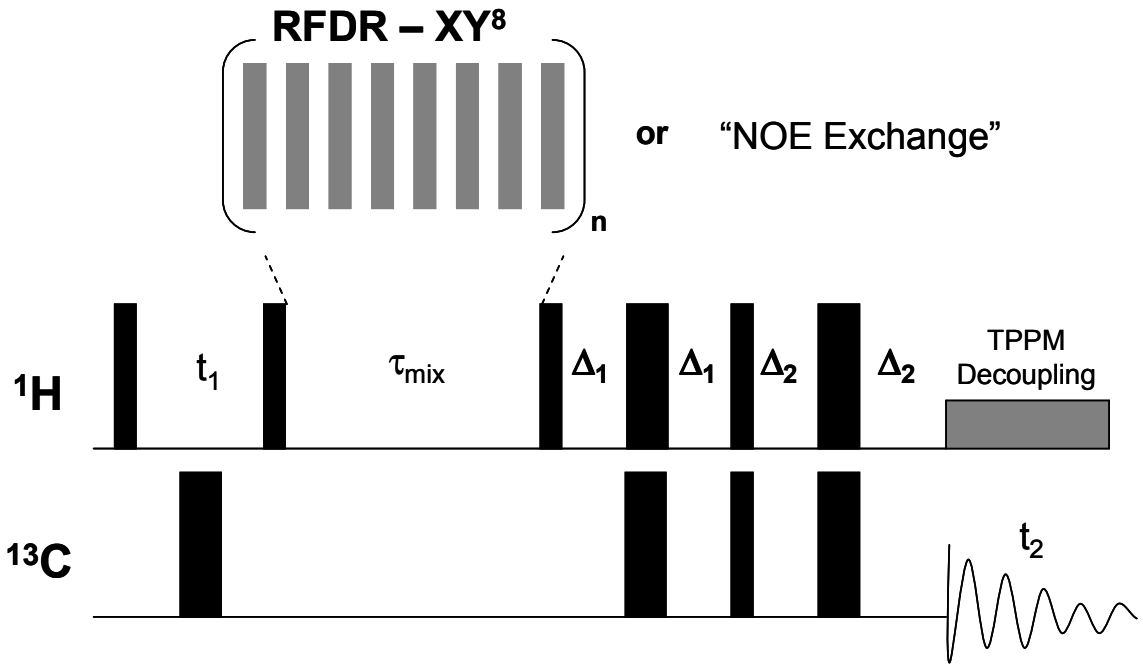

Figure 2.1. 2D refocused ^{1}H-^{13}C INEPT pulse sequence for correlation experiments where a mixing time τ_m is introduced that allows the transfer of magnetization via ^{1}H-^{1}H dipolar interactions either through NOE cross relaxation (no ^{1}H irradiation during τ_m) or recoupled dipolar interactions using a RFDR sequence. In this sequence all t_1, Δ_1 and Δ_2 delays were rotor synchronized (= $n\tau_R$ = n/ν_R, where ν_R is the spinning frequency), and were optimized as described in the text. The phase cycle for this sequence has been previously given [72].

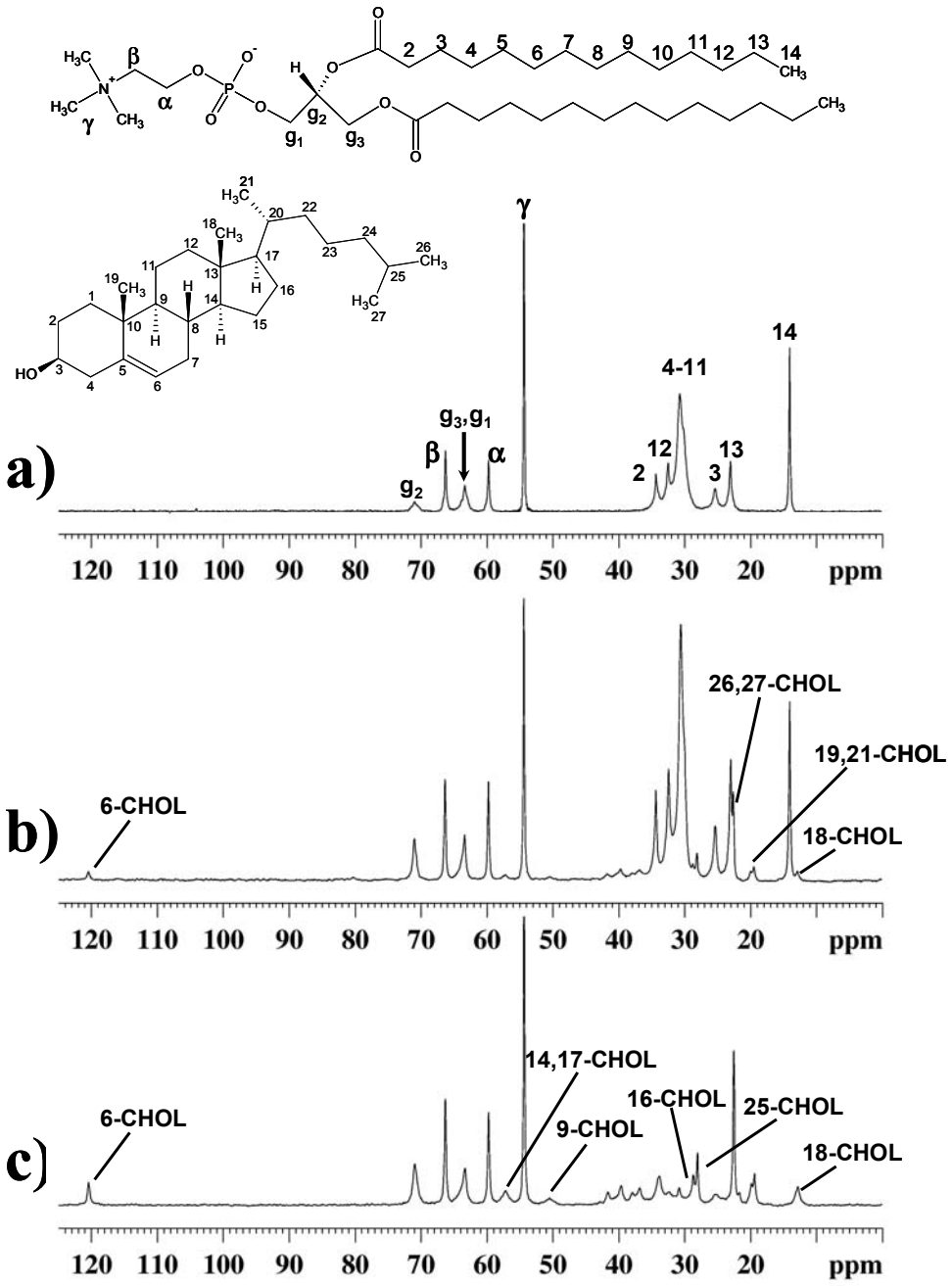

Figure 2.2. Refocused ^{1}H-^{13}C INEPT MAS NMR spectra for D_2O dispersion of (a) DMPC, ν_R = 7.5 kHz, Δ_1 = 2.1 ms, Δ_2 = 0.66 ms, 308 K (corrected for spinning/decoupling heating effects) (b) 1:1 DMPC/CHOL, ν_R = 7.5 kHz, Δ_1 = 2.1 ms, Δ_2 = 1.2 ms, 308 K, and (c) DMPC-d_{54}/CHOL, ν_R = 10 kHz, Δ_1 = 2.1 ms, Δ_2 = 1.1 ms, 313 K. The assignment numbering is shown in the molecular scheme, with the resonance assignments for DMPC given in (a) and select resonance assignments for cholesterol given in (b) and (c).

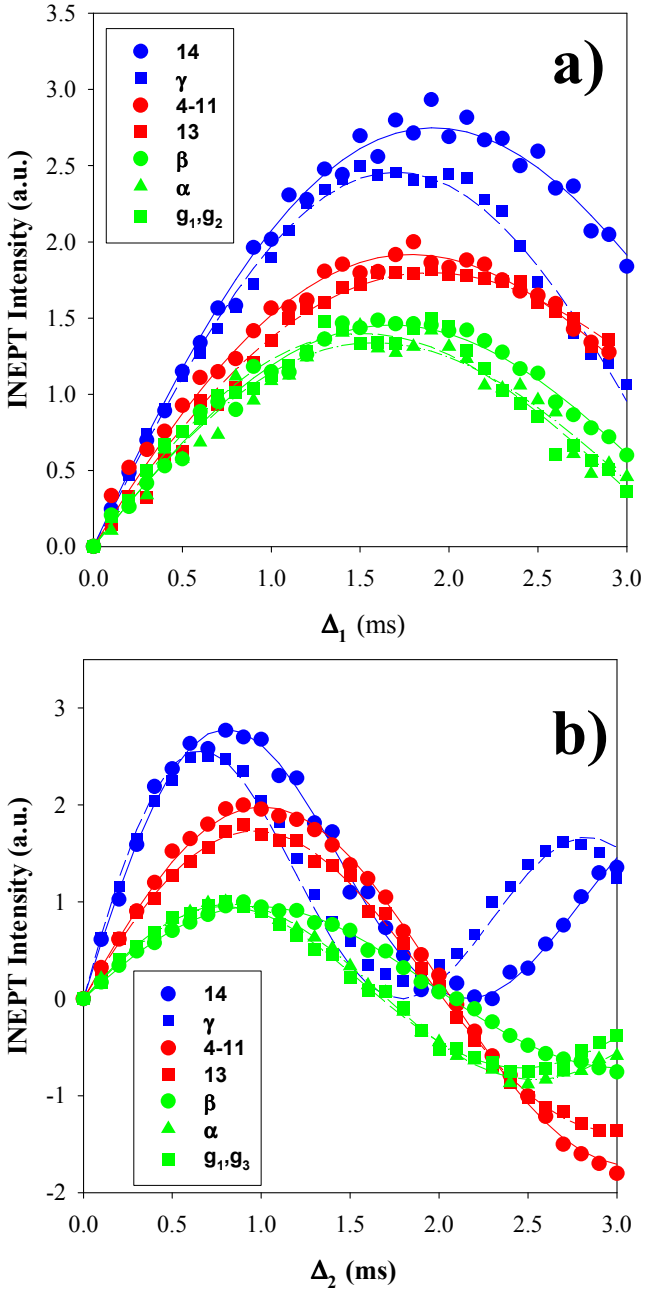

Figure 2.3. Signal amplitude variation for the ^{1}H-^{13}C INEPT MAS NMR experiment for a D_2O dispersion of DMPC at 313K, ν_R = 10 kHz, as a function of the inter-pulse delay Δ_1 and Δ_2. In (a) Δ_1 was varied while Δ_2 was held constant at 0.93 ms, while in (b) Δ_1 was kept constant at 2.0 ms and Δ_2 varied. The simulated lines were obtained using **Eqn 2.1**. The signal intensities of the different groupings were scaled to improve readability.

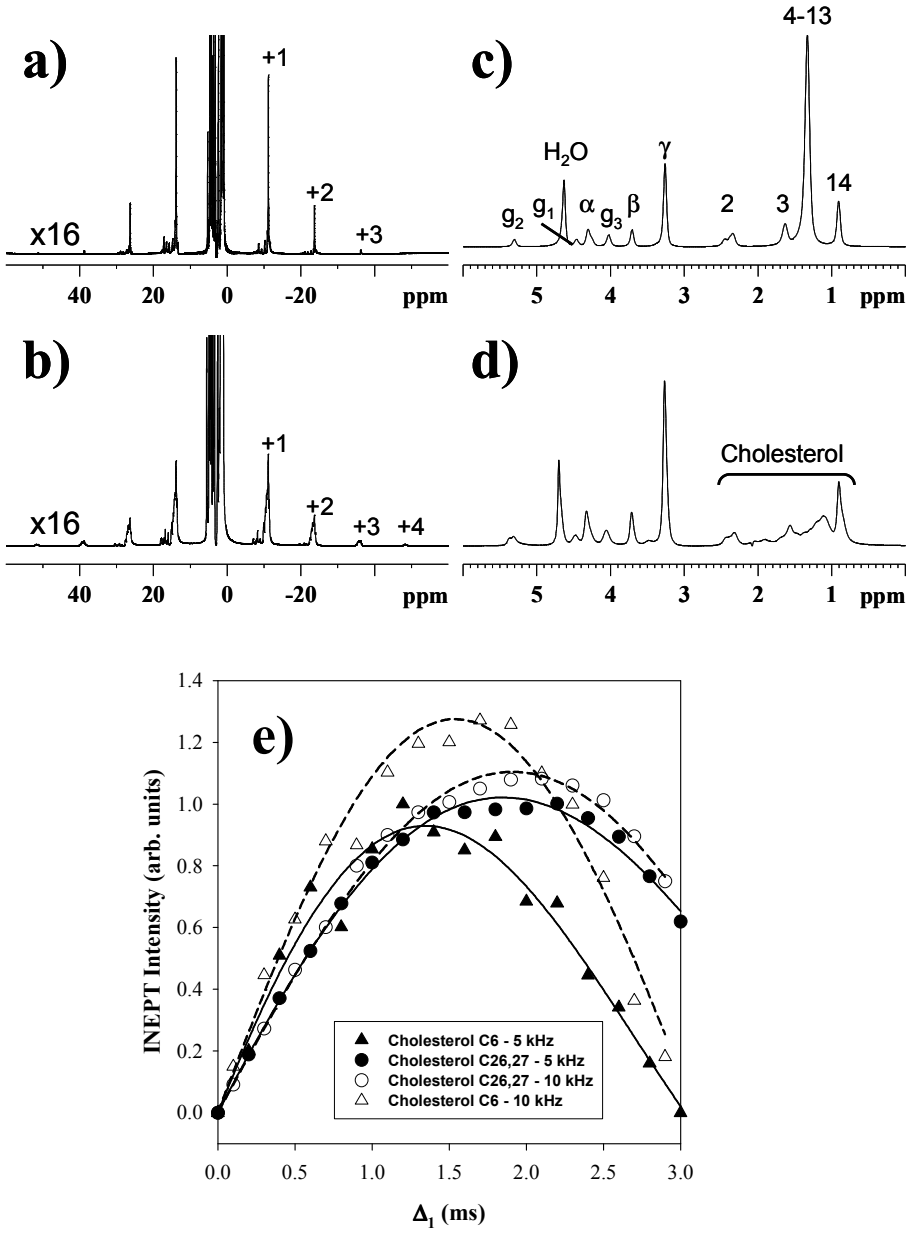

Figure 2.4. The ^{1}H MAS NMR spectra of (a) DMPC and (b) DMPC-d_{54}/Chol at 308K and ν_R = 7.5 kHz, showing the full spectral window with the different spinning sidebands marked. Expansion of the isotropic spectral region for (c) DMPC and (d) DMPC-d_{54}/Chol with the assignment of the different ^{1}H resonances in DMPC. The variation (e) of the ^{1}H-^{13}C INEPT signal intensity for the C26/C27 methyl resonances (δ = +22.6 ppm) and the C6 methine (δ = +120.4 ppm) cholesterol carbon resonances as a function of spinning speed: cholesterol C26/C27 at 5 kHz (●) and 10 kHz (○) and C6 at 5 kHz (▲) and 10 kHz (Δ).

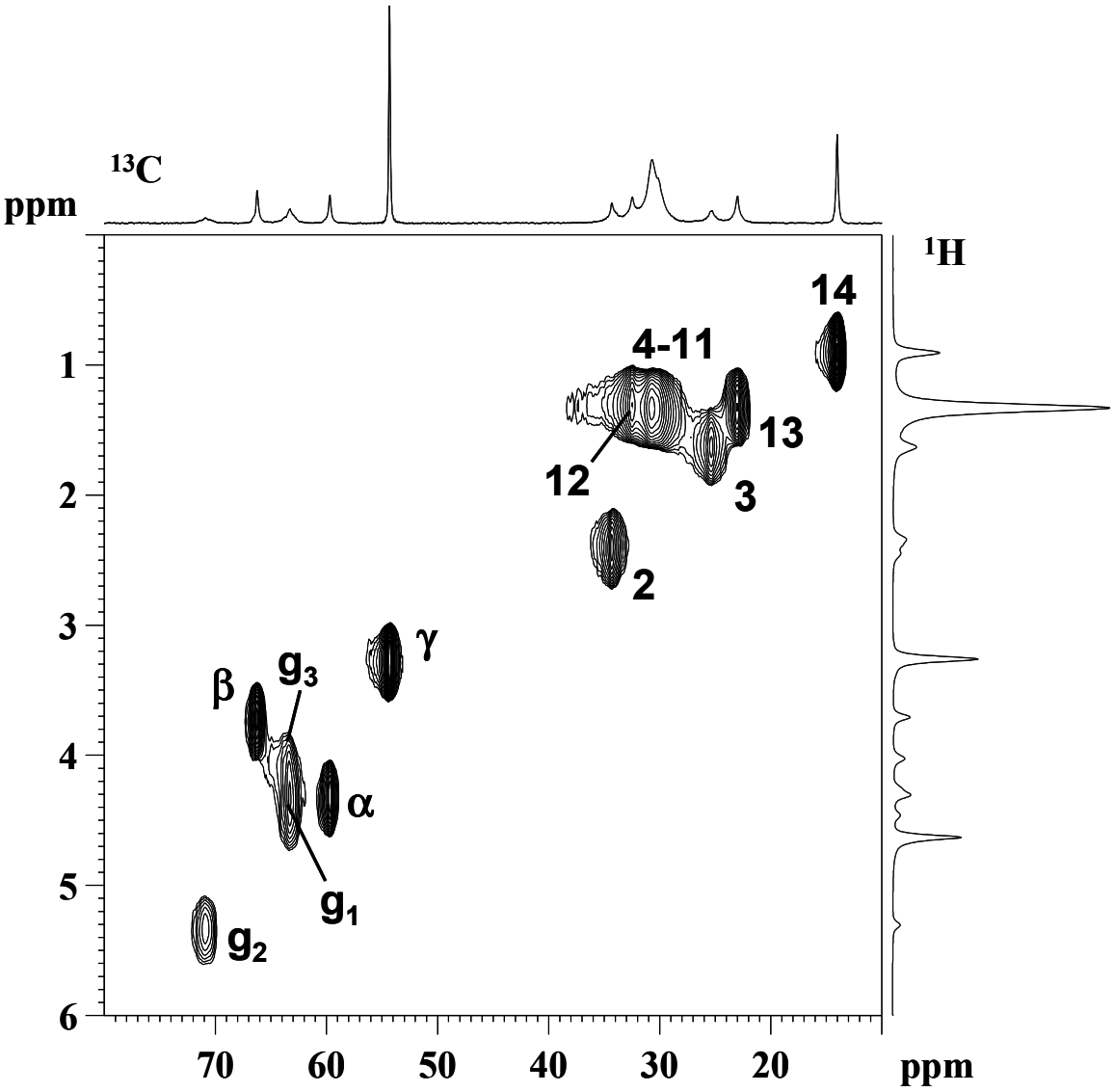

Figure 2.5. The 2D ^{1}H-^{13}C INEPT MAS NMR correlation spectra for DMPC obtained using the rotor-synchronized pulse sequence in **Figure 2.1** at ν_R = 7.5 kHz, 308K, τ_{mix} = 1 ms, Δ_1 = 2.1 ms and Δ_2 = 0.67 ms. The DMPC assignments are shown. The ^{13}C and ^{1}H projections are the 1D ^{1}H-^{13}C INEPT MAS and the 1D ^{1}H MAS NMR spectra, respectively. The low resolution in the F1 (^{1}H) dimension results from the reduced number of t_1 increments used in order to reduce experimental time.

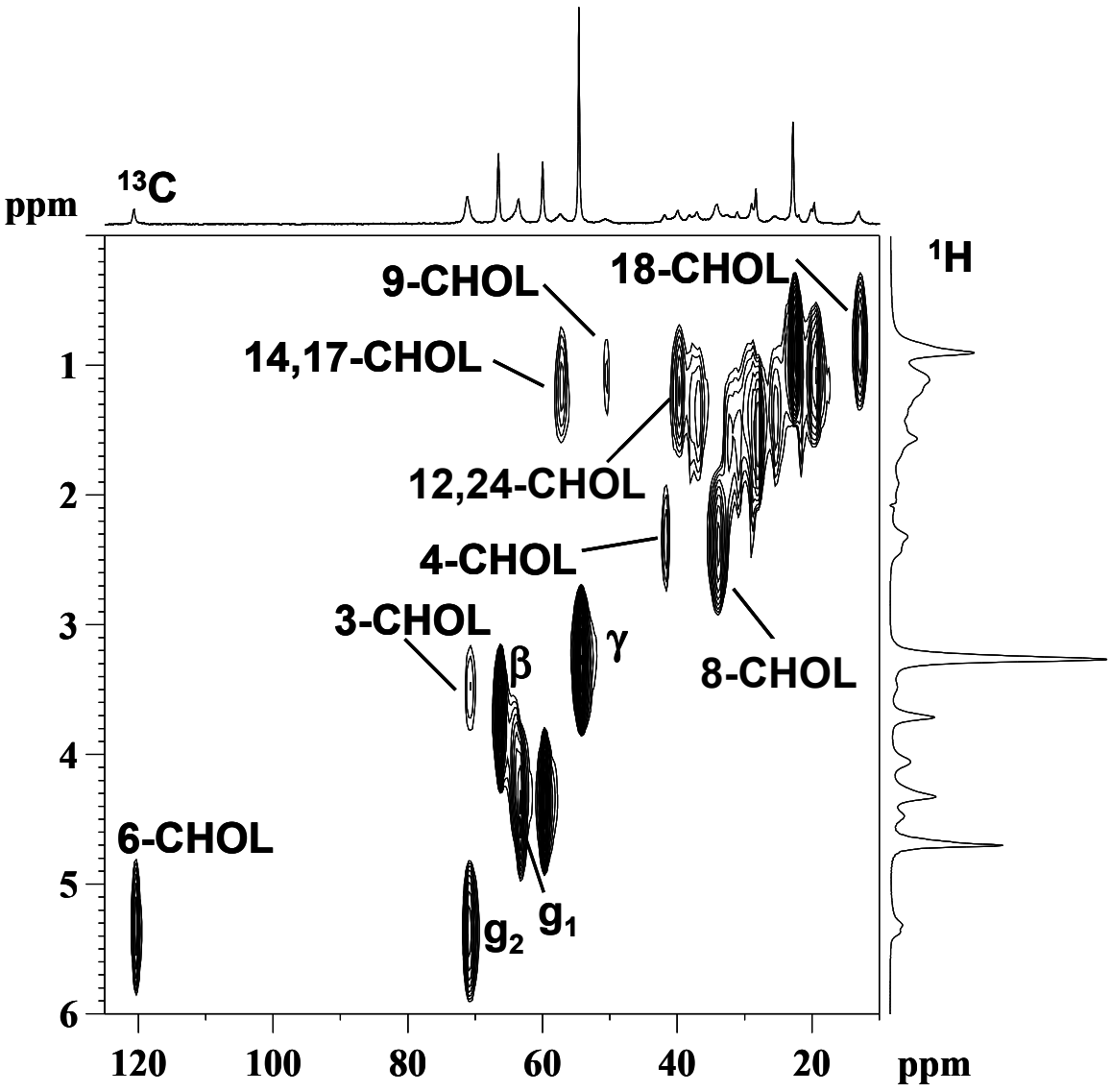

Figure 2.6. The 2D ^{1}H-^{13}C INEPT MAS NMR correlation spectra for DMPC-d_{54}/CHOL obtained using the rotor-synchronized pulse sequence in **Figure 2.1** at ν_R = 10 kHz, 313K, τ_{mix} = 1 ms, Δ_1 = 2.2 ms and Δ_2 = 1.2 ms. The undeuterated DMPC headgroup resonances and selective cholesterol assignments are shown. The ^{13}C and ^{1}H projections are the 1D ^{1}H-^{13}C INEPT MAS and the 1D ^{1}H MAS NMR spectra, respectively. The low resolution in the F1 (^{1}H) dimension results from the reduced number of t_1 increments used in order to reduce experimental time.

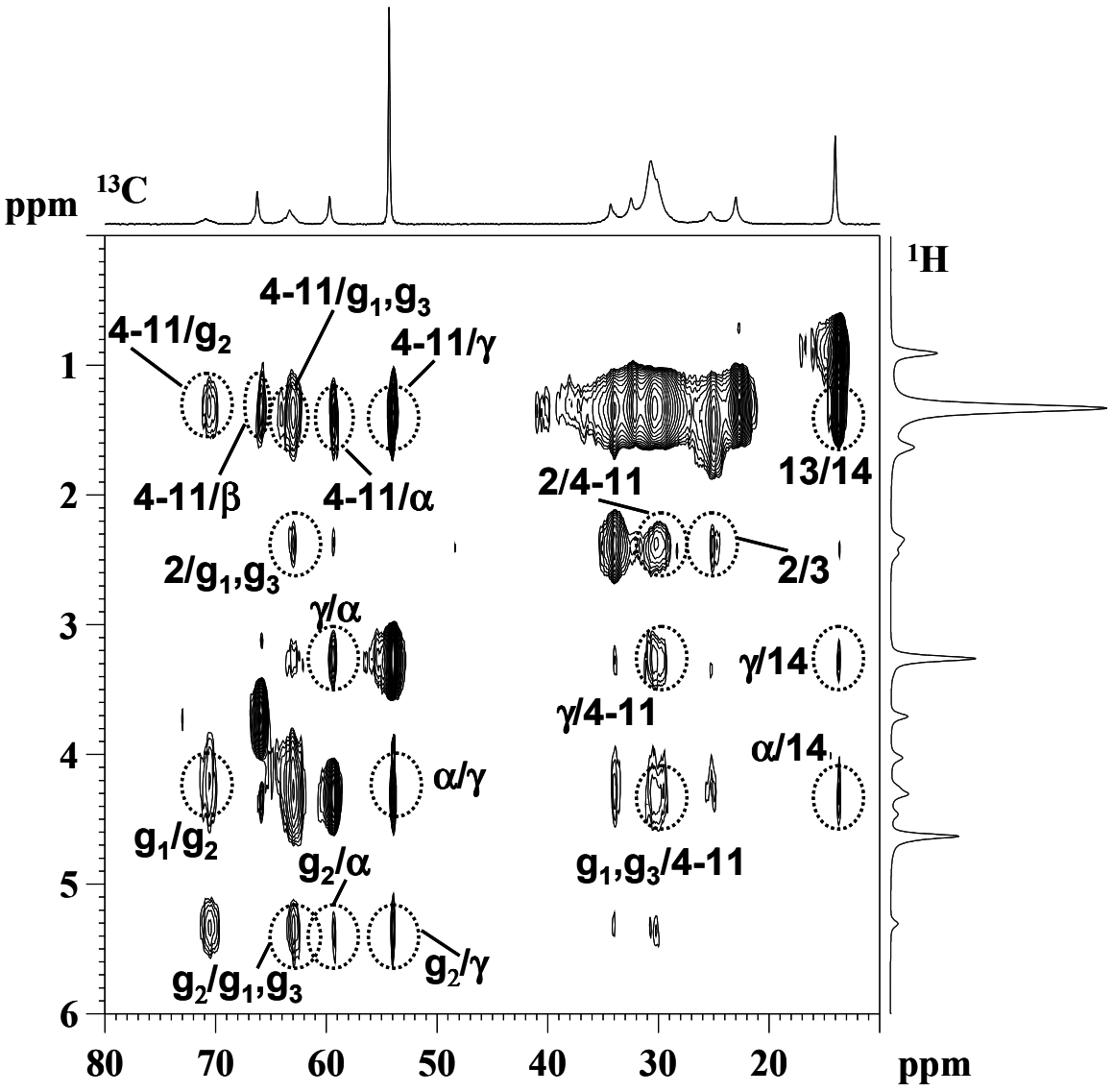

Figure. 2.7. The 2D ^{1}H-^{13}C INEPT MAS NMR correlation spectra for DMPC obtained using the rotor-synchronized pulse sequence in **Figure 2.1** at ν_R = 7.5 kHz, 308K, τ_{mix} = 300 ms, Δ_1 = 2.1 ms and Δ_2 = 0.67 ms. Selective correlation cross peaks arising from ^{1}H-^{1}H magnetization exchange are labeled. See **Figure 2.5** for assignment of standard one-bond ^{1}H-^{13}C correlations.

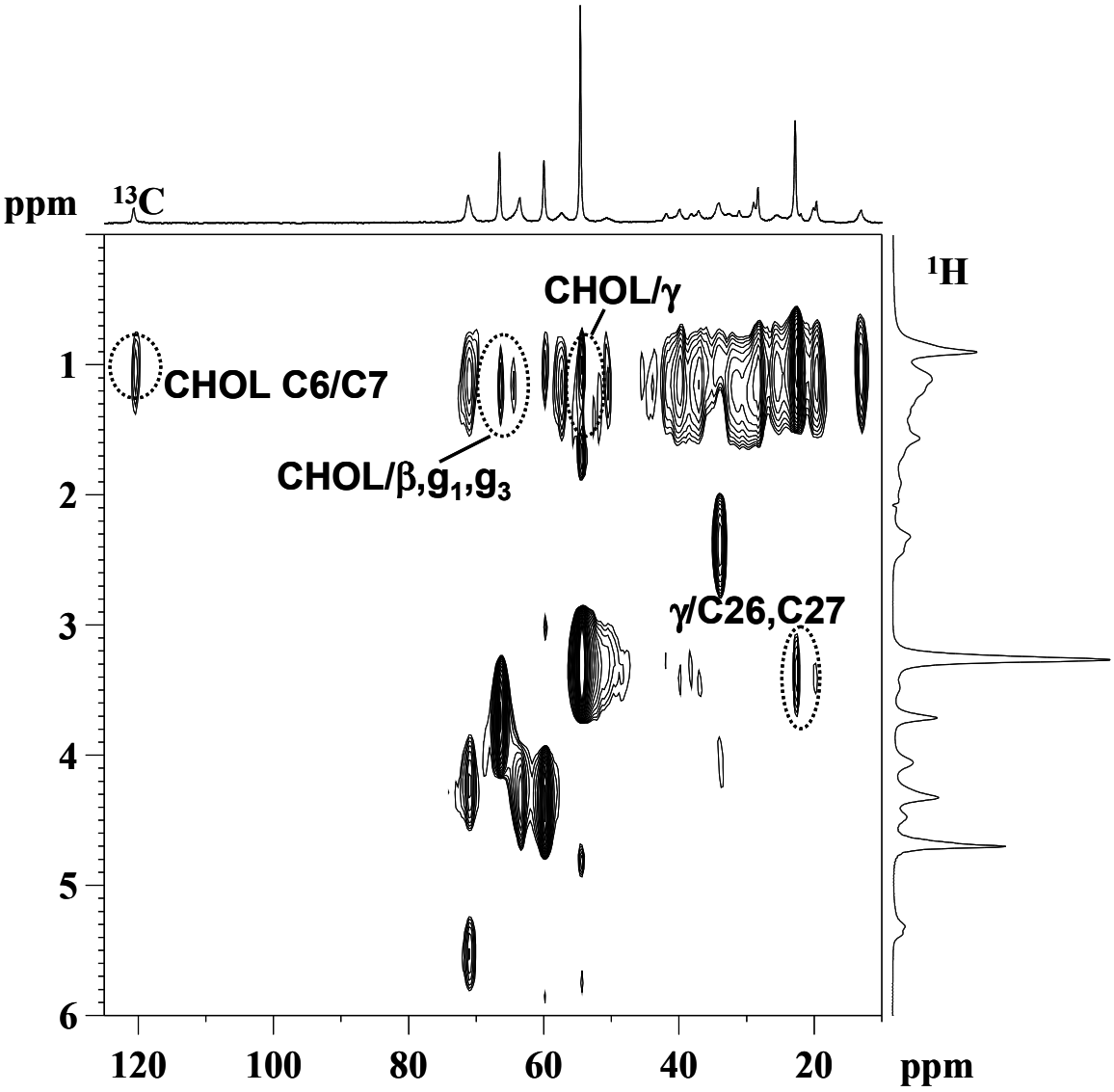

Figure 2.8. The 2D ^{1}H-^{13}C INEPT MAS NMR correlation spectra for DMPC-d_{54}/CHOL obtained using the rotor-synchronized pulse sequence in **Figure 2.1** at ν_R = 10 kHz, 313K, τ_{mix} = 250 ms, Δ_1 = 2.2 ms and Δ_2 = 1.2 ms. Selective cholesterol/lipid correlation cross peaks arising from ^{1}H-^{1}H magnetization exchange are labeled. See **Figure 2.6** for assignment of standard one-bond ^{1}H-^{13}C correlations.

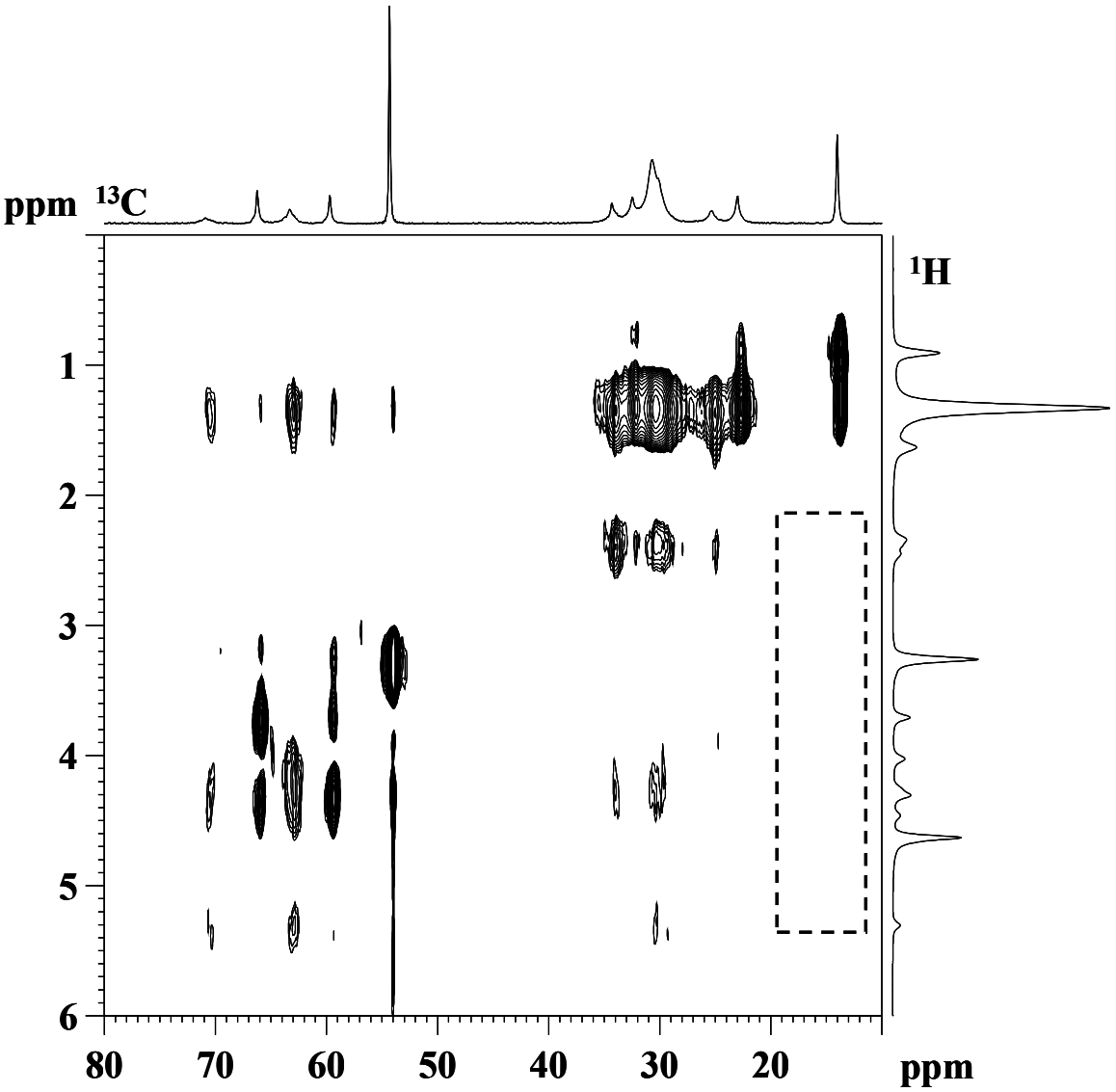

Figure 2.9. The 2D ^{1}H-^{13}C INEPT MAS NMR correlation spectra at ν_R = 7.5 kHz, 308K with RFDR mixing for (a) DMPC at τ_{mix} = 53.3 ms (50 XY-8 recoupling cycles), Δ_1 = 2.1 ms and Δ_2 = 0.67 ms, and for (b) DMPC-d_{54}/Chol at τ_{mix} = 26.7 ms (25 XY-8 recoupling cycles), Δ_1 = 2.1 ms and Δ_2 = 1.2 ms. The dashed boxes and circles mark either missing long range lipid-lipid or cholesterol-lipid ^{1}H-^{1}H magnetization exchange contacts observed in **Figure 2.7** and **Figure 2.8**.

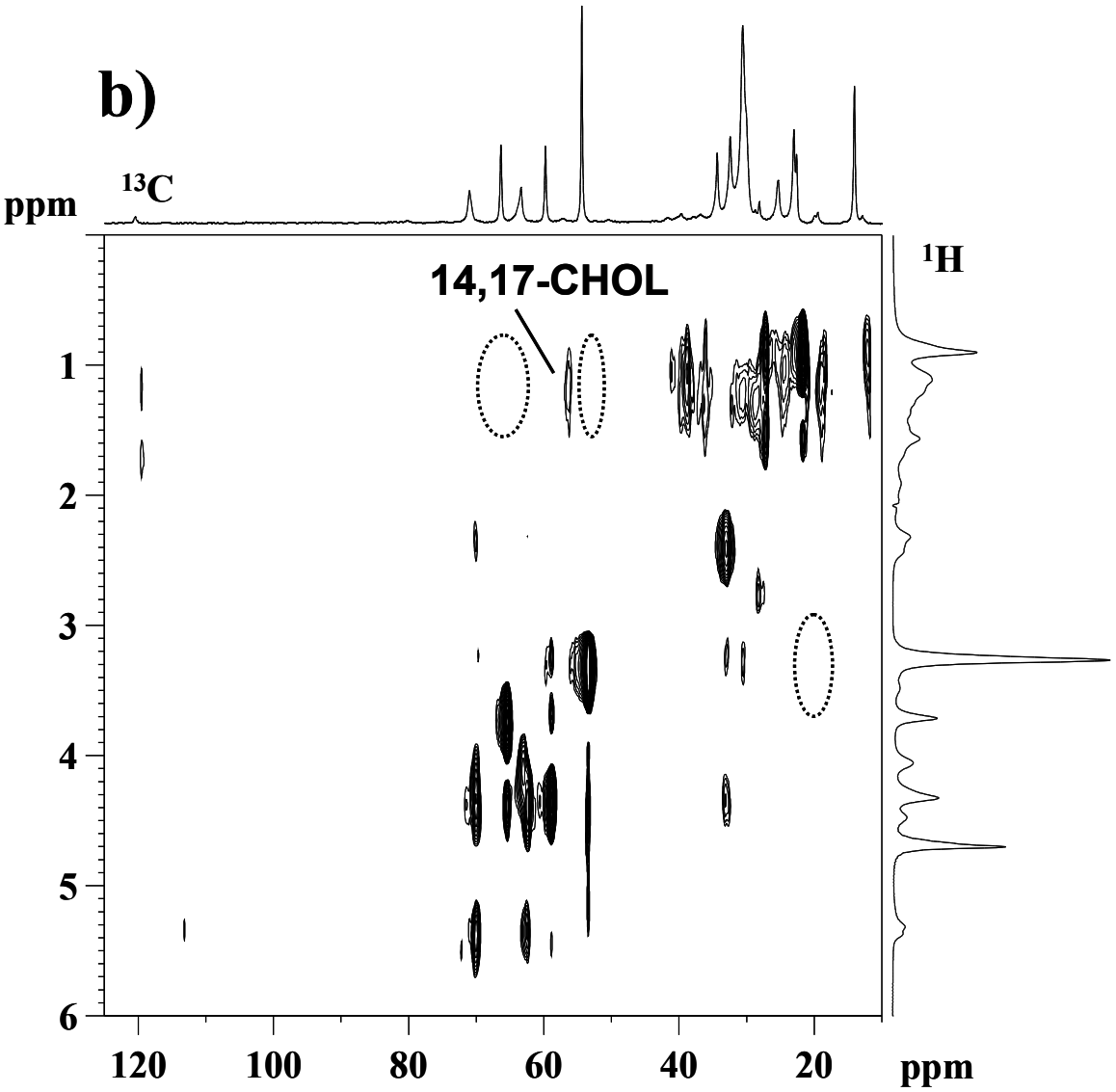

Figure 2.9b.

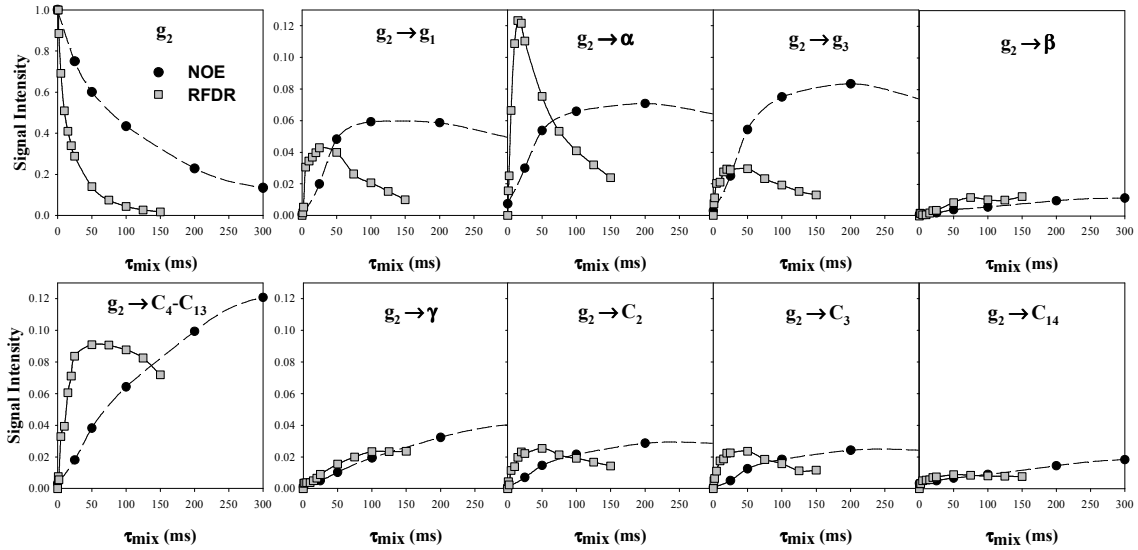

Figure 2.10. Selected normalized ^{1}H-^{1}H cross peak intensity for the glycerol g_2 proton to other lipid protons obtained from the 2D ^{1}H-^{1}H NOESY MAS NMR experiments with NOE cross-relaxation or RFDR recoupling during τ_{mix} for DMPC at 308 K. The cross peaks were normalized to the total intensity of the g_2 diagonal resonance at τ_{mix} = 0.

This Page Left Intentionally Blank

Chapter 3

Multi-Dimensional ^{1}H-^{13}C HETCOR and FSLG-HETCOR NMR Study of Sphingomyelin Bilayers Containing Cholesterol in the Gel and Liquid Crystalline States

3.1 Introduction of FSLG MAS NMR in Membranes

^{1}H magic angle spinning (MAS) and ^{13}C cross-polarization (CP-)MAS NMR spectroscopy are powerful tools for studying molecular level structure and dynamics in multilamellar vesicles (MLV's) and have been implemented in the lipid community for decades. A significant number of ^{1}H and ^{13}C NMR studies regarding the interaction of cholesterol in glycerophospholipid bilayers have appeared [47, 48, 50, 79, 98-101]. Significantly fewer NMR studies have appeared on SM [102, 103] and SM/Chol [104-106] bilayer systems. All of these studies focus primarily on the L_{α} phase due to the improved resolution observed compared to the L_{β} gel phase particularly, in ^{1}H MAS NMR spectra [47].

Most of the ^{1}H and ^{13}C NMR studies of lipid membranes that have appeared in the literature on MLV's are one-dimensional (1D) studies, although some two-dimensional (2D) ^{1}H NOESY [51, 52, 57], $^{1}H/^{31}P$ heteronuclear correlation (HETCOR) [107], and $^{1}H/^{13}C$ HETCOR [46, 65] studies have emerged. More recently 2D studies involving cholesterol containing dimyristoylphosphatidylcholine (DMPC) bilayers have also appeared [45, 62, 70, 71]. Similar to the majority of the 1D studies all these 2D studies have been limited solely to the L_{α} phase (above T_m). A better understanding of lipid cholesterol organization and sterol-lipid interactions will come from going to multi-dimensional experiments below T_m where dipolar interactions are stronger (due to reduced molecular motions) and contacts between the lipid and cholesterol can potentially be detected. In the present study, ^{1}H MAS and ^{13}C CP-MAS NMR spectra are obtained for pure SM bilayers and those containing cholesterol above and below T_m. Conventional 2D dipolar $^{1}H/^{13}C$ HETCOR on SM yield high resolution spectra above T_m, while below T_m high resolution type spectra are only observed when frequency switched Lee-Goldburg (FSLG) ^{1}H homonuclear decoupling is implemented during the evolution period [108, 109]. The isotropic chemical shifts of SM and cholesterol incorporated in SM

bilayers are reported and comparisons are made to the chemical shifts observed for cholesterol in DMPC bilayers [71].

3.2 FSLG MAS NMR Experimental

3.2.1 Materials

Egg sphingomyelin (SM) and cholesterol (Chol) were purchased from Avanti Polar Lipids (Alabaster, AL) and used as received. The SM had the following acyl chain composition: 84% 16:0, 6% 18:0, 2% 20:0, 4% 22:0, 4% 24:0 and contained no unsaturated acyl chains.

3.2.2 Sample Preparation

Pure lipid samples were prepared by mixing the lipid with de-ionized water or D_2O in a conical vial with a vortex mixer. This was followed by a minimum of 5 freeze-thaw cycles in dry ice and a warm water bath set to 60 ºC (above T_m for SM). Buffer was not used in any of the lipid mixtures. Samples containing cholesterol were first combined and dissolved in chloroform followed by vacuum drying overnight to remove the solvent. The samples were then hydrated with the above procedure. The samples are MLV's greater than 1 μm in diameter as confirmed by ^{31}P static NMR (data not shown). All lipid samples were 33 wt% phospholipid (67 wt% H_2O). The binary cholesterol-containing sample was 33 mol% cholesterol. The lipid samples were transferred to 4 mm zirconia MAS rotors and sealed with kel-F inserts and caps. The typical volume of MLV sample for NMR analysis was 50-100 μL corresponding to 25-50 mg of phospholipid. The samples were stored in a -20 ºC freezer when NMR experiments were not being performed.

3.2.3 NMR Spectroscopy

^1H MAS and ^{13}C CP-MAS NMR spectra were collected on a Bruker Avance 400 spectrometer equipped with a 4 mm broadband double resonance MAS probe. The MAS speed (ν_R) was set to 10 kHz and controlled to ± 1 Hz in all MAS experiments with a Bruker MAS control unit. The ^1H spectra were collected with a 2.5 μs π/2 and a 10 s recycle delay. The ^1H spectra were referenced to TMS (δ = 0) by setting the SM methyl resonance (H16´, H18) to 0.9 ppm [102]. The 1D ^{13}C CP-MAS experiments utilized a 4

μs ^{1}H π/2 and a 2 ms contact time. The 1D CP pulse sequence implemented a ramped (50→100%) spin-lock pulse on the ^{1}H channel and a square contact pulse on the ^{13}C channel [110]. 2D dipolar HETCOR experiments were performed to correlate ^{13}C and ^{1}H chemical shifts. This experiment is analogous to the wideline separation (WISE) experiment previously described by Schmidt-Rohr et al. with the exception that it is performed at a higher MAS speed [111]. These increased MAS speeds are known to enhance the resolution in the ^{1}H dimension [112]. HETCOR experiments with Lee-Goldburg (LG) ^{1}H homonuclear decoupling [108] were performed as previously described [109, 113] where FSLG decoupling is applied during the t_1 evolution period. The LG ^{1}H homonuclear decoupling implemented in these experiments is analogous to the flip-flop LG (FFLG) previously described by Mehring and Waugh where a frequency shift was utilized to achieve an effective field along the magic angle. In the FSLG HETCOR experiment a LG-CP condition was used for ^{1}H→^{13}C polarization transfer. The ^{1}H dimension required the theoretical scaling factor cosθ = $1/\sqrt{3}$ in the FSLG-HETCOR spectra [109]. A moderate power ^{1}H two pulse phase modulation (TPPM) decoupling field strength of 62.5 kHz was implemented during acquisition of the free induction decay in all ^{13}C detected experiments using a 15º phase shift [114]. The FSLG homonuclear decoupling field strength was also 62.5 kHz. The pulse sequences for dipolar HETCOR and FSLG-HETCOR are depicted in **Figure 3.1**. Typical acquisition parameters for 2D experiments were 256 or 512 scan averages and 64 or 128 t_1 points. A recycle delay of 5 s and 2 s was utilized in the 1D and 2D ^{13}C detected experiments, respectively. The isotropic ^{13}C chemical shift was set using a secondary reference of solid glycine (carbonyl δ = 176.03 ppm with respect to TMS δ = 0 ppm). The temperature was controlled to ± 0.2 K with a Bruker VT unit. The actual sample temperature does not correlate with the set sample temperature due to heating effects caused by MAS and decoupling. The actual sample temperature was calibrated as described previously where the chemical shift of the ^{1}H water resonance in the lipid sample is monitored under MAS and decoupling conditions [73]. The heating effect of MAS at 10 kHz and ^{1}H decoupling at 62.5 kHz for ~ 30 ms was found to be 7 °C and 9 °C, respectively. These heating effects are accounted for in all experiments reported in this paper. These heating effects can result in modest membrane dehydration that can be ignored for most applications [39]. Assignments of SM resonances were based on previous sphingolipid NMR studies [102, 115, 116]. Some additional assignments not made previously could be made by examining the 2D HETCOR spectra. The cholesterol resonances observed

in SM bilayer samples were assigned based off a previous study on cholesterol in DMPC bilayers [71]. The full width at half maximum (FWHM) or line width was extracted by fitting the resonances in the DMFIT software package [117]. The structure of SM and cholesterol are depicted in **Figure 3.2** with the nomenclature.

3.3. FSLG MAS NMR Results and Discussion

3.3.1 1D ^{1}H MAS NMR of SM Bilayers Containing Cholesterol

The ^{1}H MAS NMR spectra of SM and SM/Chol samples collected at 325 K are displayed in **Figure 3.3**. This temperature is above T_m (~ 40 °C) hence, SM is in the L_α liquid crystalline phase [118]. Both the SM/Chol (A) and the pure SM sample (B) display sharp resonances that can be assigned to SM protons (see **Table 3.1**) based on previous ^{1}H MAS NMR studies on SM bilayers [102]. Narrow ^{1}H line widths are observed in the L_α phase compared to the line widths expected in a rigid organic solid. These narrower line widths can be attributed to rapid lipid lateral diffusion, fast axial rotation about the bilayer normal, and *trans*/*gauche* isomerizations that significantly reduce the inter- and intramolecular ^{1}H-^{1}H dipole-dipole interactions [47, 48, 50]. The line widths of the cholesterol containing sample are slightly broader, FWHM = 60 Hz for SM/Chol compared to 46 Hz for SM measured at the $(CH_2)_n$ resonance. The slightly broader line widths in the cholesterol-containing sample can be attributed to a more restricted mobility of the saturated lipid chain caused by packing with cholesterol. This hinders some of the axial rotation and *trans*/*gauche* isomerizations that average the ^{1}H dipole-dipole interactions. This is consistent with previous ^{2}H static NMR studies on phospholipid/cholesterol mixtures above T_m where a larger ^{2}H quadrupole splitting was observed when cholesterol was incorporated in the bilayer. This was attributed to a decrease in chain mobility with a higher probability of *trans* conformations [119-121]. Since the structural and dynamic characteristics of phospholipid/cholesterol mixtures with significant cholesterol contents (≥25%) are intermediate between the L_β gel and L_α liquid crystalline phase, they have been termed the l_o phase [20, 50, 122]. A higher probability of *trans* conformations was also confirmed by monitoring the ^{13}C chemical shift of the $(CH_2)_n$ resonance of SM in SM/Chol mixtures with ^{13}C CP-MAS NMR (see below).

There are a few ^{1}H resonances observed for SM in the present study that were not resolved in previous ^{1}H MAS NMR spectra of SM bilayers. Particularly, the C4 and

C5, C2′ and C6, and the high ppm shoulder of the main $(CH_2)_n$ resonance that can be assigned to C3′ [102]. The assignment of these peaks was assisted by 2D dipolar HETCOR spectra discussed below. The lower resolution in the latter study can be attributed to the lower spectrometer field and slower MAS speed utilized. It should also be noted that no specific cholesterol peaks are resolved in ^{1}H MAS NMR spectra indicating a need for ^{13}C-detected NMR experiments to increase chemical shift dispersion and detect cholesterol resonances. The reason for the lack of resolved cholesterol resonances in the ^{1}H MAS NMR spectrum is attributed to the tight chemical shift range (0.5 – 2.5 ppm) and broad line widths.

The ^{1}H MAS NMR spectra of SM and SM/Chol samples at 301 K are displayed in **Figure 3.4**. At this temperature SM is below T_m and exists in the L_β gel state. Even at 10 kHz MAS the main acyl chain ^{1}H resonance is broad (FWHM = 1.3 kHz), and only the α, β, and γ resonances of the headgroup are resolved. More rapid MAS speeds could not be pursued due to a centrifugal effect where the water begins to separate from the lipid. These types of problems can result in lipid dehydration and have been discussed previously [39, 123]. The poor resolution observed in the L_β phase is due to the ^{1}H-^{1}H homonuclear dipolar coupling and has been discussed previously for phospholipids in the gel state [47]. The tight acyl chain packing and interdigitation in the L_β gel phase results in a decrease in the chain mobility that dynamically averages the ^{1}H homonuclear dipole-dipole coupling in the case of the L_α liquid crystalline phase discussed above. When cholesterol is incorporated in the bilayer the acyl chain packing and interdigitation is reduced and the fluidity of the bilayer is increased [124]. This results in a narrowing of the ^{1}H line widths, specifically for the $(CH_2)_n$ resonance, where the FWHM = 1.3 kHz in the pure SM sample compared to 400 Hz for SM/Chol. This shows that when cholesterol is in contact with the saturated chains of SM it causes an increase in chain mobility and decrease in *trans* conformations below T_m. Thus, cholesterol has the opposite effect on SM above and below T_m. Above T_m cholesterol presence decreases chain mobility (increases order) and below T_m it increases chain mobility (decreases order) compared to pure SM. This is consistent with previous interpretations from ^{13}C MAS NMR on SM/Chol and dipalmitoylphosphatidylcholine (DPPC)/Chol bilayers where the chemical shift of the $(CH_2)_n$ ^{13}C resonance is indicative of the amount of mobile *gauche* conformers present [47, 79, 104]. These results also agree with the early static ^{1}H NMR and ESR work of Olfield et al. on SM dispersions containing cholesterol [119, 125].

3.3.2 1D ^{13}C CP-MAS NMR of SM Bilayers Containing Cholesterol

The 1D ^{13}C CP-MAS NMR spectra of SM bilayers containing cholesterol below T_m are displayed in **Figure 3.5**. Numerous resonances are resolved that can be assigned to SM and cholesterol (see **Tables 3.2** and **3.3**). The subscript c denotes cholesterol resonances. The presence of cholesterol in the bilayer results in a sharpening of many of the SM ^{13}C NMR resonances. This is particularly evident for C18/C16´, C17/C15´, $(CH_2)_n$, C3, and C3´ resonances, emphasizing the impact of cholesterol on the sphingosine backbone and saturated chain region of the lipid. The resonances of the acyl chain display chemical shifts to lower ppm in the cholesterol-containing sample. This can be attributed to an increase in *gauche* conformations as discussed previously in SM/Chol bilayers [104] and mentioned in the previous section with respect to the ^1H line width. The $(CH_2)_n$, C3´, C17/C15´resonances shift downfield 0.3, 0.3, and 0.5 ppm with incorporation of cholesterol, respectively. The larger shift observed for the C17/C15´ resonance could potentially indicate a greater degree of induced chain mobility and disorder towards the end of the saturated chain when cholesterol is present in SM below T_m. The headgroup resonances: C_γ, C_α, and C_β display consistent chemical shifts and line widths when cholesterol is present. However, a slight decrease in CP efficiency is observed for these resonances indicating a decrease in the C-H dipolar coupling. This is not surprising considering ^{31}P static NMR results on SM/Chol bilayers below T_m showed that axial headgroup rotations were similar to that occurring in the L_α phase of SM [126]. It is likely that these headgroup motions, which average the ^{31}P chemical shift anisotropy, could potentially dynamically average the C-H coupling. An increase in mobility of the headgroup region is also consistent with the ^1H results where slightly sharper ^1H headgroup resonances were observed in SM/Chol sample compared to the pure SM sample. The carbonyl resonance, C1´, displays a 0.2 ppm shift downfield when cholesterol is present. This has been attributed to a change in the hydrogen bonding environment at the carbonyl site in previous studies on phospholipid/cholesterol mixtures [79, 104]. It appears that a change in water hydrogen bonding is the more probable explanation for this shift rather than a direct hydrogen bond with the OH of cholesterol [104, 105].

The ^{13}C CP-MAS spectra of SM and SM/Chol bilayers above T_m are presented in **Figure 3.6**. Comparison of the spectrum obtained for SM in the L_α phase (**Figure 3.6B, D**) to the one obtained on the L_β phase (**Figure 3.5B, D**) reveals significantly sharper

lines in the L_α phase. The acyl chain resonances: $(CH_2)_n$, C17/C15′, C3′, C6, and C16/C14′ sharpen substantially and large upfield shifts are observed between 1-2 ppm. Again, this is consistent with an increase in chain mobility and fraction of *gauche* conformers in the L_α phase compared to the primarily *trans* L_β phase. Note, C16/C14′ and C6 are not well resolved in the L_β phase of SM without cholesterol but, are clearly observed in the $L_{\square}$ phase due to the chemical shifts of the saturated acyl chain groups. These groups are assigned based on liquid state NMR sphingomyelin studies [116] and dipolar HETCOR experiments discussed below. The C4 and C5 double bond groups also display a significant sharpening in both SM and SM/Chol in comparison to the SM L_β phase indicating an increased mobility at these sites as well.

When comparing the SM/Chol ^{13}C CP-MAS spectrum to the SM spectrum above T_m some noticeable differences are observed (**Figure 3.6**). Particularly, the $(CH_2)_n$ main chain resonance is shifted to higher ppm and broadens slightly in the cholesterol-containing sample (see **Figure 3.6C, D**). The shift reflects a higher amount of *trans* conformations (more ordered) for the cholesterol containing sample in agreement with previous ^2H results on other saturated chain phospholipids above T_m [20, 119, 121]. The ^{13}C chemical shifts of the main chain $(CH_2)_n$ observed in SM and SM/Chol bilayers can be summarized: 32.5, 32.2, 31.5, and 30.5 ppm for SM L_β, SM/Chol below T_m, SM/Chol above T_m, and SM L_α, respectively. The ^{13}C chemical shift to lower ppm with cholesterol and measurements performed below and above T_m in these samples indicates a decrease in order and increase in mobility. The other noticeable difference in the ^{13}C spectrum is the significant sharpening of the C3 resonance when cholesterol is present. The C3 resonance has a FWHM = 113, 66, 49, and 37 Hz in SM L_β, SM L_α, SM/Chol above T_m, and SM/Chol below Tm, respectively. This shows that the sharpening of the C3 resonance is observed regardless of whether the sample is above or below T_m when cholesterol is present (compare **Figure 3.5A** and **3.5B** and **Figure 3.6A** and **3.6B**). This indicates that the mobility at this site is increased both above and below T_m when cholesterol is incorporated in the bilayer. An increased mobility for this site below T_m is not particularly surprising since, the fluidity of the bilayer increases and sharpening of the ^{13}C resonances is observed at many of the sites in SM/Chol. However, a sharpening of the C3 resonance above T_m is somewhat surprising at first since, the acyl chain becomes more ordered and the bilayer less fluid when cholesterol is present. One explanation for this is that cholesterol disturbs the hydrogen-bonding environment at the C3 hydroxyl group causing a decrease in the rigidity of this site. This hydroxyl group has

been postulated to participate in intermolecular and intramolecular hydrogen bonding with neighboring SM molecules at the amide and the oxygen groups of the phosphate, respectively [127]. The potential formation of water bridges between SM molecules has also been discussed [128]. This idea that cholesterol disrupts some of these hydrogen bonding motifs at the SM-water interface is in agreement with some previous X-ray diffraction results where a reduction in the inter-bilayer water thickness was reported [129, 130]. The increased mobility of this site could be a strong indicator that some of these hydrogen bonding environments at the C3 hydroxyl are disrupted by the incorporation of cholesterol regardless of whether the sample is above or below T_m. It should also be noted that when comparing the FWHM of SM/Chol above and below T_m, the line width below T_m is sharper. This probably does not indicate a higher degree of mobility below T_m at this site but, rather an increase in sample homogeneity.

3.3.3 2D ^{1}H-^{13}C Dipolar HETCOR NMR of SM and SM/Chol Bilayers

The 2D ^{1}H/^{13}C dipolar HETCOR spectra of SM bilayers in the L_β and L_α phases are presented in **Figure 3.7**. In the L_β phase (**Figure 3.7A**), the ^{1}H line widths are broad and the resolution is poor while, the L_α phase (**Figure 3.7B**) displays excellent resolution and chemical shift dispersion in both the ^{13}C and ^{1}H dimensions. The 2D HETCOR spectrum collected in the L_α phase was utilized to distinguish and assign the C6 and C16/C14´ ^{13}C resonances. It was also helpful in assigning the high ppm shoulder in the ^{1}H MAS spectrum (**Figure 3.3**) to H3´. Further, the HETCOR spectrum confirms that the ^{13}C resonance observed at 54.3 ppm is indeed an overlap of both the Cγ and C2 environments as previously proposed [102]. The ^{1}H chemical shifts of these two groups are distinct and as a result the single ^{13}C resonance is separated into two peaks in the ^{1}H dimension at the expected ^{1}H chemical shifts. It is also interesting to note that the ^{1}H correlation peak for the ^{13}C carbonyl (C1´) resonance is H2´. The carbonyl site has no directly bonded protons and the neighboring protons at C2´ site are responsible for cross polarizing the carbonyl carbon. These results show the advantage of going to multi-dimensional correlation NMR experiments in these complex lipid systems to assist in chemical shift assignment and increase resolution.

The HETCOR spectrum of SM obtained in the L_β phase (**Figure 3.7A**) displays broad resonance lines in the ^{1}H dimension as a result of the strong ^{1}H-^{1}H dipolar interactions that are not completely averaged by the combination of lipid mobility and MAS. Recently, the utilization of FSLG ^{1}H homonuclear decoupling in conjunction with

^{13}C detected dipolar HETCOR experiments has been presented in organic solids and resulted in well resolved resonances in the ^{1}H dimension [109]. This experiment was performed and is displayed in **Figure 3.7C**. The ^{1}H dimension clearly displays improved line widths compared to the conventional dipolar HETCOR spectrum (see **Figure 3.7B**). The ^{1}H line width in the FSLG-HETCOR spectrum is ~ 430 Hz compared to the line width in the conventional HETCOR experiment (L_β phase) where it was ~ 1.7 kHz measured at the $(CH_2)_n$. This shows that the FSLG technique should be successful in the study of gel phase lipids although, the resolution is not nearly as good as observed in the L_α phase. When comparing the FSLG spectrum with the conventional HETCOR spectrum it should also be noted that the signal to noise (S/N) in the FSLG-HETCOR is lower and headgroup resonances 1, 2, and 3 are not observed. This is due to the efficiency of the LG-CP transfer which is lower than the traditional CP transfer implemented in the conventional dipolar HETCOR spectrum shown in **Figure 3.7A** [131]. The breadth of these resonances in both the ^{13}C and ^{1}H dimensions make them difficult to observe. The FSLG technique does not improve the observed ^{1}H resolution when applied above T_m in SM or SM/Chol and below T_m in SM/Chol. In the latter case, the chain mobility induced by cholesterol presence approaches the line widths obtained with FSLG and no additional improvement in resolution was observed. This is in agreement with previous results where MREV-8 ^{1}H homonuclear decoupling did not improve the resolution in 2D dipolar HETCOR spectra of DMPC/Chol bilayers above T_m at similar MAS speeds [45]. The results presented here strongly indicate that ^{1}H homonuclear decoupling is not a requirement in lipid bilayers below T_m when significant amounts of cholesterol are present, however significant improvement will likely be observed in pure lipids in the gel phase as indicated by the results presented for SM in **Figure 3.7C**.

The 2D dipolar HETCOR spectra for SM/Chol above and below T_m are depicted **Figures 3.8A** and **3.8B**, respectively. As discussed above application of FSLG during the t_1 evolution period did not improve the resolution in the ^{1}H dimension thus, the spectra presented here were generated with the conventional 2D dipolar HETCOR technique. Below T_m, similar line widths are observed for SM/Chol (**Figure 8A**) in comparison to the FSLG experiment on pure SM (**Figure 7C**). This is likely the reason why no additional improvement was observed when implementing FSLG. Above T_m, line widths close to the ones observed in pure L_α SM are observed (compare to **Figure 7B**). All the observed resonances are assignable to SM and cholesterol groups. There is a decrease in intensity of the cholesterol resonances compared to the HETCOR spectrum

collected below T_m that should be mentioned. Specifically, cholesterol resonances 5^c and 6^c are not observed. This is attributed to the increased mobility above T_m that decreases the C-H dipolar coupling and hence the CP efficiency. In the 1D ^{13}C CP-MAS NMR spectrum the loss in S/N above T_m in SM/Chol was not as significant as in the HETCOR spectra. This is attributed to utilization of a longer CP contact time of 2 ms (1 ms in the HETCOR) and a ramped spin-lock pulse in the 1D case. The ramped CP sequence increases the overall S/N [110] and has been shown to be more effective in lipids above T_m than conventional CP [44]. Inclusion of a ramped CP sequence into the HETCOR will likely improve the S/N and overall quality of the 2D spectra.

3.3.4 ^{13}C Cholesterol Chemical Shifts in SM Bilayers

A complete $^1H/^{13}C$ NMR assignment of the cholesterol chemical shifts in L_α DMPC bilayers has recently been reported [71]. The cholesterol resonances observed in this study on SM bilayers were assigned based on that report since they appear at similar chemical shifts (see **Table 3.3**). However, there are some subtle differences that should be noted and discussed. The ^{13}C NMR chemical shift referencing in the previous study was set by assigning the C18 methyl group to 11.84 ppm, the chemical shift observed in the solution NMR spectrum of cholesterol in CCl_4. The chemical shift referencing in this study was based on setting the ^{13}C chemical shift to a secondary standard of glycine. Thus, the chemical shifts reported here are real chemical shifts referenced to TMS. The present results show that the cholesterol shifts in lipid bilayers can differ significantly than those observed in solution NMR studies. For example, the actual chemical shift of the C18 resonance of cholesterol in a SM bilayer below T_m is 12.7 ppm. This chemical shift is 1 ppm downfield with respect to the shift observed in solution NMR where cholesterol is dissolved in CCl_4. The cholesterol ^{13}C chemical shift differences between DMPC/Chol and SM/Chol discussed below accounts for this referencing difference.

The cholesterol ^{13}C chemical shifts observed in SM/Chol bilayers are within 0.0-0.4 ppm when compared with the shifts observed in DMPC/Chol with the exception that the C5 resonance was 0.7 ppm higher in SM/Chol above T_m. The reason for a shift to higher ppm of the C5 resonance in SM/Chol is unknown, but could indicate a difference in how this double bond environment interacts with SM compared to DMPC. A number of the cholesterol ^{13}C chemical shifts in DMPC/Chol were similar to the ones observed here in SM/Chol. Specifically, the C18, C21, C19, C10, C3 and C6 were essentially

identical. This is not surprising for the C18, C21, C19 and C10 environments since these are all methyl resonances and the latter is a quaternary carbon. The observation that the C3 resonance is identical in SM/Chol and DMPC/Chol indicates that the hydrogen bonding interaction at the C3 hydroxyl of cholesterol is probably similar in the two lipids. This is a strong indicator that there is no direct hydrogen bond between the cholesterol hydroxyl group and the lipid interfacial region considering the significant differences between the two lipid backbones (sphingosine in SM and glycerol in DMPC). One explanation for the similarity is that in both systems the hydrogen-bonding partner of the cholesterol C3 hydroxyl is water. It is also interesting to note that the shift of the C6 resonance is identical. The C6 is the other double bond resonance and the fact that it is identical yet the adjacent double bonded C5 is shifted 0.7 ppm downfield in SM/Chol is unknown.

The ^{13}C NMR chemical shifts of the cholesterol ring carbons display shifts to lower ppm between 0.1 and 0.4 ppm compared to DMPC/Chol. The reason for these variations are unknown however, as quantum chemical shift calculations get better the reason for this variability in different lipid/Chol systems should be determinable [132]. The alkyl tail of cholesterol showed some similarities and some differences. The terminal methyls C26/C27 and the C25 methine group were 0.1 ppm lower than in DMPC/Chol while, C24 was identical and C23 and C22 were 0.1 and 0.3 ppm higher, respectively. Assuming exclusively that differences in the CH_2 alkyl groups of cholesterol are due to the amount of *trans*/*gauche* conformers than the higher shifts observed for C23 and C22 carbons can be interpreted to result due to a higher fraction of *trans* conformations and thus a more ordered environment in SM/Chol compared to DMPC/Chol. Further support for this comes from the ^{13}C spectrum of SM/Chol below T_m where the shifts of the C23 and C22 carbons are to even higher ppm (0.5 ppm higher than in DMPC/Chol). Taken together these results indicate a greater degree of order of the alkyl chain in SM/Chol above T_m compared to DMPC/Chol and that this ordering of cholesterol alkyl chain increases in SM/Chol below T_m. If the assumption that the shifts of the CH_2 cholesterol alkyl chain are correct and due to changes in the ratio of *trans*/*gauche* conformers then we can conclude that cholesterol ordering is directly correlated with the ordering of the lipid environment and that the two constituents interact cooperatively.

3.4 FSLG MAS NMR Conclusions

The present chapter gives a full $^{1}H/^{13}C$ NMR assignment for SM/Chol bilayers. 2D dipolar HETCOR NMR experiments aided in the spectral assignment of SM and allowed an expansion on previous assignments. FSLG-HETCOR was presented on a bilayer lipid system for the first time and was shown to significantly improve resolution in the gel state while not being a requirement in the L_α phase or in SM/Chol bilayers below T_m. The ^{1}H line width and the ^{13}C chemical shift of CH_2 resonances are sensitive to the ordering and mobility of the SM saturated chain. The cholesterol ^{13}C chemical shifts show some significant similarities and differences compared to DMPC/Chol. It was shown that the chemical shift of the cholesterol alkyl tail can be used to measure cholesterol ordering. The cholesterol chemical shift variations observed indicate a higher degree of order in SM/Chol bilayers compared to DMPC/Chol bilayers. Other chemical shift differences indicate that the sterol-lipid interaction in SM is different than in DMPC. The NMR techniques presented herein are broadly applicable to sterol-lipid interactions in the context of understanding the lipid raft phenomenon and should also be powerful methods for the study of protein-lipid interactions.

Table 3.1 ^{1}H chemical shifts in ppm of SM extracted from MAS NMR spectrum collected above the T_m (L_α phase) of SM.

Assignment	SM L_a Phase
H18/H16´	0.9
$(CH_2)_n$	1.3
H3´	1.6
H6	2.1
H2´	2.2
Hγ	3.2
Hβ	3.7
H1,2,3	4.1
Hα	4.3
H4	5.5
H5	5.7

Table 3.2. ^{13}C chemical shifts in ppm of SM extracted from CP-MAS NMR spectra of pure SM and SM/Chol bilayers. Spectra were obtained above and below the T_m of SM.

Assignment	SM L_β Phase	SM L_α Phase	SM/Chol l_o Phase (Below T_m)	SM/Chol l_o Phase (Above T_m)
C18/C16´	14.1/14.4	13.8	14.0	13.9
C17/C15´	23.9	22.8	23.4	23.0
C3´	27.5	26.5	27.2	26.9
$(CH_2)_n$[a]	30.8	29.9	30.6	30.6
$(CH_2)_n$[a]	32.5	30.5	32.2	31.5
C16/C14´	33.9	32.2	33.2	32.7
C6	b	33.0	33.8	33.4
C2´	36.9	36.6	36.9	36.8
Cγ/C2	54.3	54.3	54.3	54.4
Cα	59.7	59.6	59.7	59.7
C1	65.4	65.4	65.5	65.4
Cβ	66.2	66.3	66.2	66.3
C3	71.6	71.3	71.2	71.2
C4	130.6	130.3	130.5	130.4
C5	133.2	133.9	133.5	133.7
C1´	174.6	174.6	174.8	174.8

[a] Acyl chain resonances including C4´-C13´/C7-C15.
[b] Not resolved in this phase.

Table 3.3. ^{13}C chemical shifts in ppm of cholesterol extracted from CP-MAS NMR spectra of SM/Chol bilayers. Spectra were obtained above and below the T_m of SM.

Assignment	SM/Chol l_o Phase (Below T_m)	SM/Chol l_o Phase (Above T_m)
C18	12.7	12.5
C21	19.5	19.3
C19	20.0	19.8
C11	21.5	21.5
C26/C27	22.4	22.4
C15	24.9	24.9
C23	25.7	25.3
C25	28.3	28.1
C16	28.7	28.6
C2	31.3	30.6
C7/C8	a	a
C10	36.9	36.8
C20/C22	37.3	37.1
C1	37.9	37.9
C24	39.8	39.7
C12	40.3	40.3
C4	42.1	42.1
C13	42.7	42.7
C9	50.4	50.5
C14/C17	57.0/57.3	57.1/57.3
C3	71.1	71.2
C6	120.6	120.7
C5	141.8	141.7

[a] Not resolved in this phase.

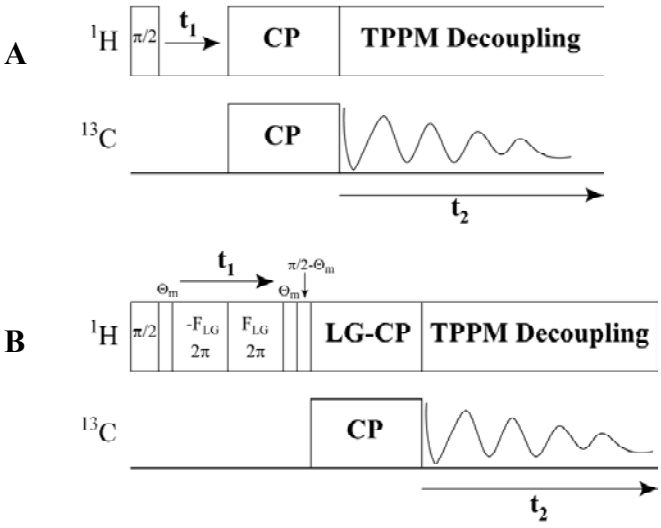

Figure 3.1. 2D NMR pulse sequences for (A) ^{1}H/^{13}C dipolar HETCOR with CP polarization transfer and TPPM decoupling and (B) FSLG-HETCOR with LG-CP polarization transfer and TPPM decoupling (B).

A

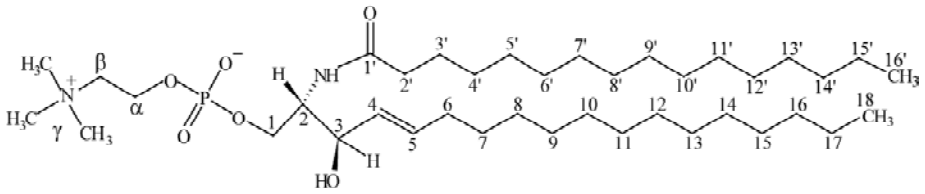

B

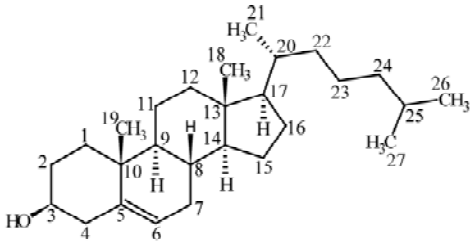

Figure 3.2. The structure of (A) the primary component of egg SM and (B) cholesterol with the numbering nomenclature.

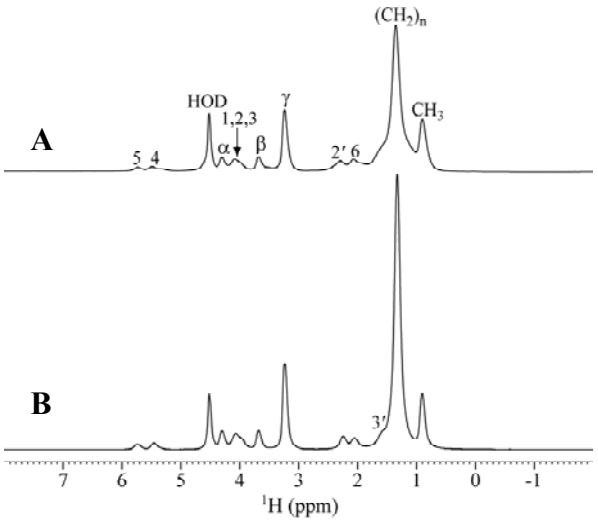

Figure 3.3. ^{1}H MAS NMR spectrum collected at ν_R = 10 kHz and 325 K (above T_m) for (A) SM/Chol and (B) pure SM bilayers.

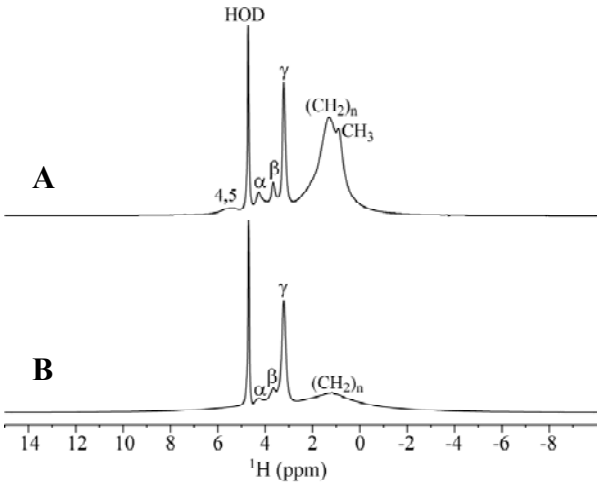

Figure 3.4. ^{1}H MAS NMR spectrum collected at v_R = 10 kHz and 301 K (below T_m) for (A) SM/Chol and (B) pure SM bilayers.

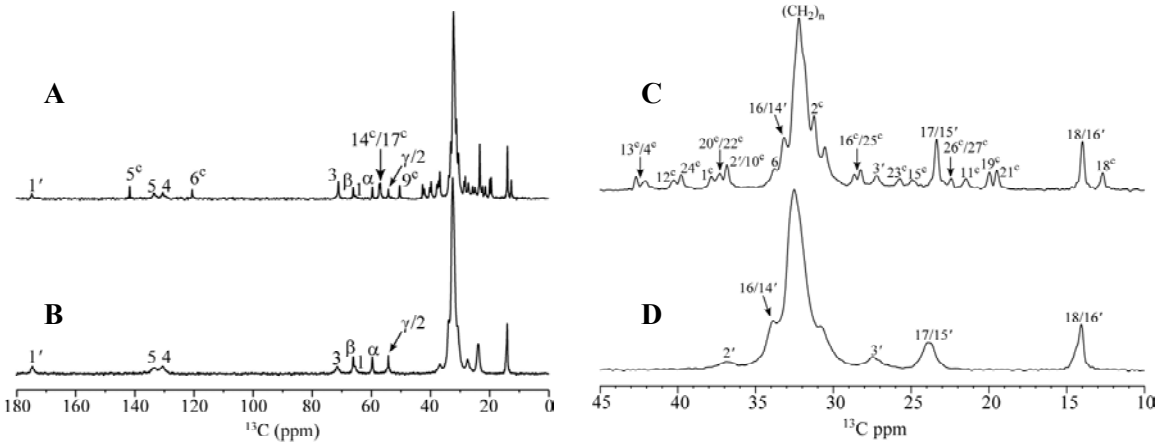

Figure 3.5. ^{13}C CP-MAS NMR spectrum collected with a 2 ms contact time at 310 K (below T_m) for (A) SM/Chol and (B) pure SM bilayers. A blow up of the crowded acyl chain region (10 - 45 ppm) is shown for (C) SM/Chol and (D) SM. The superscript c denotes cholesterol resonances.

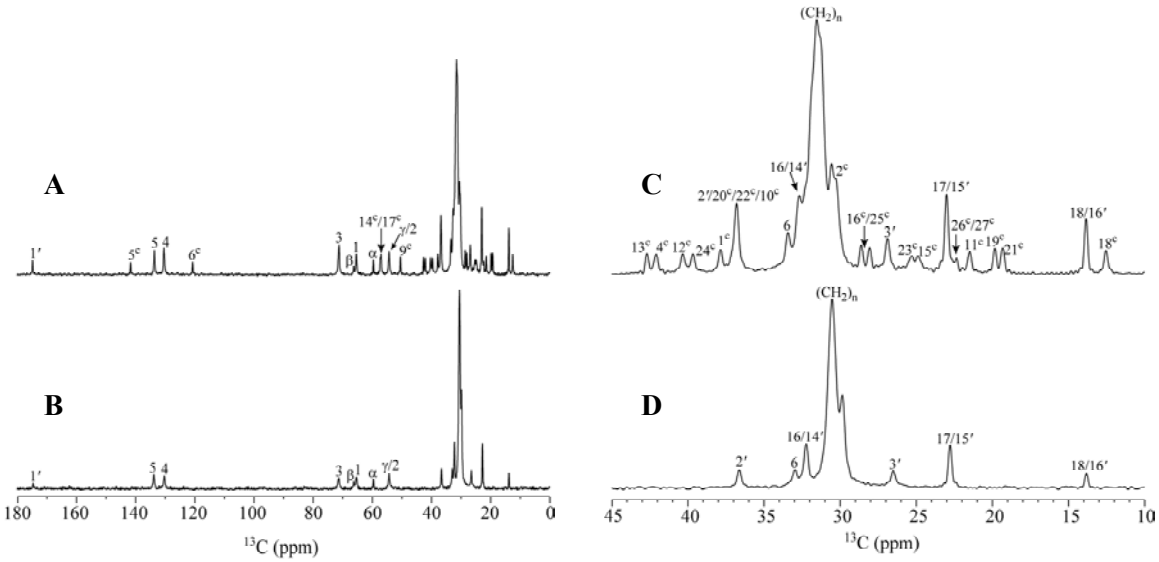

Figure 3.6. ^{13}C CP-MAS NMR spectrum collected with a 2 ms contact time at 334 K (above T_m) for (A) SM/Chol and (B) pure SM bilayers. A blow up of the crowded acyl chain region (10 - 45 ppm) is shown for (C) SM/Chol and (D) SM. The superscript c denotes cholesterol resonances.

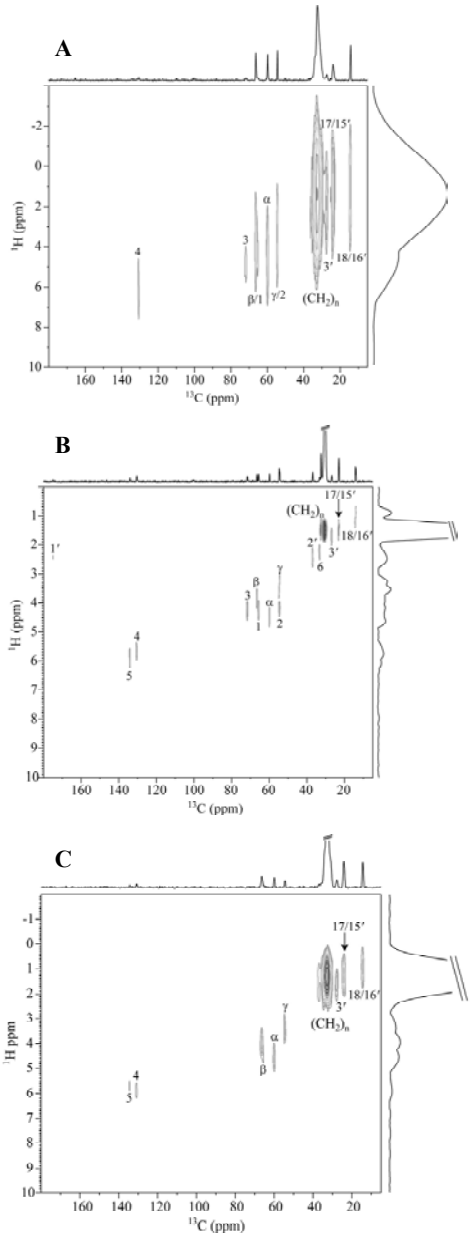

Figure 3.7. 2D ^{1}H/^{13}C dipolar HETCOR NMR spectra with 1 ms contact time for SM at (A) 310 (below T_m) and (B) 334 K (above T_m). 2D ^{1}H/^{13}C FSLG-HETCOR for (C) SM at 310 K (below T_m).

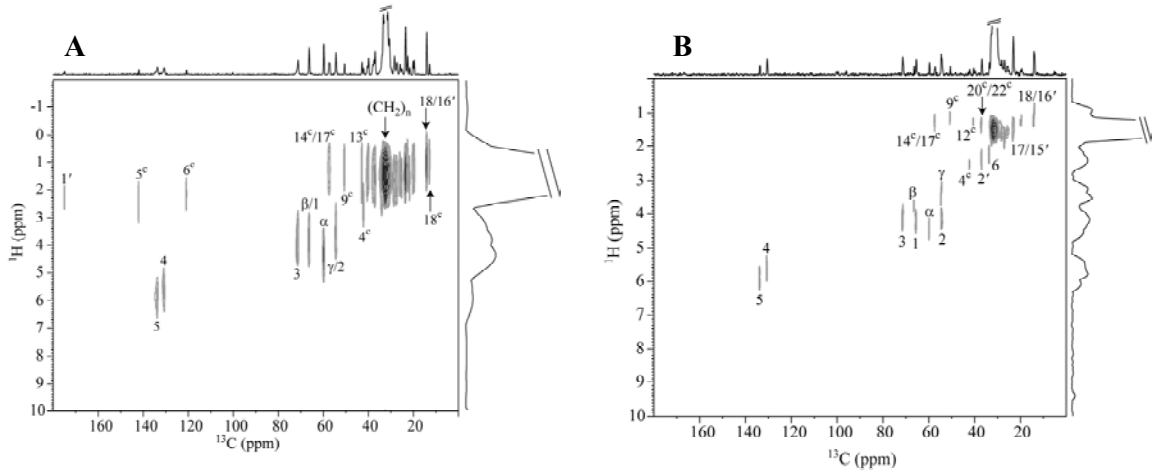

Figure 3.8. 2D ^{1}H/^{13}C dipolar HETCOR NMR spectra with 1 ms contact time for SM/Chol at (A) 310 (below T_m) and (B) 334 K (above T_m). The superscript c denotes cholesterol resonances.

Chapter 4

Distinguishing Individual Lipid Headgroup Mobility and Phase Transitions in Raft Forming Lipid Mixtures with ^{31}P MAS NMR

4.1 Introduction to ^{31}P MAS NMR of Lipid Mixtures

Static ^{31}P NMR has been extensively used for decades to study the structure and dynamics of multi-lamellar vesicles in various phospholipid systems [133-135]. These static NMR experiments produce ^{31}P powder patterns that result solely from the chemical shift anisotropy (CSA) when ^{1}H decoupling is applied. The ^{31}P CSA is sensitive to both headgroup geometry and local dynamics. The phospholipid headgroup conformation can be extracted from the ^{31}P CSA by orienting the membrane with respect to the NMR external magnetic field [136]. Since the CSA interaction is also sensitive to the headgroup dynamics, it has been successfully implemented to determine the types of local motions occurring in the gel (L_β), intermediate ($P_{\beta'}$), and liquid crystalline phases (L_α) of phospholipid membranes [137-139]. The presence of cholesterol [120, 126] and the degree of hydration [136] can greatly impact the CSA and provide insight into the interaction between the phospholipid and other select constituents.

Static ^{31}P NMR has been used to study a limited number of raft forming mixtures [140-143]. This method often suffers due to a lack of resolution resulting from overlapping powder patterns that make determination of the ^{31}P CSA of the individual lipid components difficult [142, 143]. In contrast, ^{31}P MAS NMR resolves resonances from distinct headgroup environments and is being implemented to a greater extent in the study of multi-component lipid mixtures [41, 79, 107, 144-148]. Another advantage of MAS NMR is that it requires significantly less sample compared to static NMR methods. In this work, we chose to study the mixture of DOPC/SM/Chol since the ^{31}P NMR isotropic chemical shifts of the SM and DOPC headgroups are resolvable under moderate MAS conditions. This permits extraction of the ^{31}P CSA parameters (from the spinning sideband manifold), line widths, and relaxation times of the individual lipid components that form the l_o and l_d domains.

4.2 ^{31}P Materials and Methods

4.2.1 Materials

Egg SM, DOPC, and Chol were obtained from Avanti Polar Lipids and used as received. The SM had the following acyl chain composition: 84% 16:0, 6% 18:0, 2% 20:0, 4% 22:0, 4% 24:0 and contained no unsaturated acyl chains.

4.2.2 Sample Preparation

Pure lipid samples were prepared by mixing the lipid with de-ionized water (pH = 7.5) in a conical vial with a vortex mixer. This was followed by a minimum of 5 freeze-thaw cycles in dry ice and a warm water bath set to 333 K (above the liquid crystalline phase transition for DOPC and SM). Buffer was not used in any of the lipid mixtures to prevent multilamellar vesicle (MLV) fragmentation due to freeze-thaw cycling in the presence of salt [149]. Thus, the samples in this study are large MLV's greater than ~ 1 μm in diameter. Samples containing multiple lipid constituents were first combined and dissolved in chloroform followed by vacuum drying overnight to remove the solvent. The samples were then hydrated with the above procedure. All lipid samples were 33 wt% phospholipid. The binary Chol containing samples were 33 mol% Chol to be consistent with the Chol content of the raft forming lipid mixture that was 1:1:1 mol%. The lipid samples were transferred to 4 mm zirconia MAS rotors and sealed with kel-F inserts and caps. The typical volume of MLV sample for NMR analysis was 50-100 μL corresponding to 25-50 mg of phospholipid. The samples were stored in a -20 ºC freezer when NMR experiments were not being performed.

4.2.3 ^{31}P NMR Spectroscopy

^{31}P NMR spectra were collected on a Bruker Avance 600 spectrometer equipped with a 4 mm broad band MAS probe under both static and MAS conditions. The MAS speed was set to 2 kHz and controlled to ± 1 Hz in all MAS experiments. The temperature was varied between 296 and 320 K and controlled to ± 0.2 K with a Bruker VT unit. Static spectra were obtained with a spin-echo sequence ($\pi/2 - \tau - \pi$) where the $\pi/2$ pulse was 4.5 μs and the inter-pulse delay, τ, was 20 μs. A moderate ^{1}H two pulse phase modulation (TPPM) decoupling field strength of 22.5 kHz was applied following the $\pi/2$ pulse thru acquisition of the free induction decay using a 15º phase shift [114].

For the MAS experiments, a single pulse Bloch decay without ^{1}H TPPM decoupling was utilized. Spin-spin relaxation measurements (T_2) were performed under MAS conditions with a rotor synchronized spin-echo. A recycle delay of 3 s was utilized in all experiments. The isotropic chemical shift was set using the secondary reference of solid $NH_4H_2PO_4$ (δ = +0.8 ppm with respect to phosphoric acid δ = 0 ppm). The extraction of the ^{31}P CSA ($\Delta\sigma$), asymmetry parameter (η), full width at half maximum (FWHM), and deconvolutions necessary for T_2 fitting were performed with the DMFIT software package [117]. The uncertainty in the FWHM ranged from ±2 to ±5 Hz, while the uncertainty in the determined $\Delta\sigma$ is $\pm$ 0.2 ppm.

Due to the phosphorous headgroup rotational motion about the lipid bilayer normal in MLV's, the chemical shielding tensor is averaged to an effective tensor that is axially symmetric. The anisotropic part of this time-averaged tensor has been defined by Seelig as:

$$\Delta\sigma = \sigma_{\parallel} - \sigma_{\perp} = \frac{3}{2}(\sigma_{\parallel} - \sigma_i) \tag{4.1}$$

where σ_i is the isotropic chemical shift, $\sigma_{\parallel}$ is the low intensity shoulder ($\sigma_{\parallel} = \sigma_{33}$) and $\sigma_{\perp}$ is the high intensity shoulder ($\sigma_{\perp} = \sigma_{11} = \sigma_{22}$) of the axially symmetric powder pattern [134]. This definition of $\Delta\sigma$ differs from the formalism used in the DMFIT software package by a factor of 3/2 where the anisotropy from DMFIT ($\Delta\delta$) is given by:

$$\Delta\delta = \sigma_{33} - \sigma_i \tag{4.2}$$

and has been accounted for in the $\Delta\sigma$ reported here to remain consistent with the earlier ^{31}P work on phospholipid membranes [120, 133, 134, 136, 150]. The asymmetry parameter of the ^{31}P shielding tensor is defined as:

$$\eta = \frac{\left(\sigma_{22} - \sigma_{11}\right)}{\left(\sigma_{33} - \sigma_i\right)} \tag{4.3}$$

where the principal components of the tensor are ordered in the following manner: $|\sigma_{33}-\sigma_i|>|\sigma_{22}-\sigma_i|>|\sigma_{11}-\sigma_i|$. In the DMFIT program the minimization of the fitting error uses a

quadratic distance between the simulated and experimental spectra with an iterative constrained gradient protocol involving the partial derivatives of all parameters in the line shape model [117]. For chemically shift resolved components the fits for both the static and MAS spectra were relatively sensitive to variations in $\Delta\sigma$, η and the line-width. The exception to this was the situation where an overlap of two different SM line shapes were present, in which case the fits of the MAS NMR spectra were poorly behaved. For these overlapping MAS simulations the value of η was fixed to that obtained from the static spectra to improve convergence.

4.3 ^{31}P MAS NMR Results and Discussion

4.3.1 Static ^{31}P NMR Characterization

The static ^{31}P NMR spectra for SM, SM/Chol, DOPC, DOPC/Chol, DOPC/SM, and DOPC/SM/Chol are displayed in **Figure 4.1** at two different temperatures. In all these mixtures DOPC is above its liquid crystalline phase transition temperature (T_m) of 255.7 K, and should exist in the L_α liquid crystalline state [151]. SM has a T_m of ~ 313 K and therefore, is in either the gel or liquid crystalline state, depending on the observation temperature, 296 K or 318 K, respectively [152, 153]. For SM in the gel phase (**Figure 4.1A**, 296 K), the ^{31}P powder pattern is comprised of two components: one that is axially asymmetric with $\Delta\sigma$ = 56.1 ppm and η = 0.7, and an axially symmetric pattern with $\Delta\sigma$ = 54.0 ppm and η = 0.0. This result is consistent with previous static ^{31}P NMR results on SM in the gel phase where both an axially symmetric component and an asymmetric component were required to fit the ^{31}P powder pattern [102]. When the temperature is raised above the L_α phase transition (**Figure 4.1A**, 318 K), the static ^{31}P NMR spectrum of SM collapses to a single, axially symmetric component (η = 0) with $\Delta\sigma$ = 45.2 ppm. This $\Delta\sigma$ is slightly larger than that recently reported for oriented egg SM [139] and close to the value of 45.8 ppm reported by Shaikh *et al*. on unoriented SM [140]. This dynamically averaged ^{31}P powder pattern results from axial rotation of the phosphodiester moiety about the bilayer normal, bond librations, and overall lipid fluctuations and rotations [138, 154]. The substantially smaller CSA of the L_α state compared to the L_β state is attributed to the considerable decrease in the correlation times of these headgroup motions by greater than one to two orders of magnitude [138].

The binary SM/Chol sample (**Figure 4.1B**) displays an axially symmetric powder pattern (η = 0) both above and below the L_α phase transition (~ 313 K), with a $\Delta\sigma$ ~ 44 ppm. This axially symmetric CSA is similar to pure SM in the L_α state, but the presence of Chol has reduced $\Delta\sigma$ by ~ 3%. Similar results were observed for bovine brain SM bilayers containing cholesterol, where an axially symmetric powder pattern was observed below the L_α phase transition of SM down to 0 ºC [126]. This reduction in $\Delta\sigma$ at 296 K (below T_m) presumably occurs due to a partitioning of cholesterol between the SM lipid molecules in the bilayer that disrupts the packing of the saturated chains and permits headgroup rotation similar to that occurring in the L_α phase of pure SM. The effect of Chol incorporation on phospholipid bilayers has been previously monitored with static ^{2}H and ^{31}P NMR where the dynamic averaging of the hydrocarbon chain and headgroup regions of the lipid were monitored with the two techniques, respectively [120]. ^{2}H NMR detected an increase in the ordering of the hydrocarbon chain above T_m with the incorporation of Chol while, ^{31}P NMR revealed a decrease in the ordering of the headgroup moiety below T_m when Chol is incorporated in the bilayer.

The DOPC (**Figure 4.1C**) and DOPC/Chol (**Figure 4.1D**) samples yield similar axially symmetric (η = 0) powder patterns at both temperatures since both are above the T_m of DOPC (255.7 K). The Chol containing sample reveals a CSA ~ 2 ppm smaller at 296 K and ~ 1 ppm smaller at 318 K compared to pure DOPC. This change in ^{31}P CSA is consistent with previous studies on DOPC bilayers containing cholesterol where ~ 2 ppm decrease in CSA was also observed [155]. This result shows that although small, Chol has a detectable effect on the ^{31}P CSA of DOPC in the L_α state. Similar observations have been reported for the ^{31}P CSA of DPPC and 1,2-dipalmitoyl-*sn*-glycero-3-phosphoethanolamine (DPPE) in the L_α phase, where a ~ 2 to 3 ppm decrease was observed for 1:1 mixtures with cholesterol [120, 121]. This small decrease in headgroup ordering in DOPC with incorporation of Chol occurs in conjunction with an increased degree of chain ordering as revealed by ^{2}H NMR [33].

The binary DOPC/SM mixture (**Figure 4.1E**) exhibits a single axially symmetric pattern with a CSA comparable to the pure DOPC sample or the SM/Chol mixture. There is no evidence of overlapping powder patterns as seen in the pure SM (**Figure 4.1A**) sample. This result shows that DOPC has a similar influence on the dynamics of the headgroup region of SM as cholesterol does; increasing the headgroup dynamics that occur below T_m. This experimental observation provides strong evidence that SM and DOPC are completely miscible in this mixture, displaying no sign of phase separation.

The ternary raft forming phase DOPC/SM/Chol (**Figure 4.1F**) results in a slightly asymmetric powder pattern with Δσ = ~ 43 ppm and η = 0.1 above and below the L_α phase transition of SM.

The asymmetric shape (η ≠ 0) of the raft forming mixture DOPC/SM/Chol could provide some evidence for overlapping axially symmetric CSA powder patterns. Previous static ^{31}P NMR on related POPE/SM/Chol mixtures gave results that were similar, although much clearer shoulders were observed in that study permitting the extraction of the individual CSA parameters for POPE and SM from spectral simulation of the static ^{31}P NMR line shape [140]. While DOPC and SM have indistinguishable CSA powder patterns in the ternary phase (**Figure 4.1F**), the isotropic chemical shift can be resolved under 1D MAS conditions, and was pursued to extract the ^{31}P CSA parameters of the individual components (discussed in the next section).

In a previous static ^{31}P NMR study on DOPC/SM/Chol, a splitting of the powder pattern was observed that was attributed to potential phase separation as the Chol content was increased to a value of 30 mol% [141]. This splitting of the ^{31}P powder pattern was not observed here however, the asymmetric shape could indicate the presence of two overlapping patterns. It is also important to note that no isotropic components (δ ~ 0) were observed in any of the static ^{31}P NMR spectra shown in **Figure 4.1**. This indicates that stable bilayers (> 500 nm) were formed in all of these samples with no spherical micelle structures or regions of high bilayer curvature leading to isotropic averaging of the ^{31}P CSA tensor.

4.3.2 ^{31}P MAS NMR Characterization of Binary Systems

The ^{31}P MAS NMR spectra were also collected on the six lipid mixtures and are presented in **Figure 4.2**. The spinning sideband manifold for pure SM was fit with a symmetric (Δσ = 49.4 ppm, η = 0.0) and an asymmetric (Δσ = 56.8 ppm, η = 0.7) component to maintain consistency with the static model below T_m (**Figure 4.2A**, 296 K). The line widths (FWHM = 700, 250 Hz) are broad compared to the MAS spectra of the other lipid mixtures and the two components extracted from the static ^{31}P NMR spectrum are not as apparent. As noted in the experimental section these overlapping MAS simulations are poorly constrained and required fixing of the η values from those obtained from the static NMR spectra. It is also possible to fit the pure SM (below T_m) with a single spectra component, but the error was slightly larger than that obtained with the overlapping two component simulation. This result shows an example in which it can

often be advantageous to run both static and MAS NMR to detect multiple phases in heterogeneous lipids like SM. Above T_m (**Figure 4.2A**, 318 K), the ^{31}P MAS NMR spectrum shows an axially symmetric powder pattern with a dramatically decreased CSA ($\Delta\sigma$ = 43.2 ppm) and line width (FWHM = 51 Hz) compared to the gel phase. This is in agreement with the static observations of unoriented and oriented samples and consistent with SM being in the L_α state [139].

The ^{31}P MAS spectrum of the SM/Chol sample (**Figure 4.2B**, 296 K) displayed a significant decrease in $\Delta\sigma$ compared to the pure SM sample below T_m (**Figure 4.2A**, 296 K) similar to the static results. For this mixture the MAS line width (FWHM = 270 Hz) is much broader than the line width (FWHM = 51 Hz) for the pure SM sample in the L_α phase (**Figure 4.2A**, 318 K). This shows that although the magnitude of the CSA decreases for the SM/Chol mixture (below T_m) to a value comparable to that observed in the pure SM L_α state, the SM headgroup dynamics in the Chol containing sample are not identical to the L_α phase of pure SM. Above T_m the SM/Chol sample does display a line width (FWHM = 51 Hz) comparable to the L_α phase of pure SM. This change in line width when the temperature is increased from 296 K to 318 K provides strong evidence that the SM/Chol sample does undergo some form of phase transition involving a decrease in molecular correlation times that is more easily discernable as a change in the MAS line width than a change in ^{31}P CSA (discussed further below).

The ^{31}P MAS NMR spectra of the DOPC (**Figure 4.2C**) and DOPC/Chol (**Figure 4.2D**) samples display very similar behavior compared to the static spectra at 296 K and 318 K. Axially symmetric spinning sideband patterns are observed with slightly smaller CSA's (~ 1 ppm) for the Chol containing samples at both temperatures. The line widths are very similar for measurements made on both samples at both temperatures (FWHM ≈ 40 Hz). This is consistent with DOPC being in the L_α phase in all four experiments. It should be noted that for measurements on SM and DOPC in the presence of Chol and without, the magnitude of the CSA extracted from the MAS spectra are slightly smaller than those observed under static conditions. The reason static spectra yield slightly larger CSA's compared to the MAS spectra is not clear however, one possibility for the discrepancy could be due to partial alignment of the lipid bilayers in the high NMR magnetic field. Lipid molecules have a negative anisotropic magnetic susceptibility and thus, have a tendency to align with their long axis perpendicular to the magnetic field. This results in the MLV having an ellipsoidal shape that skews the resulting ^{31}P powder pattern [156]. The fits of the static ^{31}P spectra obtained in this study assume a random

distribution of orientations. This assumption could be a possible source of error. Under MAS conditions the orientational ordering is dramatically reduced [157] therefore, the CSA's extracted from MAS spectra are presumably more accurate than the ones extracted from the static spectra. Further, it has been theoretically shown that MAS spectra give more reliable results than static spectra when extracting the magnitude of the CSA [158]. When comparing static-to-static spectra and MAS-to-MAS spectra the variations observed for the different samples are consistent.

4.3.3 ^{31}P MAS NMR Characterization of Ternary Mixtures

The ^{31}P MAS NMR spectra for the DOPC/SM and DOPC/SM/Chol samples are shown in **Figure 4.2E** and **4.2F**, respectively. The ^{31}P MAS NMR spectrum of the DOPC/SM sample resolves the isotropic chemical shift of DOPC and SM that are -1.0 and -0.4 ppm. In contrast to the glycerol backbone in DOPC, the SM lipid possesses a sphingosine backbone allowing for inter-molecular hydrogen bonding between the C3 hydroxyl group and the amide hydrogen, plus intra-molecular hydrogen bonding between the hydroxyl group and the phosphoryl oxygen of the headgroup. Molecular dynamics (MD) simulations [127, 159] and ^{31}P liquid-state NMR [128] results favor the later intra-molecular hydrogen bonding pair although, a finite possibility also exists for intra-molecular hydrogen bonding between the phosphoryl oxygen and the amide hydrogen according to one of the MD studies [127]. This 0.6 ppm decrease in the ^{31}P chemical shift in comparing DOPC and SM has been attributed to the presence of these hydrogen bonding motifs within SM that do not exist in phosphatidylcholines [160]. The presence of these different hydrogen bonding arrangements may result in differences in the headgroup interaction with water between the two lipids. An expansion of the isotropic chemical shift range is shown in Figure 4.3 where the resonance lines of the pure components can be compared with the mixtures. The isotropic ^{31}P chemical shifts for the individual lipid headgroups in the DOPC/SM mixture was identical to the pure lipid chemical shifts and did not vary as a function of temperature or with addition of cholesterol (33 mol%) arguing that if hydrogen bonding is responsible for the decrease in the ^{31}P chemical shift of SM the hydrogen bonding motif does not appear to vary for the different mixtures and temperatures investigated.

4.3.4 Variation of ^{31}P CSA for Mixtures

It is interesting to compare the magnitude of the CSA extracted from the ^{31}P MAS spectra of DOPC/SM and DOPC/SM/Chol to those of the pure lipid mixtures. In the DOPC/SM mixture at 296 K (below T_m of SM), the CSA of DOPC is ~ 2 ppm larger (~ 5 %) than the CSA observed in pure DOPC, while the CSA of SM is ~ 10 ppm smaller (~ 18 %) than the CSA observed for pure SM (**Figure 4.2**). For the DOPC/SM mixture the DOPC resonance also displays ~ 2 ppm decrease in CSA at 318 K compared to the measurement at 296 K; however, the value of the DOPC ^{31}P CSA is ~ 1 ppm larger than that observed for pure DOPC at 318 K. These results, along with the continued observation of the SM gel to L_α phase transition with temperature (see discussion below on SM ^{31}P CSA temperature variation) demonstrates that the SM is still in the ordered gel phase at 296 K. It is known that for phospholipids with different T_m that either the mixture can remain uniform or cooperative phase separation can occur, with a coexisting gel and L_α phases. If a phase separation did occur there are limits to the lipid composition of the coexisting phases. In one limiting case the gel phase can be assumed to be composed entirely of SM, which would predict a $\Delta\sigma$ ~ 55 ppm (pure SM at 296 K) significantly larger than observed experimentally. This would also predict the L_α phase to be composed entirely of DOPC, giving rise to $\Delta\sigma$ ~ 42 ppm, which is smaller than the $\Delta\sigma$ ~ 45.4 ppm observed experimentally. Based on the observed headgroup dynamics this type of pure phase separation does not appear to occur. Intermediate to this limit is a gel phase enriched in SM with a minor concentration of DOPC, along with a minor concentration of SM in the DOPC rich L_α phase. There is no evidence of two SM phases (or two DOPC phases) coexisting in the present ^{31}P NMR experiments, but it would be difficult to resolve overlapped SM (or DOPC) phases with small differences in $\Delta\sigma$. In addition, it may also be possible for the coexisting gel and L_α phases to be in rapid exchange giving rise to an averaged $\Delta\sigma$ (see discussion below on time and length scales). To distinguish these possibilities using ^{31}P NMR will be difficult and will require careful studies of these mixtures as a function of relative concentration. For the present study we will report the single parameter or averaged $\Delta\sigma$ values assuming these lipid mixtures are homogeneous. Under this assumption, these results illustrate a cooperative effect between lipid constituents. The presence of DOPC greatly increases the SM headgroup mobility and subsequent motional averaging of the SM ^{31}P CSA tensor. These experiments also reveal that the ^{31}P CSA of DOPC does not remain unchanged with the incorporation of SM, but increases slightly, consistent with a decrease in DOPC

headgroup motions, although the impact of DOPC on SM appears to be larger than the SM impact on DOPC. These observations are in agreement with the static ^{31}P experiments; however, the ^{31}P MAS NMR results are unique in that they yield an exact measure of the variation in the ^{31}P CSA for the two individual components.

A similar argument can be made for the DOPC/SM/Chol mixture where the ^{31}P CSA of SM is ~ 5 ppm smaller than the binary DOPC/SM sample at both 296 K and 318 K. Similarly, the ^{31}P CSA of DOPC in the DOPC/SM/Chol mixture is ~ 3 ppm smaller than the binary mixture. In this case a pure phase separated gel phase SM/Chol composition would predict a $\Delta\sigma$ ~ 43.2 ppm at 296 K for SM, while experimentally it is ~ 42.0 ppm. The corresponding pure DOPC L_α would predict a $\Delta\sigma$ ~ 43.2 ppm, while again a smaller value of 42 ppm was observed. Again in these ^{31}P MAS NMR studies there is no evidence of this type of phase separation, but additional experiments would be required to fully unravel this. Assuming a homogeneous mixture these experiments show that the presence of Chol increases the headgroup motion of both lipids, although the impact of Chol on the SM headgroup is larger. The fact that the SM ^{31}P CSA is smaller in the DOPC/SM/Chol mixture both above and below T_m compared to the SM/Chol (33% Chol) binary mixture could indicate a higher relative amount (> 33%) of Chol present in the SM domain of the ternary mixture. However, considering the large effect DOPC has on the headgroup of SM (**Figure 4.2E**) the cooperative effect of DOPC and Chol presence cannot be ruled out as the cause of the SM ^{31}P CSA reduction in the ternary mixture. Further work is in progress where the Chol concentration is varied to distinguish these cooperative lipid effects and the sole impact of Chol, and will be presented elsewhere. These results also show that if phase separation occurs into cholesterol-rich SM domains below T_m, that there must still be some Chol present and interacting with the DOPC component since it too displays a decrease in ^{31}P CSA to a value comparable to that observed in the DOPC/Chol binary mixture. This is in agreement with previous ^{2}H NMR and AFM results that indicate there is cholesterol present in the DOPC l_d domains [28, 33] as well as more recent PFG studies on the DOPC/SM/Chol mixture which shows that there is preferential enrichment of Chol and SM in the l_o domains, but with lateral diffusion rates between those of pure ternary DOPC/Chol and SM/Chol mixtures. Again note that the resolution of the individual headgroup resonances afforded by ^{31}P MAS NMR allows these subtle variations in the lipid headgroup dynamics to be directly measured.

4.3.5 Variation of ^{31}P Line Width for Mixtures

The line widths of the ^{31}P isotropic resonances are different for the mixtures and pure lipid samples, and change as a function of temperature particularly for SM. The ^{31}P line width of SM below its T_m is much narrower (FWHM = 102 Hz) in the mixture with DOPC (**Figure 4.3B**, 296 K) than in the pure SM sample where the FWHM = 250 and 700 Hz (**Figure 4.3D**, 296 K). However, above the T_m of SM the ^{31}P line widths (FWHM = 58 Hz) are comparable in the DOPC/SM mixture. In the DOPC/SM/Chol sample below T_m the line widths of the different lipid resonances are not identical, where the FWHM = 71 Hz for SM and 53 Hz for DOPC. Above T_m comparable ^{31}P line widths are observed with the FWHM = 58 Hz for both lipid headgroups. These results show that SM undergoes a liquid crystalline phase transition and the difference in line width between SM and DOPC below the SM T_m indicates a lower degree of mobility and/or an increased heterogeneity of headgroup environments for SM compared to DOPC. Additional discussion about this change is presented in the T_2 section below. This variation in the ^{31}P line width is consistent with prior interpretations regarding ternary mixtures of saturated lipids, unsaturated lipids and cholesterol that form coexisting liquid phases below T_m. The saturated lipid is in a l_o state while the unsaturated lipid is in a liquid crystalline l_d state [21-24, 26]. This separation into l_o and l_d phases presumably results in slight differences in mobility that are borne out in the line width. Above T_m both DOPC and SM have comparable line widths and therefore, both appear to exist in a liquid crystalline l_d state.

4.3.6 Variation of the SM ^{31}P CSA with Temperature

While variations in the ^{31}P CSA have been noted above for changes in the lipid composition, it is also instructive to take a detailed look at the variation in the SM ^{31}P CSA as a function of temperature. The CSA of SM extracted from the ^{31}P MAS spectra as a function of temperature for the different lipid mixtures is displayed in **Figure 4.4**. For pure SM, the ^{31}P CSA decreases as the temperature increases and displays two transitions: a small one at 306 K that is attributed to a gel-gel transition and a major one at 314 K that is attributed to the gel-liquid crystalline phase transition. This is in excellent agreement with previous static ^{31}P NMR results that report a gel-gel transition at 306 K and the formation of an almost exclusively L_α bilayer at 314 K for SM [102]. For the pure SM there is also a small reduction in the ^{31}P CSA observed at 300 K, along with a gradual decrease in the CSA approaching the L_α phase transition. This gradual decrease

is not surprising considering that naturally occurring SM is heterogeneous having different acyl chain lengths producing complex phase behavior where multiple different gel phases have been proposed [102, 161] and a very broad asymmetric L_α phase transition is observed by differential scanning calorimetry (DSC) [118, 162]. For the other lipid mixtures (**Figure 4.4**), changes in the ^{31}P CSA at the phase transitions are much less apparent, although some minor variations are observed. The relative decrease in the SM ^{31}P CSA occurs in the following order: SM > SM/DOPC > SM/Chol > DOPC/SM/Chol. From these trends cholesterol has a larger impact than DOPC on the reduction of the SM ^{31}P CSA (and correspondingly the increased headgroup dynamics). Also note that DOPC and Chol have the largest combined effect on SM where the smallest ^{31}P CSA was observed for the ternary DOPC/SM/Chol mixture, again suggesting cooperative lipid effects in these mixtures. The ^{31}P CSA variations for DOPC in these mixtures as a function of temperature are very minor, reflecting that DOPC is in the L_α phase for the entire temperature range investigated.

4.3.7 Line Width Variation for SM with Temperature

Since the ^{31}P MAS NMR line width (FWHM) of SM varies greatly in the different mixtures it was also monitored as a function of temperature as shown in **Figure 4.5**. For pure SM, the FWHM increases as the temperature is increased and the L_α phase transition is approached (~ 314K). Above this transition a drastic, order of magnitude decrease in the ^{31}P FWHM is observed. The increase in ^{31}P FWHM prior to the L_α transition was initially surprising because the ^{31}P CSA decreases across this range indicating an increase in motional averaging yet, a broadening of the ^{31}P resonance could be an indication of a change in motional correlation time. This increased line broadening might also be attributed to heterogeneities in the SM sample resulting in a distribution of chemical shifts commonly observed in NMR spectra of disordered and/or heterogeneous systems. Contributions of the chemical shift distribution to the line width were estimated by measuring the ^{31}P MAS T_2 relaxation time which is found to correlate well with the line width observations (see below). Therefore, it appears that for pure SM there is a restriction in some motional process prior to the main L_α transition. Similar observations have been made in DPPC [162] and 1,2-Dimyristoyl-sn-Glycero-3-Phosphocholine (DMPC) [138] where the formation of a rippled phase, $P_{\beta'}$, occurs prior to the main transition. It has been shown by ^{14}N MAS NMR [163] and ^{31}P NMR [138] that some of the motional dynamics, particularly in the headgroup region, are slower in

the $P_{\beta'}$ rippled phase than in the $L_{\beta'}$ gel phase or L_α liquid crystalline phase. This difference in dynamics has been detected as a broadening of the line width in the ^{14}N MAS NMR of DPPC and a decrease in ^{31}P T_2 relaxation time of DMPC in the $P_{\beta'}$ phase. This $P_{\beta'}$ rippled phase is usually detected as a distinct pre-transition that occurs prior to the main L_α phase transition of saturated chain phosphatidylcholines like DPPC and DMPC using DSC. This distinct pre-transition is not observed in the DSC of SM [118, 162] however, some reports do indicate the existence of a rippled morphology in naturally occurring SM [162, 164]. The ^{31}P MAS NMR line width results presented here for pure SM further support the existence of a dynamically restricted, presumably $P_{\beta'}$ rippled phase in egg SM.

The ^{31}P FWHM of SM or DOPC in the other lipid mixtures (DOPC, DOPC/Chol, DOPC/SM, SM/Chol) do not show any indication of a similar dynamically restricted environment across the temperature range studied. The SM ^{31}P line width does decrease as the L_α phase transition is approached in the other mixtures, but it is not nearly as sharp as the transition observed for pure SM. These observations are consistent with reports on phosphatidylcholine/Chol mixtures that indicate a disappearance of the rippled phase pre-transition in the presence of cholesterol for concentrations greater than 20% [165-168].

4.3.8 Variation of ^{31}P MAS NMR T_2 with Temperature

To confirm that the trends observed in the ^{31}P FWHM were due to mobility variations and not chemical shift heterogeneities, the ^{31}P NMR T_2 relaxation times were measured across the same temperature range. The ^{31}P T_2 of pure SM and SM/Chol is shown in **Figure 4.6A** as a function of temperature. For the pure SM sample the results are very similar to the ^{31}P FWHM results depicted in **Figure 4.4**. The T_2 shows a decrease prior to the liquid crystalline phase transition that correlates well with the observed increase in the FWHM, followed by a large increase as the L_α phase transition is reached, and finally a leveling off as the transition is surpassed. The ^{31}P T_2 value for pure SM below L_α predicts a line width ~4 times narrower than the observed value. Therefore, it appears that below L_α some of the SM ^{31}P line width contributions can be attributed to chemical shift distributions as a result of the heterogeneous nature of egg SM, and is in agreement with the multi-component static ^{31}P powder pattern observed in **Figure 4.1A**, (296K). The decrease in ^{31}P T_2 observed prior to the L_α transition correlates well with the increase in the ^{31}P FWHM, arguing that this observed variation is

the result of a decrease in headgroup dynamics. The decrease in the ^{31}P T_2 is again consistent with formation of a motionally restricted phase (similar to the rippled phase) prior to the L_α transition. In the SM/Chol mixture, the ^{31}P T_2 gradually increases until the L_α phase transition is reached displaying no sign of this motionally restricted headgroup dynamic. Again this is consistent with the previously observed elimination of the pre-transition and rippled phase in DPPC mixtures with similar amounts of cholesterol [165-168]. The phase transition of the SM/Chol mixture is significantly broader than the pure SM sample consistent with DSC results [129, 130].

The ^{31}P T_2 as a function of temperature for SM in the DOPC/SM and DOPC/SM/Chol mixtures are displayed in **Figure 4.6B**. For DOPC/SM, the SM T_2 increases with a step at 306 K and the main L_α phase transition (314 K). The initial ^{31}P T_2 value is comparable to that observed in pure SM in the gel state which suggests that SM in the DOPC/SM mixture is in a solid ordered gel state below T_m. The slight dip in T_2 at 306 K could provide some evidence that there is a small gel-gel transition that is still observed similar to pure SM. In the raft forming DOPC/SM/Chol lipid mixture, the ^{31}P T_2 of SM gradually increases towards the L_α phase transition and then levels off above 314 K. These trends are consistent with SM in the DOPC/SM/Chol mixture being in a l_o state below T_m (T_2 between 9-10 ms) where the dynamics are not as slow as in the solid ordered gel state which is observed for SM in DOPC/SM (T_2 = ~2 ms) and still undergoes a broad phase transition to a l_d liquid crystalline state (T_2 between 11 and 13 ms). This transition is extremely broad, but observable by monitoring subtle variations in dynamics from T_2 measurements and the line width. The ^{31}P T_2 of DOPC remains relatively consistent across the temperature range in all the lipid mixtures studied with a value between 14.5 and 16.5 ms.

It is interesting to note the contributions from heteronuclear dipolar coupling to the ^{31}P line broadening observed for SM in these lipid mixtures. The ^{31}P MAS NMR spectra presented in this report were collected without ^{1}H decoupling. For pure SM (below T_m) the inclusion of ^{1}H decoupling narrows the line width from ~400 to ~200 Hz, demonstrating that residual ^{1}H-^{31}P dipolar coupling are still present under MAS at 2 kHz. Above T_m, there is no change in the ^{31}P MAS line widths with the incorporation of ^{1}H decoupling, demonstrating that in the L_α phase any residual ^{1}H-^{31}P dipolar coupling is completely averaged by the combination of phospholipid headgroup motion and MAS. By obtaining ^{31}P MAS spectra without ^{1}H decoupling subtle differences in headgroup dynamics could be distinguished by changes in the ^{31}P line width and T_2 due to the

presence of the residual heteronuclear dipolar coupling. These small variations in headgroup dynamics were not readily determined from ^{31}P CSA variations.

4.3.9 Limits on Time and Length Scales

The observation of powder patterns and spinning sidebands in the ^{31}P NMR spectra provides a way to determine limits for motional timescales and domain sizes. The CSA is the dominant nuclear interaction for ^{31}P, and scales linearly with magnetic field strength. For a 14.1 T magnetic field the observed residual ^{31}P anisotropy of $\Delta\sigma$ ~ 42 ppm, corresponds to a ~ 10 kHz interaction. As noted above the lack of an observable isotropic resonance in the static spectra of any of the lipid mixtures investigated in this study demonstrates that there are no large scale motions on a time scale <100 μs. In some systems such rapid motions may exist for high curvature regions or isotropic phases giving rise to a motionally averaged isotropic resonance; but that is not observed for the present DOPC/SM/Chol systems. The observation of a typical, non-distorted ^{31}P CSA powder patterns and spinning sidebands patterns also provides a limit on the size of the MLV. It has been previously demonstrated that rapid lateral diffusion of the lipid along the curvature of the liposome results in a change of the lipid normal orientation with respect to the magnetic field and can give rise to averaging or exchange of different frequencies within the ^{31}P CSA pattern. This liposome radius (R) is related to the effective lipid lateral diffusion (τ_D) by $R = \sqrt{6D_L\tau_D}$, where D_L is the lateral diffusion coefficient. Recent PFG ^{1}H NMR measurements of D_L in the DOPC/SM/CHOL raft forming mixture have measured D_L to range between 1-10 x 10^{-12} m^2/s, depending on the temperature, cholesterol content, phase (l_o vs. l_d) and the lipid measured [169]. For this range of diffusion constants, the lack of a distorted CSA line shape limits the curvature to R >> 50 nm. This is consistent with ^{31}P two-dimensional exchange experiments that have measured the radii in pure lipid MLV between 300 and 1000 nm [170, 171].

For the DOPC/SM and the raft forming DOPC/SM/Chol mixture below T_m the lack of discernable different CSA patterns overlapping for SM (or DOPC) would suggest that SM is predominantly incorporated in the l_o phase, with no or a very low concentration in the l_d (L_α) phase which is predominantly DOPC (see additional discussion above in section on variation of ^{31}P CSA for mixtures). The other possibility is that the ^{31}P CSA observed is a weighted average due to *rapid* exchange of the lipids between the l_o and l_d

phase on the timescale of 100's μs (assuming a ~10 ppm difference in the CSA between l_o and l_d phases). This averaging would require very small domain sizes on the order of 10's of nm. Interestingly recent PFG NMR studies on this ternary lipid mixture found that the exchange between the phases was *slow* on the PFG time scale of 50 - 250 ms. Obviously additional studies will be required to unravel this information.

The final timescale limit involves the variation of line width in SM as a function of temperature (**Figure 4.5**). Based on the differences between the line width with and without ^{1}H decoupling, there is a residual heteronuclear ^{1}H-^{31}P dipolar coupling under MAS of ~ 200 Hz. The sensitivity of the line width during this temperature range suggests that motions on the 5 ms timescale are occurring in SM during the phase transition. This time scale is slower, but consistent, with an increased rotational correlation time (~30 μs) of SM compared to DMPC reported by Malcolm and co-workers [139]. These longer SM correlation times were attributed to the existence of inter- and intra-molecular hydrogen bonding in SM.

4.4 ^{31}P MAS NMR Conclusions

The ^{31}P MAS NMR for the model lipid membrane mixtures SM, SM/Chol, DOPC, DOPC/Chol, SM/DOPC and SM/DOPC/Chol have been obtained. The ^{31}P MAS NMR is complementary to static ^{31}P NMR measurements and allowed the ability to resolve the SM and DOPC lipids within raft forming mixtures. The individual ^{31}P CSA parameters were measured for the SM and DOPC components that comprise the l_o and l_d phases within these mixtures. The ^{31}P MAS line widths and T_2 measurements detected subtle differences in the headgroup dynamics for the different lipids as a function of mixture composition and temperature. These ^{31}P MAS NMR results show that cholesterol is not completely excluded from the DOPC l_d domains during raft formation. Similarly the headgroup dynamics support a l_o state for SM below T_m in the ternary mixture. These results also highlight cooperative lipid effects within these raft forming mixtures and demonstrate that ^{31}P MAS NMR is a powerful tool for probing raft formation in the more complex ternary samples.

These ^{31}P NMR results provide additional insight into the current view of raft formation in lipid systems. Two main arguments are typically presented when discussing the formation of raft phases from a molecular point of view. The first argument is that chain packing effects (i.e. cholesterol prefers to interact with saturated chain lipids over unsaturated lipids) help drive lipid raft formation. Headgroup

interactions may also play an indirect role in chain packing. The second molecular interaction forwarded for impacting raft formation is the potential for hydrogen-bond formation between the cholesterol OH moiety and the lipid backbone and/or hydrogen bonding between lipid headgroups. In the case of SM the cholesterol/lipid interaction can occur at the OH, NH or carbonyl sites and may involve bridging water molecules between the sphingolipid and OH of cholesterol. Presently the chain packing argument appears to be favored when discussing the main driving force for phase separation into co-existing liquid phases. These chain packing effects are most directly measured using ^{2}H NMR, and as such will be the molecular level interactions highlighted by such studies. However, headgroup and backbone interactions need to be explicitly considered, especially in light of the impact of DOPC on the SM headgroup dynamics shown in the present study along with recent results that indicate cholesterol prefers SM over DPPC in model raft formers [33]. SM and DPPC have identical headgroups, similar saturated chain lengths, and a comparable T_m, but have substantially different backbones. These observations suggest that the sphingosine backbone may influence the preference of cholesterol for sphingolipids over glycerophospholipids. The ^{31}P MAS NMR results presented here show that there are subtle variations in the headgroup dynamics of SM in raft forming mixtures and may provide some evidence for variability in inter- and intramolecular hydrogen bonding motifs when cholesterol-rich SM rafts are formed. It is clear that any future models describing the formation of rafts in lipid mixtures must include the impact on both acyl chain and headgroup dynamics, and that ^{31}P MAS NMR provides an alternative probe of these dynamics.

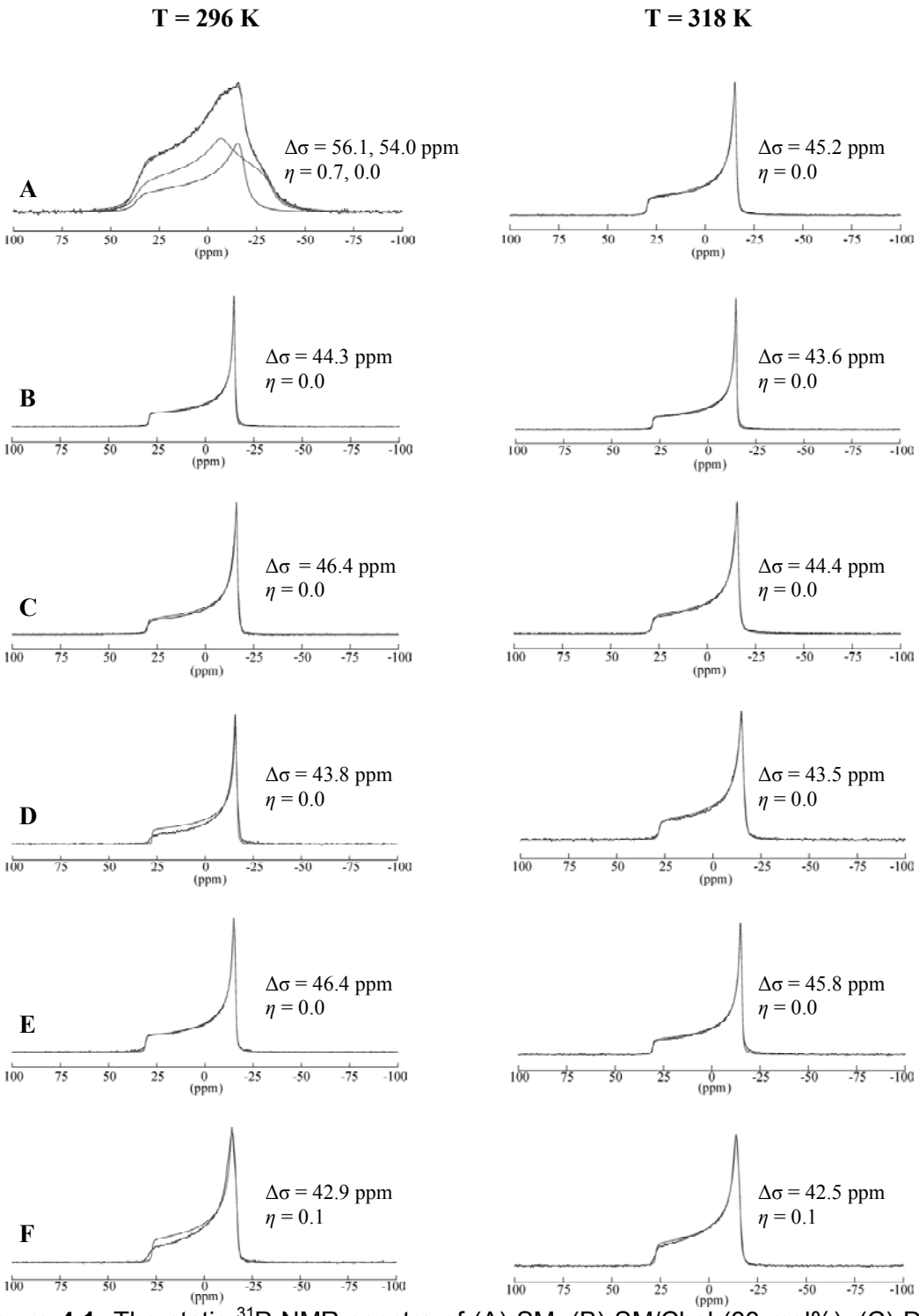

Figure 4.1 The static ^{31}P NMR spectra of (A) SM, (B) SM/Chol (33 mol%), (C) DOPC, (D) DOPC/Chol (33 mol%), (E) DOPC/SM, and (F) DOPC/SM/Chol. Spectra collected at temperatures below (296 K) and above (318 K) the T_m (~ 313 K) of SM are shown. The fits with the extracted CSA parameters are also displayed in the figure. The parameters extracted for SM are indicated first for samples containing both SM and DOPC.

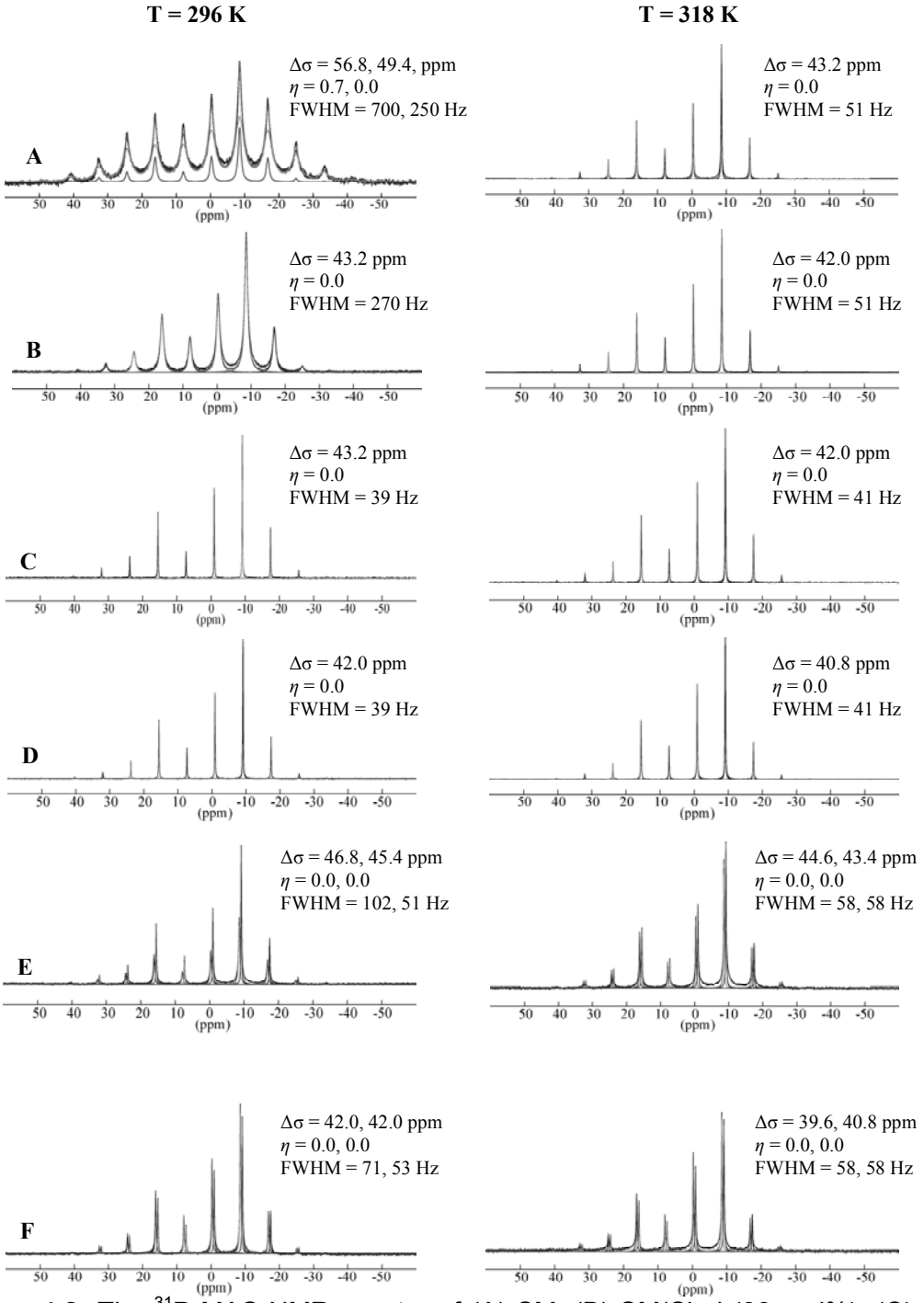

Figure 4.2 The ^{31}P MAS NMR spectra of (A) SM, (B) SM/Chol (33 mol%), (C) DOPC, (D) DOPC/Chol (33 mol%), (E) DOPC/SM, and (F) DOPC/SM/Chol. Spectra collected at temperatures below (296 K) and above (318 K) the T_m of SM are shown. The fits with the extracted CSA parameters are also displayed in the figure. The parameters extracted for SM are indicated first for samples containing both SM and DOPC.

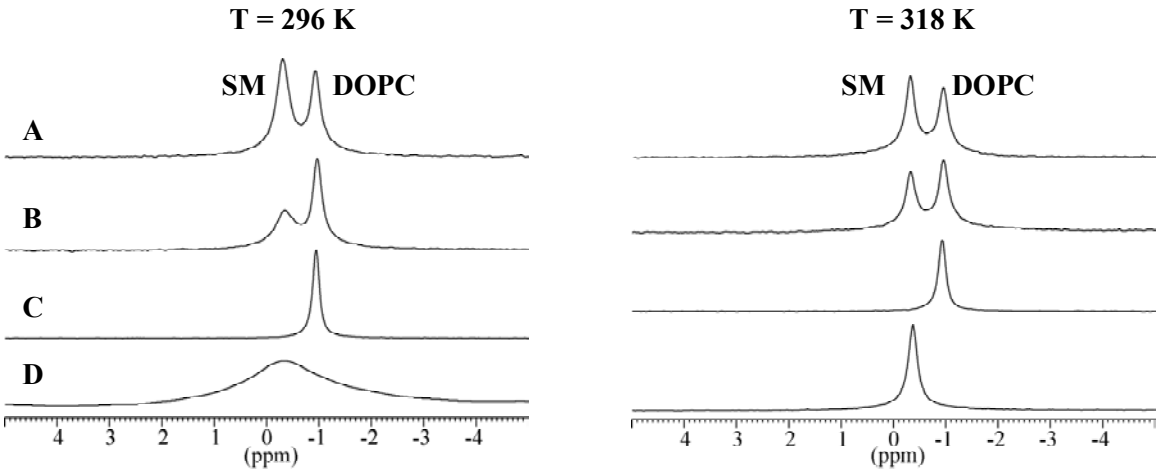

Figure 4.3 Isotropic chemical shift region of ^{31}P MAS NMR spectra of (A) DOPC/SM/Chol, (B) DOPC/SM, (C) DOPC, (D) SM. Spectra collected below (296 K) and above (318 K) the T_m of SM are shown.

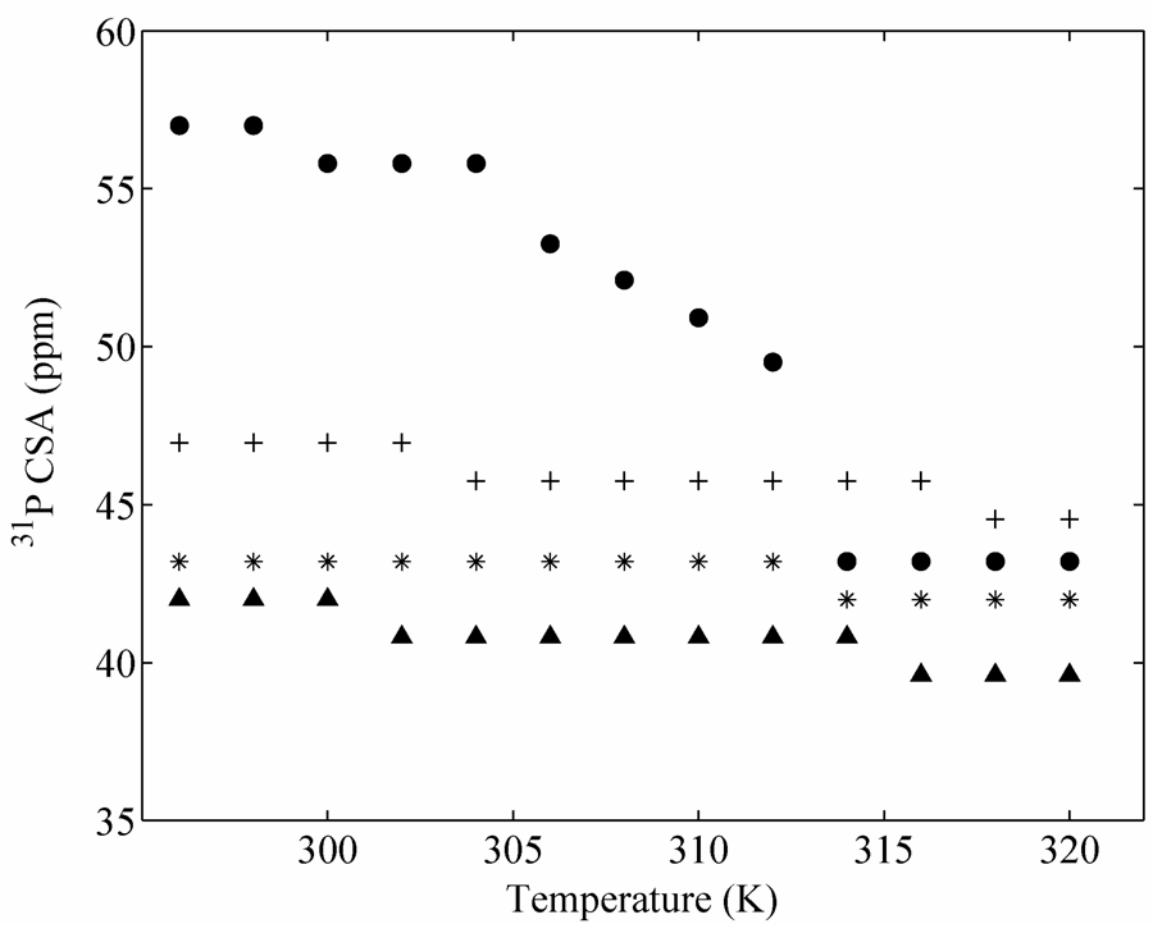

Figure 4.4 The magnitude of ^{31}P CSA (Δσ) extracted from fitting the MAS spinning sideband manifold for SM component as a function of temperature in lipid bilayer mixtures: (•) SM, (+) DOPC/SM, (*) SM/Chol, (▲) DOPC/SM/Chol.

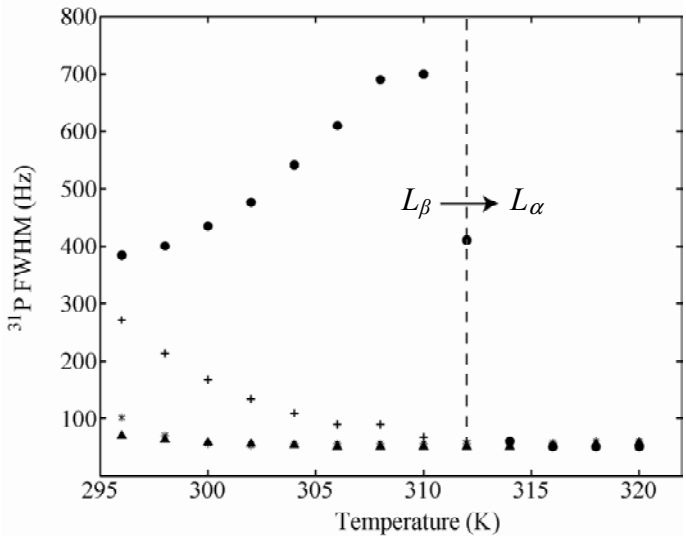

Figure 4.5 The ^{31}P MAS NMR full width at half maximum (FWHM) for SM resonance as a function of temperature in lipid bilayer mixtures: (•) SM, (+) DOPC/SM, (*) SM/Chol, (▲) DOPC/SM/Chol.

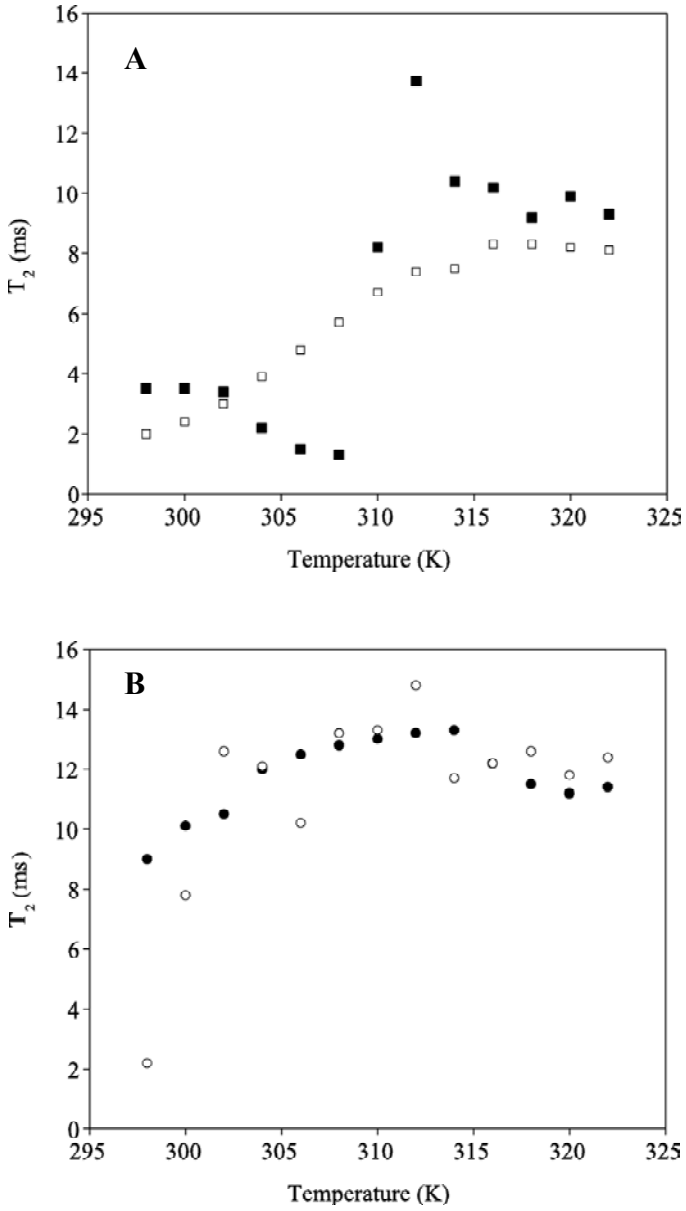

Figure 4.6 The ^{31}P MAS NMR T_2 relaxation times measured for SM resonance with rotor synchronized spin-echo on MAS spectra as a function of temperature in lipid mixtures: (A) (■) SM and (□) SM/Chol and (B) (○) DOPC/SM and (●) DOPC/SM/Chol.

Page Left Intentionally Blank

Chapter 5

Using ^{31}P MAS NMR to Monitor a Gel Phase Thermal Disorder Transition in Sphingomyelin-Cholesterol Bilayers

5.1 Introduction Gel Phase Transition

Previous studies show that the incorporation of cholesterol into the lipid bilayer broadens and lowers the main gel to liquid crystalline phase transition temperature (T_m) [124, 129, 172], decreases (increases) the lipid hydrocarbon chain ordering below (above) T_m [173, 174], decreases the acyl chain tilt angle in the gel phase [175], and diminishes/eliminates the gel phase pretransition prior to T_m [172]. Below T_m, the addition of cholesterol can lead to the formation of a coexisting two-phase region involving the low cholesterol content solid-ordered (s_o) phase and the high cholesterol content liquid-ordered (l_o) phase [25], while above T_m a two-phase region involving the low cholesterol content liquid-disordered (l_d) phase and the high cholesterol content l_o phase results [25, 35, 176-178].

Cholesterol appears to have a higher affinity for sphingomyelin (SM) than for other phospholipids [104, 174, 179-183], most likely due to the distinct structural properties of SM. Sphingomyelin has a large phosphoryl choline headgroup that is well hydrated, allowing more favorable insertion of cholesterol and shielding for the hydrophobic cholesterol molecules [181, 182, 184-187]. The backbone and acyl chain regions of SM distinguish it from other lipids with the same headgroup (i.e. phosphatidylcholines, PCs) [179, 186]. The sphingosine backbone consists of two H-bond donor groups (OH and NH group) and one H-bond acceptor group (carbonyl), compared to the glycerol backbone of PC which only has two carbonyl H-bond acceptors. The main SM-cholesterol interaction has been experimentally shown to occur between the NH group of SM and the OH group of cholesterol [188-190], a finding also supported by molecular dynamic simulations [174]. The hydrophobic acyl chain regions of SM and PC also have an important impact on chain packing effects. Natural SMs have a high degree of saturation in the acyl chain, resulting in stronger van der Waals interactions between SM and cholesterol. Naturally occurring PCs, on the other hand,

have a high occurrence of unsaturation which weakens the PC-cholesterol interaction [124, 180, 181].

Until recently, only saturated phosphatidylcholines (e.g. DPPC) were known to form a rippled phase ($P_{\beta'}$), or pretransition phase. This rippled phase is intermediate to the motionally restricted gel phase and the fluid liquid crystalline phase [191] and is characterized by a long-wavelength rippling of the bilayer and a swelling of the membrane [192]. In the past two decades, several reports of gel phase pretransitions in sphingomyelin bilayers have emerged. These pretransitions have been detected by differential scanning calorimetry [105, 118, 124, 161, 162, 172, 175, 193-196], freeze-etch electron microscopy [162, 164, 195] and x-ray diffraction [175]. Several factors seem to effect the pretransition, including chain length, headgroup size, hydration, and possibly chain tilt [191]. In addition to these factors, the observation of a pretransition in SM appears to be dependent upon the type of SM sample. Thus far, pretransitions have been observed for brain SM [118, 162, 164], purified egg SM [105, 172, 196], synthetic C24 SM [124, 175, 194, 195], synthetic C18 SM (D- and L- isomer) [161], synthetic C16 SM (D-isomer) [193], but not detected in racemic mixtures of SM [161, 193] or unpurified egg SM. Interestingly, the x-ray diffraction data [37, 124, 175] for SM with long C24 chains indicate other processes are occurring in the bilayer, e.g. chain interdigitation, resulting in the presence of another type of transition prior to the main transition. Thus, for SM, hydration, chain length, chain heterogeneity, and chirality seem to be factors in the occurrence and/or detection of a gel phase pretransition.

Previous NMR studies have revealed important information regarding the conformation and molecular dynamics in the SM bilayer. SM was shown to have similar headgroup motions and conformations as the glycerol-based phospholipids using ^{31}P NMR [126]. However, unlike PC, intermolecular H-bonding between SM amide groups and intramolecular H-bonding between the SM OH group and the phosphate headgroup was shown to be a significant factor in the rigidity of SM membranes using ^{1}H and ^{31}P NMR [160, 197]. This result was further supported by molecular dynamic simulations [159, 173, 174, 198, 199]. In addition, restricted mobility in the gel phase was detected for both the SM headgroup and the acyl chains using ^{31}P and ^{13}C NMR, respectively. The mobility of the headgroup increased as cholesterol was added to the bilayer and resembled that seen in the liquid crystalline phase [104, 122, 143]. Multiple gel phases for SM have also been seen in ^{31}P NMR and ^{13}C NMR [102]. More recently, Holland *et al.* suggested an additional gel phase transition was observable in the ^{31}P MAS NMR

spectra of SM mixtures [122]. However, the appearance of this additional gel phase transition was quenched by the inclusion of 33% cholesterol. This chapter continues this work with a ^{31}P MAS NMR analysis of the SM system at cholesterol concentrations below 33% to study the structural/dynamical changes occurring immediately prior to the main gel to liquid crystalline phase transition.

5.2. Gel Phase Materials and Methods

5.2.1 Materials and Sample Preparation

Egg SM and Chol were obtained from Avanti Polar Lipids (Alabaster, AL) with no further purification. The SM contained the following acyl chain composition: 84% 16:0, 6% 18:0, 2% 20:0, 4% 22:0, 4% 24:0. Multilamellar vesicles (MLVs) of SM and SM/Chol were prepared in deionized water using five freeze-thaw cycles with a two minute vortex time between each cycle. The freeze-thaw cycles were accomplished using a dry ice bath and a water bath set to 333 K (above the SM T_m). Hydrated samples contained 33 wt% phospholipid with varying mol% of Chol. Lipid samples were transferred to 4mm zirconia MAS rotors and sealed with kel-F inserts and caps. Sample volume for MAS experiments was ~ 50 µL of lipid MLV and ~100 µL of lipid MLV for static experiments. Samples were stored at -20°C when not in use. The differential scanning calorimetry (DSC) spectra were obtained using a TA Instruments Q100 with a scan rate of 5°C/min from 20°C to 60°C.

5.2.2 ^{31}P NMR Spectroscopy

The NMR experiments were performed on either a Bruker Avance 600 at 242.9 MHz (14.1 T), or a Bruker Avance 400 at 162.0 MHz (9.4 T) using a 4 mm broad band MAS probe for both MAS and static conditions. A Bruker BVT 3000 temperature controller maintained the sample temperature to ± 0.2 K for all experiments. Samples were allowed to equilibrate for 5 minutes at each temperature before acquisition. The ^{31}P MAS NMR experiments used a spinning speed of 2 kHz ± 1 Hz unless otherwise noted. An increase in sample temperature due to frictional heating from sample spinning is ~1 K for speeds ≤ 4 kHz and is ~ 3 K for a rotor speed of 6 kHz. Sample temperatures reported here have been calibrated using the method described previously [200]. The ^{31}P MAS NMR experiments utilized a single pulse Bloch decay with a 4.5 µs π/2 pulse,

either without ^{1}H decoupling or with moderate (22.5 kHz) ^{1}H TPPM decoupling. Spin-spin relaxation times (T_2) were obtained under MAS conditions with a rotor synchronized spin-echo without ^{1}H decoupling. All MAS experiments utilized a 3 s recycle delay. Static ^{31}P NMR spectra were obtained using a Hahn spin-echo sequence (π/2-τ-π) with a π/2 pulse of 4.5 μs and an interpulse delay of 20 μs and moderate ^{1}H TPPM decoupling (22.5 kHz).

All ^{31}P chemical shift anisotropy (CSA) tensor fits were performed on the experimental spectra as previously described [122] using the DMFIT software package as described in Chapter 4 [117].

5.3 Pre-Transition Results and Discussion

The ^{31}P MAS NMR spectra for pure SM MLVs below and above the main gel to liquid crystalline phase (L_α) transition temperature (T_m ~ 313 K [152, 153, 172]) are shown in **Figure 5.1**. Below T_m the broad spinning sideband (SSB) manifold (**Figure 5.1a**) reveals an asymmetric ^{31}P CSA tensor ($\Delta\sigma$ **=** 56.8 ppm, η = 0.65) consistent with previously reported gel phase ^{31}P NMR spectra [122]. Above T_m, the ^{31}P MAS NMR spectrum (**Figure 5.1b**) is axially symmetric (η = 0) with a significantly smaller CSA value ($\Delta\sigma$ **=** 43.2 ppm), consistent with a change in headgroup orientation and/or the increased motional averaging of the headgroup in the liquid crystalline L_α phase, as previously discussed [122, 143].

5.3.1 Variation of ^{31}P Isotropic Line Width with Temperature and Cholesterol Concentration

Previously, it was noted that the line widths of the isotropic resonance in the ^{31}P MAS NMR spectra of SM were temperature sensitive, and revealed some type of disordering or motional transition event (i.e. pretransition, gel → gel) occurring in the gel phase region (298 K to 310 K), prior to the main gel → L_α phase transition. The same type of ^{31}P MAS NMR line width variation can be seen in **Figure 5.2**, where the isotropic line width of SM increases from ~328 Hz at 292 K to 530 Hz at 310 K, then drops dramatically to ~ 167 Hz following the main gel → L_α transition at ~ 312 K. The overall increase in FWHM for this SM gel phase transition is 202 Hz. This change is ~100 Hz smaller than previously reported [122] and is being attributed to the slight variability of lipid chain length distribution between different samples. Anecdotal evidence has shown that lot-to-lot variations of egg SM impacts the magnitude of the observed temperature

variations in the line width, such that for the work reported in this manuscript a single SM lot was employed for all samples.

It can also be seen in **Figure 5.2** that the addition of Chol impacts the extent of this ^{31}P MAS NMR line width variation just prior to the main gel → L_α transition. For example, increasing the Chol content to 5 mol% reduces the line width variation, with the maximum occurring at 306 K and an overall line width change reduced to 118 Hz (versus 202 Hz in pure SM). As the Chol content increases to 7.5 mol% this gel phase line width variation diminishes to ΔFWHM = 50 Hz. For Chol concentrations > 10 mol% this unique increase in the line width was not observed; instead revealing only a gradual decrease with increasing temperature throughout the gel phase.

A more detailed look at the effects of Chol on the ^{31}P MAS NMR line widths are shown in **Figure 5.3**. Below T_m the line widths of SM bilayers with low Chol concentrations are broader compared to other SM/lipid mixtures (*e.g.* SM/DOPC, SM/DOPC/Chol [122]) and suggest either restricted phosphorus headgroup mobility and/or heterogeneity in the headgroup environment within the SM gel phase. With the addition of 5 or 7.5 mol% Chol to the SM bilayer, no changes in the line width are observed (**Figure 5.3b**). At 10 mol% Chol, a 15.5 % reduction in the line width occurs, and at 21 mol % Chol, an overall FWHM reduction of 34 % was observed. SM with 33 mol% Chol (previous work) shows a slightly larger line width value (FWHM = 270 Hz) [122] than the 21 mol% value (FWHM = 236 Hz) reported, here but remains consistent with the overall trend. For cholesterol concentrations greater than 10 mol%, this reduction of the gel phase line width mirrors the reduction of the ^{31}P CSA values at higher cholesterol contents (see discussion below). Interestingly, below 10 mol% Chol no changes in the line width were observed at 296 K. Therefore, at 296 K (in the gel or s_o phase, and prior to the observation of the pretransition shown in **Figure 5.2**) the inclusion of Chol at concentrations > 10 mol% results in either an increased headgroup mobility or change in headgroup orientation, while below 10 mol% Chol changes in the headgroup dynamics on the timescale of the ^{31}P line width ($1/\Delta\delta_{so}$) are not occurring. These results are consistent with previous studies in which increased head group mobility or changes in headgroup orientation were observed as cholesterol was added to the bilayer [122, 143]. The phase diagram for *N*-palmitoyl-D-sphingomyelin (PSM)/Chol below T_m has been reported [25]. For intermediate Chol concentrations a two-phase region exists between the low cholesterol content s_o and l_o phases. The observed line width of 357 Hz (296 K) and 0 mol% Chol corresponds to the s_o phase, while the line

width of 272 Hz of the 33 mol% Chol sample is characteristic of the l_o phase. The change in the ^{31}P MAS NMR line width between 10 and 20 mol% Chol may reflect the averaging within the mixed s_o+l_o phase, but is complicated by the presence of multiple gel phases [102].

Above T_m (318 K), the isotropic line width is ~140 Hz for all bilayers with concentrations up to 21 mol % Chol (**Figure 5.3b**), after which a dramatic decrease in line width is seen at 33 mol% Chol. The phase diagram for SM/Chol above T_m also reveals the existence of a two-phase region, with the coexistence of the l_d and l_o phases [25, 35, 176, 178]. At 0 mol% Chol the line width of 140 Hz (318 K) corresponds to the l_d phase while at 33 mol% Chol the line width of 51 Hz (318 K) represent the l_o phase. The lack of variation in the line width between 0 and 22 mol% Chol shows that the ^{31}P MAS NMR line width is not sensitive to the presence of the two-phase l_d+l_o region. This result is in contrast to the gradual decrease in the lateral diffusion rates observed between 2.5 and 20 mol% Chol reported by Filippov and co-workers [35, 178]. The invariance of the ^{31}P MAS NMR line width to changing Chol concentration above T_m is most likely the result of timescale differences, with the line width time scale being much shorter than the lateral diffusion process.

The most notable item in the ^{31}P MAS NMR line width variation is the pronounced effect that cholesterol has on the appearance of the gel phase pretransition (**Figure 5.2**). Inclusion of < 10 mol% cholesterol diminishes this pretransition, and for Chol concentrations > 10 mol %, the gel phase pretransition is completely eliminated. Several explanations have been forwarded to explain this observed ^{31}P MAS NMR line width variation in the gel phase, including the presence of a distinct gel → gel phase transition, dynamical changes in the bilayer, and changes in headgroup motional correlation times. These possibilities will be addressed in the following sections.

5.3.2 Differential Scanning Calorimetry

One possible explanation for the observed gel phase ^{31}P MAS NMR line width variation is a gel → gel transition, such as that observed in the gel phase to rippled phase [162] or the gel-*α* to gel-*β* transition [161]. Differential scanning calorimetry (DSC) was used to investigate a possible phase transition in the temperature region prior to the main gel to liquid crystalline transition. The calorimetric heating scans for SM and SM with 7.5 mol% Chol are displayed in **Figure 5.4**. For SM, the endothermic gel → L_α phase transition is marked by a broad peak centered at 313.7 K (40.7 °C), while there is

no visible indication of a pretransition (inset). The 7.5 mol% Chol bilayer also shows a broad main transition (313.1 K, 40.1°C) with no measurable pretransition (inset). The main phase transition temperature for SM and the 0.6°C shift to lower temperatures seen with the inclusion of Chol correlates well with previous reports [129, 130, 152, 153, 172, 201]. Although pretransitions have been reported in the DSCs of SM, they have only been observable for synthetic and/or purified SM, with pretransition temperatures at approximately 301 K for purified 16:0-SM [172, 193, 195, 196], from 293 K to 309 K for synthetic 18:0-SM (depending upon hydration) [161, 202], and ~312 K for 24:0-SM [124, 175, 195]. The lack of an observable pretransition in the DSC shown here suggests the pretransition observed in the ^{31}P MAS NMR line width data between 300 K and 310 K is not the result of a bulk gel → gel phase transition.

5.3.3 Variation of ^{31}P MAS CSA with Cholesterol and Temperature

A second argument is that the observed line width variation during this gel phase pretransition is the result of purely dynamical changes occurring on the ^{31}P CSA timescale. The variations of the CSA parameters from the ^{31}P MAS NMR spectra as a function of cholesterol concentration and temperature have therefore been explored. The ^{31}P MAS NMR CSA parameters for pure SM and SM with varying mol% of Chol are displayed in **Figure 5.5a** while the temperature variation for these mixtures is shown in **Figure 5.5b**. For samples with < 33 mol% Chol there is a dramatic reduction in the ^{31}P CSA at T_m, and the production of a symmetric ^{31}P CSA tensor. This change is indicative of the main gel to L_α phase transition, and shows that there are headgroup motions on the order of a ~ 15 ppm (3600 Hz) leading to partial averaging of the ^{31}P CSA tensor.

Below the main gel to L_α phase transition the 0 mol% Chol (pure SM) sample has ^{31}P CSA value of $\Delta\sigma$ = 56.8 ppm (296 K) and corresponds to the gel (s_o) phase. The ^{31}P CSA anisotropy decreases to $\Delta\sigma$ = 55.6 ppm with the addition of 5 mol% Chol. The CSA again decreases for the 7.5 mol% Chol mixture ($\Delta\sigma$ = 54.3 ppm), and remains at the same value for bilayers containing 10 and 21 mol % Chol. Only at 33 mol % Chol is an additional ~10 ppm decrease in CSA observed with $\Delta\sigma$ = 44.3 ppm (296 K), which corresponds to the l_o phase. In the intermediate Chol concentration range no distinct ^{31}P NMR spectral signature for the co-existing s_o+l_o phase was observed. The decrease in the ^{31}P CSA with the addition of Chol is consistent with the averaging between the two phases, with increasing l_o concentration at higher Chol content. Analysis of this ^{31}P CSA trend is complicated by the presence of multi-component gel (s_o) phase ^{31}P NMR spectra

[122], and variation in the degree of magnetic alignment. A detail discussion of the ^{31}P NMR CSA variation will be presented in a future publication.

Above T_m the ^{31}P CSA shows only a minor variation ranging from $\Delta\sigma$ = 44.5 ppm (318 K) for the l_d phase (0 mol% Chol) to $\Delta\sigma$ = 43.6 ppm (318 K) for the l_o phase (33 mol% Chol). These results support the argument that the SM headgroup dynamics are very similar for the concentration range of Chol studied. The invariance of the ^{31}P CSA to the two-phase (l_d+l_o) regions most likely results from the rapid exchange of lipid between the l_o and l_d phases on the time scale of hundred of μs, suggesting very small domain sizes (~10 nm) as previously discussed [122], or that the ordering of the acyl chains in the l_o phase has a minimal impact on the dynamics detectable through measurement of the ^{31}P CSA tensor.

The overall decrease in ^{31}P CSA with increasing temperature in the gel phase does not correlate with the increasing ^{31}P MAS NMR line width shown in **Figure 5.2**, since the predicted increase in headgroup dynamics should narrow the ^{31}P isotropic line width in this region. Because this predicted trend was not observed in the FWHM data, the observed gel phase pretransition is not being attributed to a purely dynamical change on a timescale measurable by the ^{31}P CSA (~ 12 kHz). It has been suggested that the ^{31}P CSA reduction results purely from a change in the headgroup orientation near T_m, such that the increasing ^{31}P MAS NMR line width in the gel pre-transition reflects an increase in the heterogeneity of this orientation. The observation of a symmetric ^{31}P CSA tensor above T_m and an asymmetric tensor below T_m argues against the CSA reduction occurring entirely from a change in headgroup orientation.

5.3.4. Variation of ^{31}P NMR T_2 with Cholesterol and Temperature

Spin-spin (T_2) relaxation measurements were also performed to complement the ^{31}P CSA results. The ^{31}P T_2 relaxation times are sensitive to molecular processes with correlation times equal to the inverse chemical shift anisotropy determined from the width of the SSB pattern (**Figure 5.1a**, $\Delta\sigma$ ~80 ppm or ~20 kHz) [138]. The results of the ^{31}P T_2 relaxation measurements as a function of temperature are displayed in **Figure 5.6**. Below T_m, the T_2 relaxation times are similar for pure SM, 5 mol% Chol, and 7.5 mol% Chol mixtures (1-2 ms), consistent with a dynamically restricted headgroup. At the main phase transition temperature, a sharp increase in T_2 is seen for SM bilayers with less than 10 mol% Chol and the L_α phase is marked by values ranging from 8 – 10 ms, indicating a dynamically mobile phase. For >10 mol% Chol the T_2 measurements display

a gradual increase with higher temperatures, throughout the gel (s_o) phase and into the L_α (or l_d) phase. For the higher Chol concentrations the main phase transition is not clearly distinguishable with the T_2 measurements, similar to the ^{31}P MAS NMR line width measurements. The increasing T_2 values correlate well with the decreasing FWHM values for SM bilayers with > 10% Chol, indicating an increase in the motional processes of the phosphorous headgroup and a reduction in the correlation time governing T_2. The similarity of ^{31}P T_2 relaxation times for intermediate Chol content also shows that these relaxation measurements are not sensitive to the presence of the two-phase s_o+l_o or the l_d+l_o regions. The ^{31}P NMR T_2 measurements are also in agreement with the ^{31}P CSA observations, revealing no pretransition in the gel phase for SM with Chol concentrations <10 mol%. These results supports the conclusion that the molecular motions measurable by the ^{31}P T_2 and CSA (12-20 kHz) are not responsible for the ^{31}P MAS NMR line width gel phase pretransition observed in the FWHM data.

5.3.5 Impact of Proton Decoupling, Field Strength, and Sample Spin Rate on Line Width Broadening

The ^{31}P CSA is the dominant nuclear interaction for ^{31}P at high frequencies [203], and therefore the ^{31}P MAS NMR spectra reported here were collected without ^{1}H decoupling at 14.1 T. However, due to the unusual increase in line width, the effects of heteronuclear ^{1}H-^{31}P dipolar coupling, magnetic field strength, and sample spin rate were also explored in an effort to explain the observed gel phase pretransition. Previously, Holland *et al.* [122] showed that residual ^{1}H-^{31}P dipolar coupling was still present under ^{31}P MAS conditions at a spinning speed of 2 kHz, while in the L_α (or l_d) phase, the heteronuclear dipolar coupling was averaged out. A similar effect can be seen in **Figure 5.7a**, where a narrowing of ~ 113 Hz is seen in the ^{31}P MAS NMR line width of SM (0 mol% Chol) at 296 K with the addition of ^{1}H decoupling. Despite this narrowing, the overall change in ^{31}P MAS NMR line width during the pretransition range is the same with and without ^{1}H decoupling supporting the argument that ^{1}H-^{31}P dipolar interactions are not responsible for the observed line width variations.

The impact of magnetic field strength on ^{31}P MAS line width is shown in **Figure 5.7a**. These experiments show that the gel phase pretransition is essentially unaffected by changes in the magnetic field, with the overall change in ^{31}P line width (ΔFWHM) in the same temperature range (296 K – 310 K) reveals similar values for SM at 9.4 T (140 Hz) and SM at 14.1 T (173 Hz). The dramatic decrease in line width marking the main

transition at both fields is also approximately the same (320 Hz at 9.4 T compared to 380 Hz at 14.1 T). In the L_α (or l_d) phase, however, the 9.4 T line widths are slightly narrower (~ 50 Hz) than the line widths seen at higher field, partially due to the difference in the field homogeneity and quality of shimming with a different magnet. Spin-spin T_2 relaxation measurements were also conducted at a lower magnetic field (data not shown) and did not reveal any correlated change in T_2 values. These results suggest that the observed ^{31}P MAS NMR line width variation in the gel phase pretransition is not directly tied to the magnitude of the ^{31}P CSA.

It has also been suggested that the increase in line width observed in the gel phase pretransition arises from destructive interference between the coherent averaging of MAS and incoherent molecular averaging processes [204, 205]. To address this possibility, the ^{31}P MAS NMR line width was measured at different spinning speeds at 9.4 T (**Figure 5.7b**). Increasing the sample spinning speed from 2 kHz, to 4 kHz and finally 6 kHz dampens the observed gel phase pretransition, with a reduction in the ^{31}P MAS NMR line width variation of 60 (ν_r = 4 kHz) and 80 Hz (ν_r = 6 kHz). Temperature effects due to frictional spinning under MAS have been accounted for, and result in a shift of the pretransition, not a dampening of the transition with increasing spin rate. This result shows that the gel phase pretransition observed in the ^{31}P MAS line width variation results from slow headgroup motions with correlation times on the order of 2 to 6 x10^{-5} s ($\tau_c \sim 0.7/\omega_r$, where ω_r is the MAS rotor frequency in rad/s) [205]. This is a slightly slower timescale than measured by the ^{31}P T_2 relaxation and CSA studies, which showed no clear evidence of a pretransition. The addition of Chol increases the rate of the headgroup motions reducing the interference with the coherent averaging of the MAS.

One final possibility for this observed gel phase pretransition in SM is a subtle change in the local headgroup structural environments (leading to a distribution of chemical shifts) just prior to the gel $\rightarrow L_\alpha$ phase transition that is eliminated with the addition of cholesterol. Compared to other lipids with a glycerol backbone, SM has been shown to have unique intra- and intermolecular hydrogen bonding properties due the hydroxyl and amide groups on the sphingosine backbone [115, 160, 197, 198], that may be disrupted by the addition of Chol. The SM headgroup may undergo significant structural changes during the gel $\rightarrow L_\alpha$ transition with the ^{31}P MAS NMR line width variations reflecting SM preparing for this transition. With increasing Chol content, these intra- and intermolecular bonding interactions are reduced, and correspondingly the

required structural changes in SM diminished. On the other hand this increased distribution of ^{31}P NMR chemical shifts should not be influenced by the variation in spinning speed as was observed experimentally.

5.4 Conclusions

The ^{31}P MAS NMR spectra for SM and SM with 5, 7.5, 10, and 21 mol% Chol have been presented. The variations in ^{31}P MAS NMR line width indicate a transition is occurring in the gel phase prior to the main gel → L_α. The incorporation of Chol into the bilayer diminishes this gel phase transition. Possible explanations for this observation included a gel → gel phase transition, dynamical changes, and changes in correlation times. The DSC results show it is not a bulk gel → gel transition. Analysis of the ^{31}P NMR data show that it does not result from CSA, ^{1}H-^{31}P dipolar coupling or T_2 relaxation effects. The observed pretransition appears to be due to slow motions on the order of the MAS spinning speed or a result of a local disorder in the headgroup region, possibly due to changes in intramolecular and/or intermolecular hydrogen bonding. Although subtle, these changes are readily apparent in the ^{31}P MAS NMR as an increase in line width that is diminished with the addition of 10 mol % cholesterol. The results demonstrate how low concentrations of cholesterol can have an impact on the headgroup structure/dynamics of sphingomyelin, further illustrating the complexity of the sphingomyelin in membrane systems.

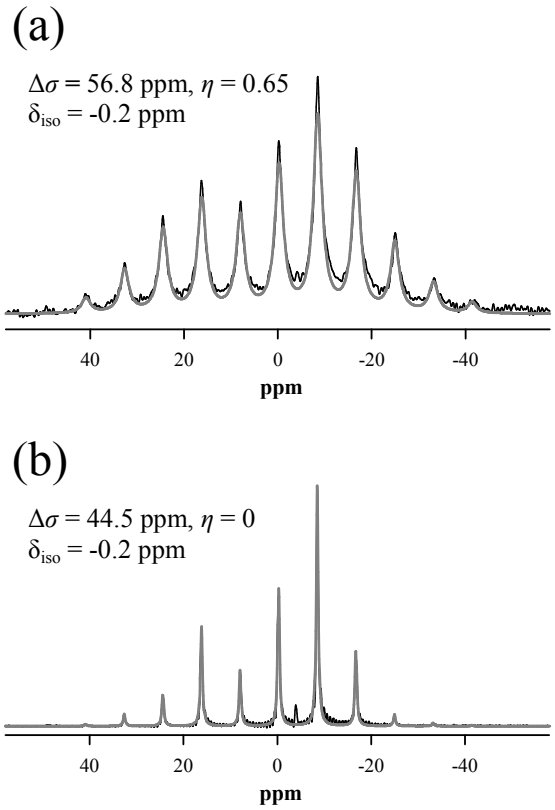

Figure 5.1 The ^{31}P MAS NMR spectra (black lines) and simulations (gray lines) of SM bilayers (v_r = 2 kHz) at (a) 296 K (below T_m ~ 313 K) and (b) 318 K. The ^{31}P CSA parameters obtained from simulations are shown.

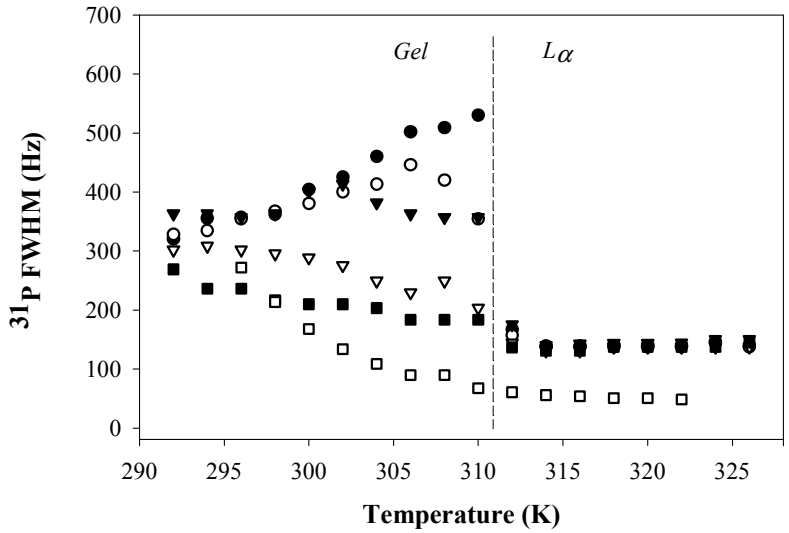

Figure 5.2 The ^{31}P MAS NMR isotropic full width at half maximum (FWHM) line width as a function of temperature for (●) SM, (○) 5 mol% Chol, (▼) 7.5 mol% Chol, (∇) 10 mol% Chol, and (■) 21 mol% Chol. SM and 33 mol% Chol (□) is shown for comparison and is from a previous work [122].

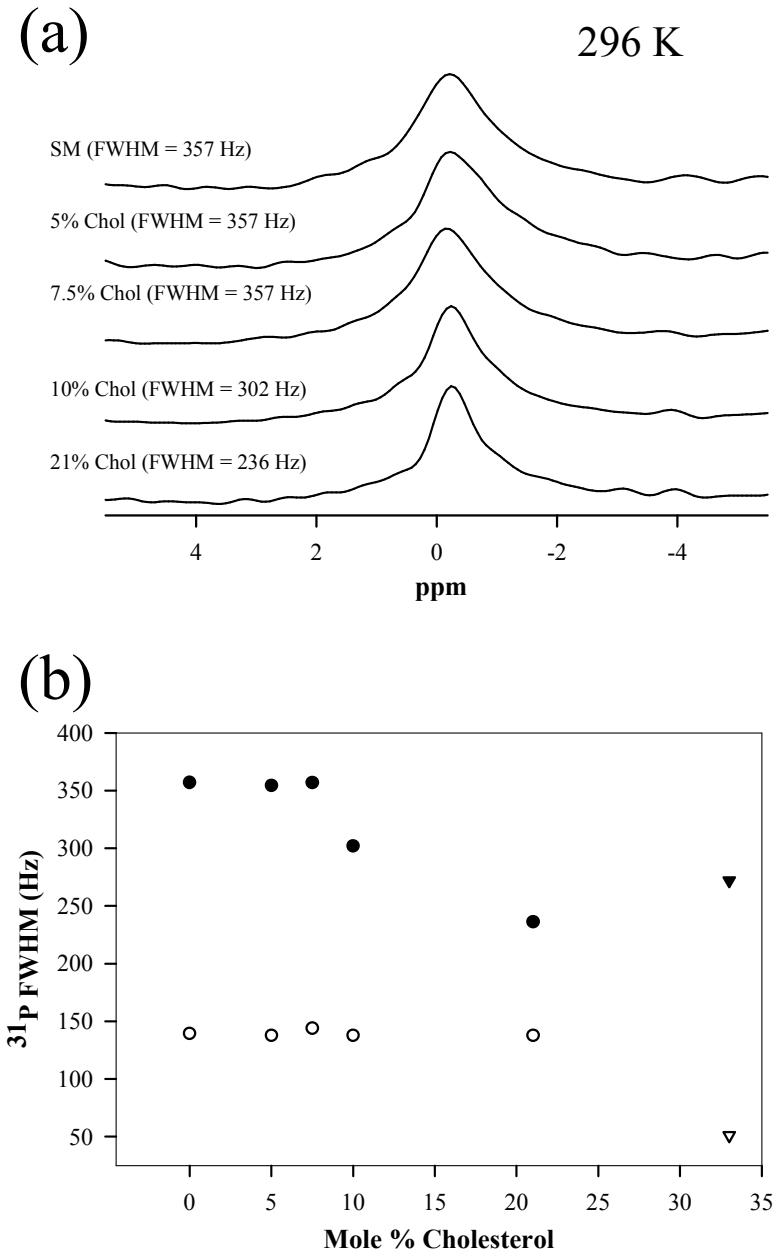

Figure 5.3 The (a) ^{31}P MAS NMR isotropic chemical shift region of pure SM and SM with 5, 7.5, 10 and 21 mol% Chol at 296 K. The line width (b) as a function of Chol concentration at (●) 296 K and at (○) 318 K. SM and 33 mol% Chol at (▼) 296 K and (∇) 318 K from previous studies are also shown [122].

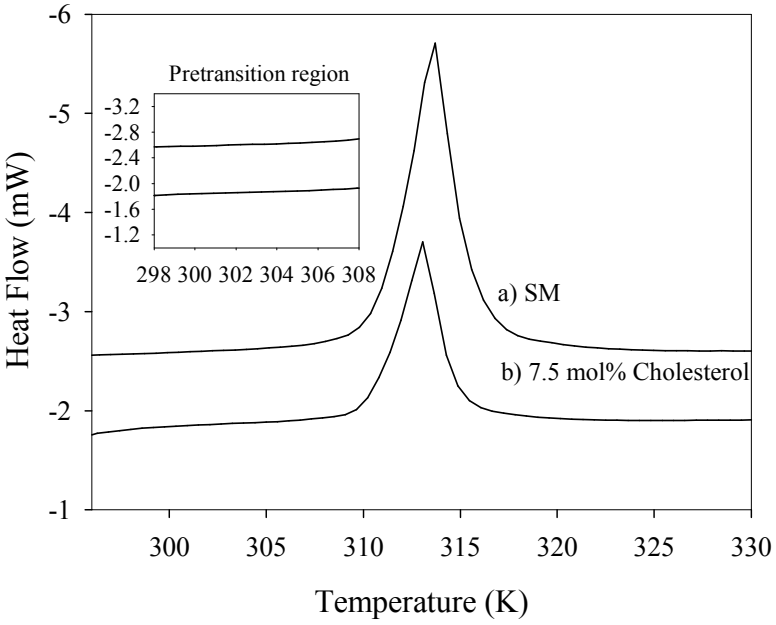

Figure 5.4 DSC profiles of (a) SM and (b) SM with 7.5 mol% cholesterol. The pretransition temperature range is expanded in the inset.

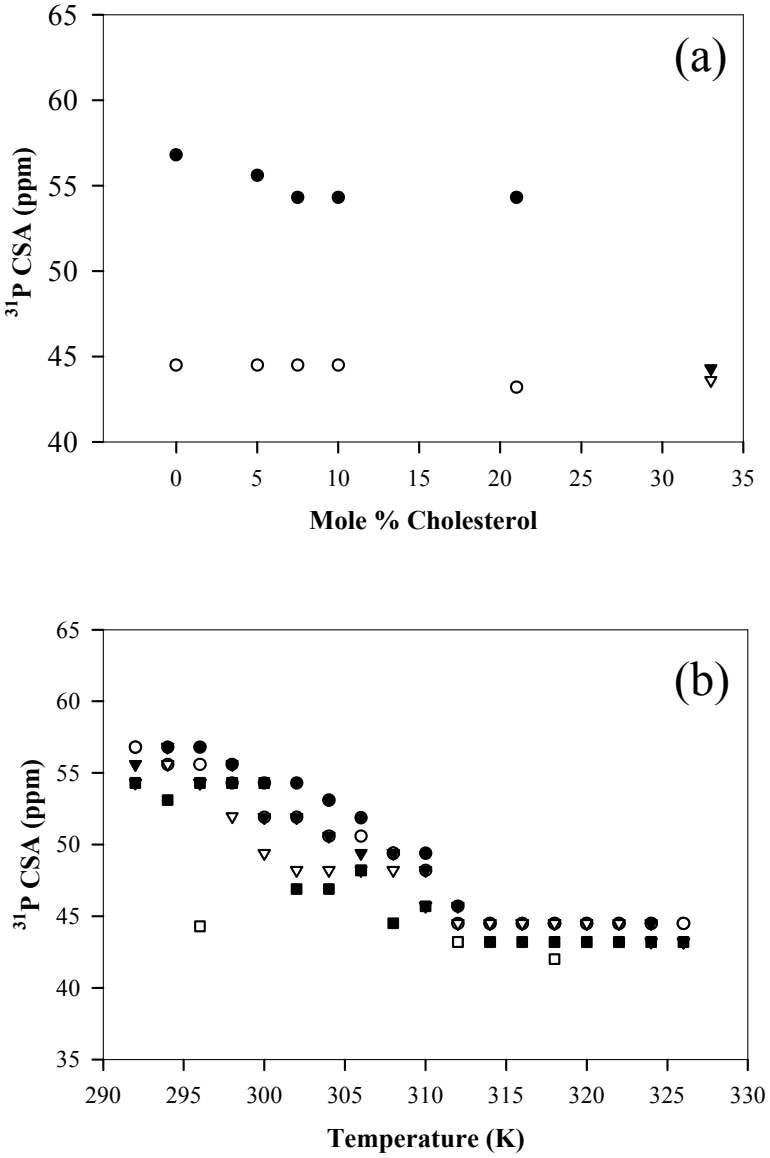

Figure 5.5 (a) The ^{31}P CSA ($\Delta\sigma$) parameters extracted from ^{31}P MAS NMR fits of the spinning sideband manifold at (●) 296 K and (○) 318 K as a function of Chol concentration. SM and 33 mol% Chol at (▼) 296 K and (▽) 318 K from previous studies are also shown [122]. (b) The ^{31}P CSA parameters as a function of temperature for (●) SM, (○) 5 mol% Chol, (▼) 7.5 mol% Chol, (▽) 10 mol% Chol, and (■) 21 mol% Chol. SM and 33 mol% Chol (□) is shown at select temperatures for comparison and is from a previous work [122].

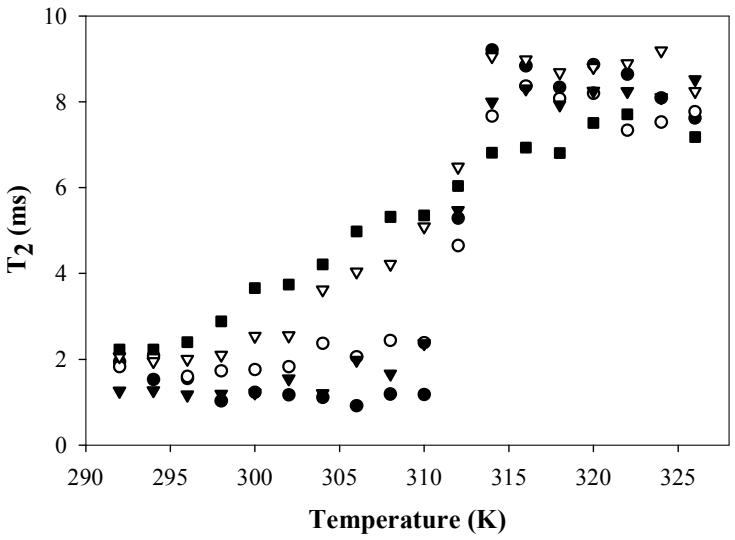

Figure 5.6 ^{31}P MAS NMR T_2 relaxation times as a function of temperature for (●) SM, (○) 5 mol% Chol, (▼) 7.5 mol% Chol, (∇) 10 mol% Chol, and (■) 21 mol% Chol.

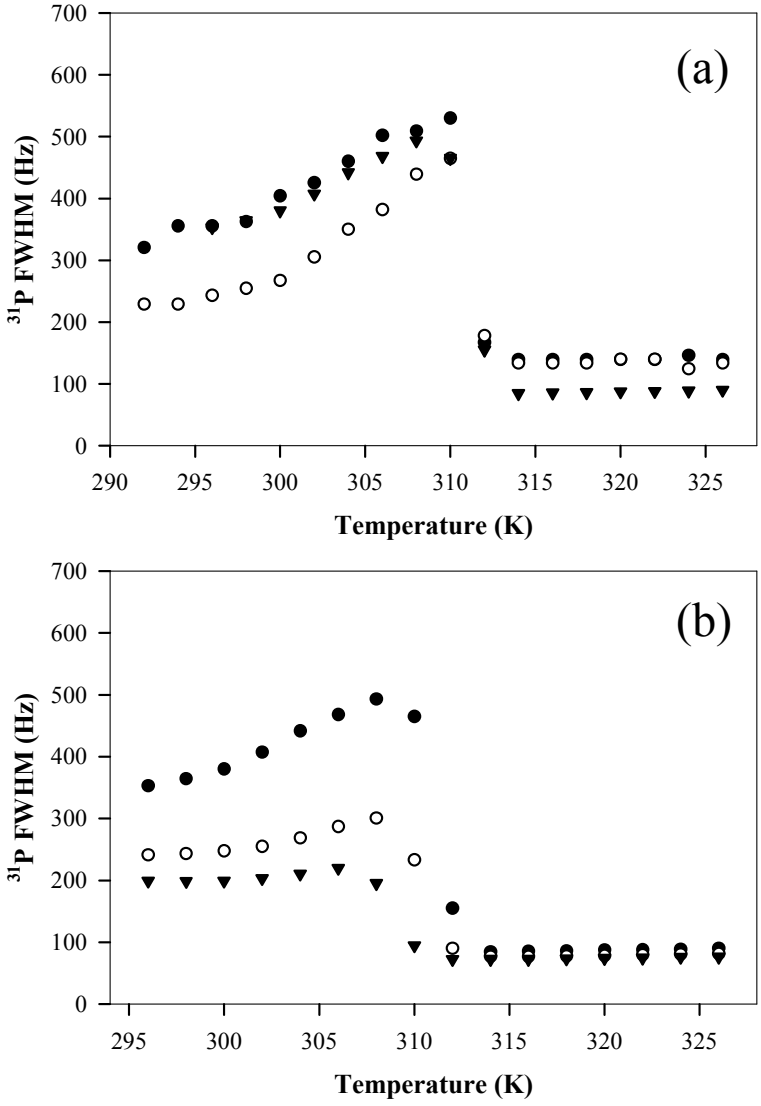

Figure 5.7 (a) The ^{31}P MAS NMR isotropic full width at half maximum (FWHM) line width as a function of temperature for (●) SM at 14.1 T, (○) SM with ^{1}H decoupling at 14.1 T and (▼) SM at 9.4 T. (b) The ^{31}P isotropic full width at half maximum (FWHM) line width for SM at 9.4 T as a function of temperature and rotor frequency at (●) ν_r = 2 kHz, (○)ν_r = 4 kHz, and (▼)ν_r = 6 kHz.

Chapter 6

Unique Backbone-Water Interaction Detected in Sphingomyelin Bilayers with $^{1}H/^{31}P$ and $^{1}H/^{13}C$ HETCOR MAS NMR Spectroscopy

6.1 Introduction SM Water Interactions

Sphingomyelin (SM) and phosphatidylcholine (PC) comprise the majority of eukaryotic cell membranes [30]. Sphingomyelin is particularly interesting because of its role in the formation of lipid rafts [5]. There is increasing evidence that cholesterol prefers to interact with saturated chain sphingolipids over saturated chain glycerophospholipids of similar chain lengths [33]. There are only two main structural differences between these two classes of lipids: (1) the sphingosine backbone in sphingolipids compared to the glycerol backbone in the glycerophospholipids and (2) the trans double bond between the C4 and C5 carbon of the acyl chain in sphingolipids (see structure in **Figure 6.2**) compared to no double bond in glycerophospholipids (see structure in **Figure 6.4**). The presence of the double bond in sphingolipids is thought to be responsible for the tighter acyl chain packing and thus, higher chain order parameter observed for sphingolipids over glycerophospholipids [31, 206].

The unique role of SM in membrane function and the formation of raft phases could be due to the sphingosine backbone. The sphingosine backbone has both hydrogen bond acceptors (the amide group and carbonyl group) and a hydrogen bond donor (the hydroxyl group) while the glycerol backbone of PC contains only hydrogen bond acceptors (the carbonyl groups). This unique backbone of SM permits participation in both intra- and intermolecular hydrogen-bonding interactions. The formation of a possible hydrogen bonded network at the interfacial region of sphingomyelin may explain a more favorable interaction with cholesterol by shielding it from interactions with water. This is similar to the previously proposed “Umbrella model” where the main requirement for cholesterol incorporation in a lipid bilayer is the phospholipid headgroup’s ability to cover the hydrophobic cholesterol molecules from interactions with water [187, 207]. This model was used to explain the cholesterol solubility limits in

different lipids including why PC with its larger headgroup can incorporate more cholesterol than the smaller headgroups of phosphatidylethanolamine (PE) [187, 207]. Water could potentially be involved in this hydrogen-bonded network at the SM interface and the possibility of intermolecular hydrogen-bonded water bridges between neighboring SM molecules in bilayers has been proposed [128]. Unfortunately, experimental evidence that supports the existence of this hydrogen-bonded network in SM bilayers and the involvement of water at the sphingosine backbone is limited. Infrared and Raman spectroscopies have been used to investigate the role of inter- and intra-molecular bonds in SM, unfortunately the results are inconclusive with respect to assignments in the amide I and amide II bands. High resolution ^{1}H and ^{31}P NMR have argued for an intramolecular hydrogen bond between the SM hydroxyl and the phosphodiester group [115, 116, 128], while more recent ^{2}H NMR studies have probed the interfacial polarity and the water/hydroxyl and water/amide exchange rates [208] suggesting that it is the amide residue involved in intermolecular hydrogen bonding.

One-dimensional ^{31}P MAS NMR techniques have been extensively applied to the study of lipid bilayer systems and have been recently utilized to study raft formation in tertiary lipid systems containing cholesterol [122]. A few reports on the application of two-dimensional (2D) $^{1}H/^{31}P$ heteronuclear Overhauser effect spectroscopy (HOESY) [107, 209] have appeared on PC and PE lipids, although the bulk of ^{31}P NOE studies are of the 1D variety [185, 210]. NMR experiments involving $^{1}H/^{13}C$ cross-polarization (CP) have also been shown to be useful in the study of lipid membrane systems and have been implemented in both 1D and 2D experiments (as detailed in Chapter 2). NMR studies involving ^{31}P CP have not been implemented to a large extent because of the long ^{1}H-^{31}P distances and high degree of head group mobility that further averages the dipolar coupling. Only a limited number of lipid reports based on ^{31}P CP have appeared in the literature. In this chapter we present an example of a 2D MAS NMR experiment that utilizes ^{1}H-^{31}P CP and a NOE mixing period. These $^{1}H/^{31}P$ dipolar HETCOR NMR methods are particularly useful for studying intra- and intermolecular interactions in SM by including a NOE mixing period prior to the CP step in the pulse sequence (see **Figure 6.1**). Of specific interest is the ability to probe interactions at the lipid headgroup and backbone. A unique dipolar network involving strongly associated water is detected at the backbone of SM that is not detected in PC lipids. Further characterization of this intermolecular dipolar proton network was provided by 2D $^{1}H/^{13}C$ INEPT HETCOR experiments with NOE mixing.

6.2 SM Interaction Materials and Methods

6.2.1 Materials

Egg SM, 1,2-dipalmitoyl-*sn*-glycero-3-phosphocholine (DPPC), 1,2-dimyristoyl-*sn*-glycero-3-phosphocholine (DMPC) and 1,2-dioleoyl-sn-glycero-3-phosphocholine (DOPC) were obtained from Avanti Polar Lipids and used as received. The SM had the following acyl chain composition: 84% 16:0, 6% 18:0, 2% 20:0, 4% 22:0, 4% 24:0 and contained no unsaturated acyl chains.

6.2.2 Sample Preparation

Pure lipid samples were prepared by mixing the lipid with de-ionized water (pH = 7.5) in a conical vial with a vortex mixer. This was followed by a minimum of 5 freeze-thaw cycles in dry ice and a warm water bath set to 333 K (above the liquid crystalline phase transition for all lipids). Buffer was not used in any of the lipid mixtures to prevent multilamellar vesicle (MLV) fragmentation due to freeze-thaw cycling in the presence of salt [149]. Thus, the samples in this study are large MLV's greater than ~ 1 μm in diameter. Samples containing multiple lipid constituents were first combined and dissolved in chloroform followed by vacuum drying overnight at room temperature to remove the solvent. The samples were then hydrated with the above procedure. All lipid samples were 33 wt% phospholipid. The lipid samples were transferred to 4 mm zirconia MAS rotors and sealed with kel-F inserts and caps. The typical volume of MLV sample for NMR analysis was 50-100 μL corresponding to 25-50 mg of phospholipid. The samples were stored in a -20 ºC freezer when NMR experiments were not being performed.

6.2.3 NMR Spectroscopy

NMR spectra were collected on a Bruker Avance 600 spectrometer equipped with a 4 mm broadband double resonance MAS probe spinning at 5 kHz. The temperature was set above the liquid crystalline phase transition of the lipid and controlled to ± 0.2 K with a Bruker VT unit. The reported temperature is adjusted to account for heating effects due to MAS and ^{1}H decoupling as described previously [73]. The spectra were collected in a two-dimensional HETCOR fashion with $^{1}H \rightarrow ^{31}P$ ramped

CP. A moderate ^{1}H two pulse phase modulation (TPPM) [114] decoupling field strength of 22.5 kHz was applied following the CP contact pulse thru acquisition of the free induction decay using a 15º phase shift [114]. CP was achieved with a ramped (50→100%) spin-lock pulse on the ^{1}H channel and a square pulse on the ^{31}P channel [110]. The ^{1}H $\pi/2$ pulse length was 4 μs and the RF field strength for CP at 100% power was 62.5 kHz. In order to monitor ^{1}H magnetization exchange via the NOE, a mixing period, τ_m, was included in the 2D HETCOR pulse sequence (see **Figure 6.1**) as previously described [111]. We refer to these 2D NMR experiments as $^{1}H/^{31}P$ dipolar HETCOR with NOE mixing. Typical acquisition parameters for 2D experiments were 128 scan averages, 128-256 t_1 points, and a 3 s recycle delay. The ^{1}H-^{13}C INEPT MAS NMR HETCOR experiments with ^{1}H-^{1}H magnetization exchange were performed as previously detailed [200]. For these INEPT experiments a 10 kHz spinning speed was utilized with the INEPT interpulse delays or Δ_1 = 2.2 ms and Δ_2 = 1.2 ms, respectively. Additional optimization details are described elsewhere [200].

6.3 SM Water Contacts Results and Discussion

6.3.1 $^{1}H/^{31}P$ Dipolar HETCOR NMR of SM Bilayers

The 2D $^{1}H/^{31}P$ dipolar HETCOR NMR spectra of SM bilayers collected with two distinct ^{1}H-^{1}H NOE mixing periods, τ_m, are displayed in **Figure 6.2** where (A) τ_m = 20 μs and (B) τ_m = 500 ms. In **Figure 6.2A** the mixing period can be considered essentially zero and no ^{1}H-^{1}H magnetization exchange via the NOE effect is observed. This can be considered a baseline spectrum where ^{1}H cross peaks only appear for proton environments that CP to the ^{31}P nuclei. For a 1 ms contact time, strong cross peaks are observed for the Hα and the SM lipid backbone protons: H1, H2, and H3 (See **Figure 6.2** for numbering scheme and assignments). The correlation with these different ^{1}H environments is as expected since they are spatially closest to the ^{31}P headgroup and thus, have the strongest dipolar coupling with similar local dynamics. It is assumed that the ^{1}H resonance at δ = +4.0 ppm is dominated by the H1 proton environment due to its close proximity however, contributions from the H2 and H3 protons can not be discounted since these three ^{1}H resonances overlap [102, 122]. Weaker ^{1}H-^{31}P correlations are also observed for the 2′ proton adjacent to the carbonyl and the main chain $(CH_2)_n$ protons. Observation of a correlation peak for the 2′ group is not surprising

considering that orientation of the phospholipid headgroups are essentially perpendicular to the lipid bilayer normal positioning the ^{31}P close enough to CP from this proton, particularly if an intramolecular hydrogen bond between the amide proton and the phosphate ester oxygen is considered [159, 160]. However, the distance between the main chain $(CH_2)_n$ protons and the ^{31}P headgroup is too large for the observed correlation at this contact time to be ascribed to an intramolecular contact. Instead the ^{1}H-^{31}P correlation involving the $(CH_2)_n$ results from intermolecular contact with adjacent lipid molecules. The observation of unusual intermolecular ^{1}H-^{1}H NOE contacts in phospholipids has been discussed in depth and attributed to the high degree of disorder within the lipid bilayers [51, 52, 57]. The lack of a CP correlation between H_2O and ^{31}P reveals that there is not a H_2O environment with significant direct ^{1}H-^{31}P dipolar coupling, suggesting that H_2O molecules interacting with the phosphate group are not bound strongly enough to efficiently CP ^{31}P at these contact times. Contact times as long as 5 ms were attempted with no observation of a H_2O cross peak. The result shown in **Figure 6.2A** demonstrates that 2D $^{1}H \rightarrow ^{31}P$ CP MAS NMR is a powerful tool for studying both intermolecular and intramolecular contacts near the headgroup and backbone of SM.

The 2D ^{1}H-^{31}P dipolar HETCOR MAS NMR spectrum of SM presented in **Figure 6.2B** was collected with a τ_m = 500 ms ^{1}H-^{1}H mixing period to probe proton magnetization exchange via the NOE effect. The observed ^{1}H-^{31}P correlations represent ^{1}H magnetization originally from different proton environments that interact via dipolar cross relaxation with protons involved in the final CP to the ^{31}P nucleus (i.e. the H1, H2, H3, H2′ and Hα proton environments). For this long mixing period the Hα, H1, and the H2′ resonances have completely disappeared. The loss of these Hα, H1 and H2′ correlations results from spin-lattice relaxation and from cross relaxation between these protons and other lipid protons that do not CP to the ^{31}P headgroup. In these long mixing time experiments (τ_m = 500 ms) several new resonances corresponding to the choline Hγ protons, the terminal methyl CH_3 protons, and H_2O have emerged. It should also be noted that the ^{1}H-^{31}P correlation involving the $(CH_2)_n$ has increased in intensity. Of particular interest is the observation of a strong correlation involving H_2O ($\delta(^{1}H)$ = + 4.8 ppm) due to intermolecular contact between H_2O and a proton involved in the final ^{1}H-^{31}P CP step. A stack plot of the indirectly detected ^{1}H spectra as a function of mixing time (τ_m) for SM bilayers provides more insight into this interaction and is depicted in **Figure 6.3**. At mixing times as short as 10 ms a H_2O resonance is clearly observed indicating a strong ^{1}H-^{1}H magnetization exchange between H_2O and SM. When

comparing the ^{1}H spectrum collected with a 1 ms and 10 ms mixing period the following observations are made: (1) the intensity of Hα decreases by ~ 8% (2) the intensity of H1 decreases by ~ 23% (3) the $(CH_2)_n$ increases by 52% (4) H2′ increases by ~ 11% and (5) a H_2O resonance is observed that accounts for 13% of the total proton intensity. Since both Hα and H1 decrease in intensity, these protons participate in dipolar cross relaxation where magnetization is rapidly transferred to the other proton environments. The large increase in intensity of the $(CH_2)_n$ is not due to cross relaxation from H1 or Hα (since the increase is greater than the combined decrease in signal intensity), but is assumed to result from additional magnetization exchange between neighboring $(CH_2)_n$ groups on the chain and protons involved in the final ^{1}H-^{31}P step. The appearance of a strong H_2O resonance with rapid intensity buildup must therefore result from cross relaxation between the H_2O and the Hα and/or H1 environments (involved in the final ^{1}H-^{31}P CP step). This argument is also supported by the observation of the $(CH_2)_n$ correlations being smaller than the H_2O correlations (for τ_m > 10 ms); this precludes a H_2O to $(CH_2)_n$ to backbone proton multi-step exchange process. This is also consistent with the faster decrease in the H1,2,3 correlation with increasing mixing time compared to the intensity of the Hα correlation. This result indicates that there is a unique H_2O environment located within the lipid backbone region, however, the observed magnetization exchange process is complicated and quantifying the exact contribution from H1 and Hα to H_2O and/or H2′ is somewhat ambiguous. The $^{1}H/^{13}C$ INEPT HETCOR NMR with NOE mixing results presented below clarify this problem and show that the H_2O is indeed located at the SM backbone.

6.3.2 $^{1}H/^{31}P$ 2D Dipolar HETCOR of DOPC Bilayers

The observation of this strong H_2O correlation in the 2D $^{1}H/^{31}P$ dipolar HETCOR spectra of SM as a function of NOE mixing time prompted the study of other lipid membrane systems. The 2D $^{1}H/^{31}P$ dipolar HETCOR spectra of DOPC bilayers with a NOE mixing period, τ_m = 20 μs and 500 ms, are shown in **Figure 6.4A** and **6.4B**, respectively. Again, for short mixing times only correlations between proton environments that CP and the ^{31}P headgroup are observed. It is interesting to note that all the glycerol backbone protons (g1, g2, and g3), along with the headgroup Hα, and Hγ protons are observed. The latter is surprising considering these methyl groups are located 6 bonds apart suggesting that instead of an intramolecular interaction that these

correlations result from an intermolecular interaction with neighboring DOPC molecules due to membrane disorder. The choline Hγ protons do not CP to ^{31}P at the same contact time in SM indicating that DOPC are more disordered than SM bilayers, or that these protons environments in SM are more dynamic. The other interesting difference between SM and DOPC is the significant ^{1}H-^{31}P correlation observed for $(CH_2)_n$ and C2′ in SM (Fig. 2B) that is essentially not observed in the spectrum of DOPC (**Figure 6.4B**) for the same length mixing periods. Since the $(CH_2)_n$ interaction is intermolecular in origin, this strong correlation is consistent with the tighter chain packing of SM versus DOPC previously observed by ^{2}H NMR studies [206]. For a 500 ms mixing period ^{1}H-^{31}P correlations are observed for almost all environments (**Figure 6.4B**) consistent with rapid ^{1}H-^{1}H magnetization exchange resulting from lipid disorder as previously proposed [51, 52]. The one exception is that no correlation between H_2O and the ^{31}P of the headgroup is observed for mixing times between 1 – 500 ms (see **Figure 6.5** for a stack plot of the ^{1}H dimension through the ^{31}P DOPC resonance as a function of τ_m); in contrast with the SM results presented in **Figures 6.2** and **6.3**. In addition, other PC lipids systems such as DMPC and DPPC displayed similar results to DOPC with no $^{1}H/^{31}P$ HETCOR correlation between H_2O and ^{31}P observed (data not shown). This again supports that the strong dipolar network observed between SM and H_2O arises from unique interactions at the sphingosine backbone.

6.3.3 $^{1}H/^{13}C$ 2D INEPT HETCOR of SM and DOPC Bilayers

To further investigate these water-backbone interactions in SM a series of 2D ^{1}H-^{13}C INEPT HETCOR MAS NMR experiments were performed as shown in **Figure 6.6**. By utilizing the INEPT component the final ^{1}H-^{13}C transfer results from ^{1}H-^{13}C J couplings, such that for the interpulse delays utilized the final ^{13}C correlation results from directly bonded protons and does not arise from through space ^{1}H-^{13}C dipolar couplings. This is confirmed in **Figure 6.6A** were only the expected direct one-bond C-H correlations are observed. Inclusion of a 50 ms ^{1}H-^{1}H NOE mixing period in this sequence [200] now allows correlations between different proton environments to be measured in the ^{13}C dimension (analogous to a ^{1}H-^{1}H relay experiment) as seen in **Figure 6.6B**. In this 2D spectrum multiple new correlation resonances are observed. We are particularly interested in the interactions with H_2O. The ^{13}C NMR spectrum along the ^{1}H chemical shift of H_2O (δ = +4.8 ppm) is shown as the upper projection in **Figure 6.6B**. Correlations between H_2O and the protons on the C4, C5, C3 and C2/Cγ carbons are

observed. The ^{13}C resonances of the C2/Cγ environment overlap not allowing us to identify which interaction is occurring, but it assumed it is primarily with the C2 environment. Minor correlations between H_2O and the protons on the C1, Cα and Cβ carbons were also detected. H_2O correlations with protons at other carbon environments were not observed. Similar 2D ^{1}H-^{13}C INEPT experiments on DOPC with an equivalent 50 ms mixing time revealed no correlations between H_2O and any of the protons on that lipid system (results not shown). These results also support the argument that there is a unique H_2O environment associated with the sphingosine backbone in SM.

6.3.4 $^{1}H/^{31}P$ 2D Dipolar HETCOR of SM/DOPC Bilayers

The 2D $^{1}H/^{31}P$ dipolar HETCOR spectrum for a 50:50 lipid mixture of SM and DOPC is shown in **Figure 6.7**. For a short τ_m = 20 μs mixing time the ^{31}P resonances for SM (δ = -0.3) and DOPC (δ = -0.9) are clearly resolved. The 0.6 ppm increase in the chemical shift of SM has been attributed to hydrogen bonding motifs that are not present in phosphatidylcholines [160]. The ^{1}H dimension displays resonances resulting from protons that CP to the headgroup ^{31}P nuclei similar to the pure lipid samples (see **Figure 6.2A** and **Figure 6.4A**). The higher intensity of the DOPC spectrum compared to SM, indicates an improved CP efficiency for DOPC at 1 ms contact time. This suggest that the ^{1}H-^{31}P dipolar coupling is smaller in SM than DOPC in agreement with previous measurements of the ^{1}H-^{31}P dipolar coupling in similar SM and PC lipids [46]. Measurements of the ^{31}P chemical shift anisotropy in SM/DOPC mixtures indicate similar headgroup dynamics in the liquid crystalline phase [122] pointing towards different ^{1}H-^{31}P distances and different headgroup configurations producing the changes in the dipolar coupling. When the spectrum is collected with τ_m = 500 ms ^{1}H-^{1}H mixing period (**Figure 6.7B**) a significant H_2O resonance is observed for SM while, DOPC only displays a minor H_2O cross peak. This shows that even in mixtures with DOPC a significant interaction between SM and H_2O persists and DOPC has a minor but, detectable interaction with H_2O. This is in contrast with the pure DOPC 2D $^{1}H/^{31}P$ dipolar HETCOR spectrum where no detectable interaction with H_2O was observed under similar conditions (see **Figure 6.5**). This provides some evidence that H_2O may facilitate the interaction between neighboring lipids in mixtures with SM by forming water bridges as proposed previously [128].

6.4 SM Water Contacts Discussion

It is thought that the H_2O contact detected when an NOE mixing period is included in the $^1H/^{31}P$ dipolar HETCOR and $^1H/^{13}C$ INEPT experiments presented here differs from the H_2O that was observed in previous $^1H/^{31}P$ HOESY studies of lipids [107]. In the HOESY studies, a H_2O contact was detected in both PC and SM lipids in contrast with the dipolar HETCOR results presented here, where a H_2O contact is only observed in SM. This is due to the difference between the two NMR experiments utilized in the two studies. In the previous study, ^1H-^{31}P NOEs are detected while, in this study ^1H-^1H NOEs are detected indirectly by the final CP step to ^{31}P. It was concluded in the HOESY work that the contact observed is due to H_2O hydrogen-bonded to the phosphate group in close enough proximity to display a ^1H-^{31}P NOE contact. These H_2O molecules do not CP to ^{31}P (see **Figures 6.2A** and **Figures 6.4A**). This is probably due to a combination of rapid H_2O dynamics and long distances (weak dipolar coupling), resulting in poor ^1H-^{31}P CP efficiency. The H_2O correlations observed in the present study (which are dipolar coupled to Hα and H1 in SM but show no significant dipolar coupling to the headgroup or backbone protons of pure PC lipids) is believed to originate from H_2O hydrogen bonded at the backbone NH or OH groups. If the H_2O contact observed here was simply due to the ones bound to the phosphate group a contact would be expected in the other PC lipids similar to the HOESY studies. Thus, in the SM system the H_2O contact must result from H_2O hydrogen-bonded at the SM backbone.

In a 2D ^1H NOESY NMR spectrum cross-peaks arising from cross-relaxation correlations in the spin-diffusion or slow-tumbling limit ($\omega_0\tau_0$ >>1, negative NOE) will have the same sign as the autocorrelation diagonal (positive phase), and would be expected for both intra- and inter-molecular lipid contacts, as well as water-lipid contacts where the water is closely associated with the lipid and has a lifetime greater than ~ 1 to 10 ns. An example of these positive phase water/lipid correlations are seen in the ^1H NOESY spectrum of SM (supplemental material – Appendix A). Cross-relaxation correlations arising from rapid motion in the extreme narrowing limit will have a negative phase (positive NOE) as observed for small molecules, including water with short association lifetimes (< 1 ns). The latter NOE effects (negative phase) have been reported previously in DOPC lipid systems (34), DMPC (supplemental material – Appendix A), along with the careful characterization by Gawrisch et al. in a ^1H NOESY study on 1-palmitoyl-2-oleoyl-sn-glycero-3 phosphocholine (POPC) where a water/lipid lifetime of 100 ps was determined [211]. Cross-peaks that arise from chemical

exchange involving water will also have the same phase as the diagonal (positive phase), and are not readily distinguished from correlations produced from interactions in the spin-diffusion limit. Positive phase water/lipid correlation peaks have been reported in the NOESY spectrum of monomethyldioleoyl phosphatidylethanolamine and were attributed to either water contacts with long lifetimes or to the exchange process. A similar phase argument holds for the ^{1}H-^{31}P and ^{1}H-^{13}C dipolar HETCOR experiments presented in this paper, since the magnetization exchange during the mixing period occurs via the same mechanism as the NOESY experiment.

It should be noted that we were unable to detect any negative phase correlations involving water in the pure SM or DOPC dipolar HETCOR experiments, or in the HETCOR experiments of the SM/DOPC mixture (**Figures 6.2 – 6.7**). There are a few possible reasons for this result. In the ^{31}P (or ^{13}C) detected NOE exchange experiments described in this paper the final CP (or INEPT) transfer involves magnetization arising from NOE exchange to these specific ^{1}H environments (the Hα, H1, H2 and H3 of SM), as well as the magnetization of these environments that did not undergo exchange (essentially the diagonal intensity of the NOESY spectrum). This produces a dynamic range issue, since the observed NOESY diagonal intensities (positive phase) are typically 2 to 3 orders of magnitude larger than the small negative phase H_2O/lipid NOE correlations. In addition, the other lipid/lipid NOE exchange (positive phase) are also commonly an order of magnitude larger than these H_2O/lipid NOE effects. This would suggest that these small negative phase H_2O/lipid NOE are being swamped by the larger positive phase correlations in the HETCOR experiments. Another factor that may contribute to not observing these negative phase H_2O/lipid NOE correlations is the diminished resolution in the F_1 dimension (128 to 256 points), giving rise to t1 noise. This is why in many NOESY analyses the water correlations are extracted from the F_2 dimension where higher spectral resolution is obtained. This is not an option in the dipolar HETCOR experiments. The resolution in F_1 could also be improved by increasing the number of t_1 increments, but unfortunately this would prove to be highly time extensive for these types of dipolar HETCOR experiments.

In large biomolecules chemical exchange between water and exchangeable protons followed by relay or transfer to non-exchangeable protons is a documented phenomena. These exchange cross-peaks will also have a positive phase in both the ^{1}H NOESY and dipolar HETCOR spectra, are not readily distinguished from the more direct cross-relaxation process, and in many instances may be the dominant process. The

strong positive NOESY cross peaks are clearly observed in 2D ^{1}H NOESY MAS NMR of SM (see supplemental material – Appendix A), as well as the positive correlations observed in the ^{1}H-^{31}P dipolar HETCOR (**Figure 6.2**) and the ^{1}H-^{13}C dipolar HETCOR (**Figure 6.6**) of SM and SM/DOPC are consistent with an exchange process involving the NH and OH protons in the SM backbone. Previous ^{2}H NMR studies of SM have measured the OH exchange rate at ~ 600 s^{-1} (at 45 ^{o}C), consistent with these protons being in rapid exchange with the inter-lamellar waters. This same study was unable to detect the NH exchange arguing that the NH is involved in strong hydrogen bonding. Molecular dynamics [198] simulations also indicate that it is primarily the NH group that participates in intermolecular hydrogen-bonding with H_2O in SM. It should be noted that the detection of the H_2O correlation in the HETCOR experiments would still requires the additional NOE magnetization transfer between the exchanged NH and OH protons to the protons involved in the final CP step. It would be a bit surprising if this multi-step exchange gave rise to the dramatic buildup in the H_2O correlation observed in SM, but on the other hand the H_2O concentration in these hydrated MLV's is high. Even if the strong water correlations are entirely the result of an exchange process these results clearly demonstrate the presence of a strong water interaction at the SM backbone that is not detected at the backbone of PC lipids.

These HETCOR results strongly support the presence of strong H_2O interactions at the backbone of SM. The detection of a H_2O contact between both SM and DOPC in a 50:50 mixture may provide some evidence for the existence of bridging H_2O molecules in lipid mixtures containing SM. It will be interesting to use the techniques presented here to detect the presence or absence of this water-backbone interaction when cholesterol is incorporated in the bilayer and in more complex raft forming lipid mixtures.

6.5 SM Water Contacts Conclusions

^{1}H/^{31}P dipolar HETCOR and ^{1}H/^{13}C INEPT HETCOR MAS NMR methods are useful for the study of intra- and intermolecular contacts in lipid mixtures when a mixing period is included in the pulse sequence to monitor ^{1}H-^{1}H NOEs. A specifically interesting result of this work is the detection of a strong interaction between H_2O and backbone protons in SM that is not observed in PC lipids. This results from the unique hydrogen-bonding properties of the sphingosine backbone of SM. The lack of water contacts to the acyl chain of the lipid supports previous arguments that the water content in the hydrophobic core is very low. It is also interesting that a H_2O contact is observed in DOPC when it is

in a 50:50 mixture with SM. This provides some evidence that bridging hydrogen-bonded water molecules are present between lipids in mixtures with SM. The presence of these hydrogen bonded H_2O species at the backbone is consistent with the low H_2O permeability in SM. These unique waters may also impact the membrane chemical potential and play a unique role in bilayer repulsion and cell fusion, as well as influence the targeting of amphiphilic peptides and proteins at the membrane surface.

It should be possible with future NMR experiments of this type to determine whether this unique water contact is indeed present at the NH moiety and if it exists in mixtures with cholesterol and in raft forming systems containing SM. The NMR experiments with ^{31}P detection have the unique advantage over ^{1}H detected NOESY methods in that unique lipids can be resolved in mixtures. This is not always the case with ^{1}H detected NOESY experiments where the ^{1}H resonances of lipids with different headgroups are typically not well resolved and thus, only single component lipid mixtures are typically studied.

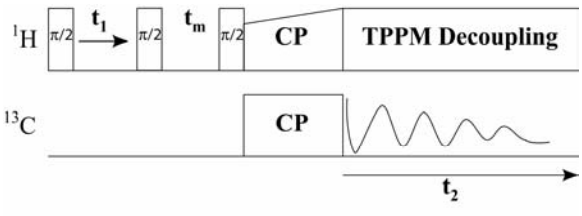

Figure 6.1 Pulse sequence for 2D dipolar HETCOR MAS NMR experiment with NOE mixing period, τ_m.

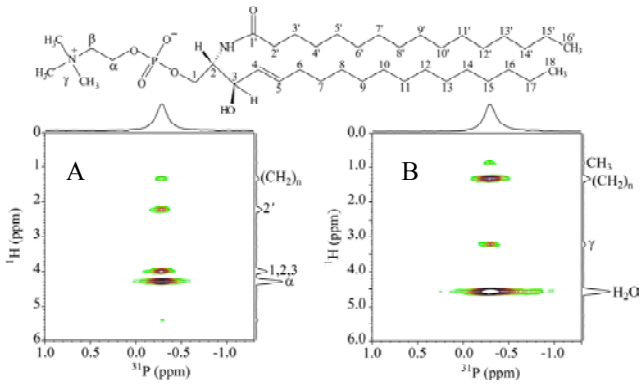

Figure 6.2 The 2D ^{1}H-^{31}P CP dipolar HETCOR MAS NMR spectrum for SM recorded at a sample temperature of 318 K with two different ^{1}H-^{1}H NOE mixing periods; A) τ_m = 20 μs and B) τ_m = 500 ms. The structure of SM with the nomenclature is depicted above the NMR spectra.

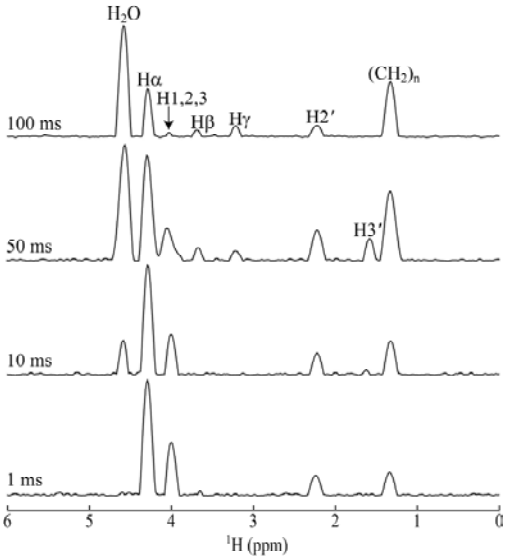

Figure 6.3 The ^{1}H projections from the 2D ^{1}H-^{31}P CP dipolar HETCOR MAS NMR spectra for SM (Figure 2) at increasing mixing periods τ_m.

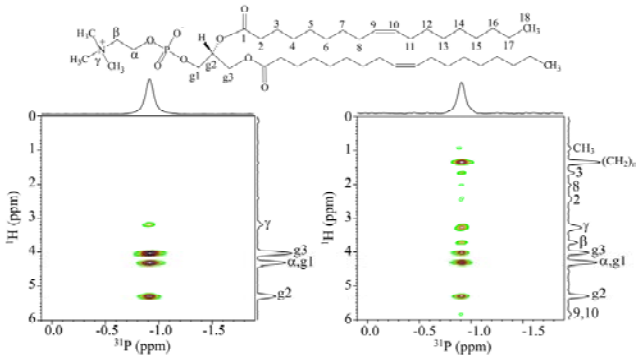

Figure 6.4 The 2D ^{1}H-^{31}P CP dipolar HETCOR MAS NMR spectra for DOPC recorded at a sample temperature of 301 K with two different NOE mixing periods; A) τ_m = 20 μs and B) τ_m = 500 ms. The structure of DOPC with the nomenclature is depicted above the NMR spectra.

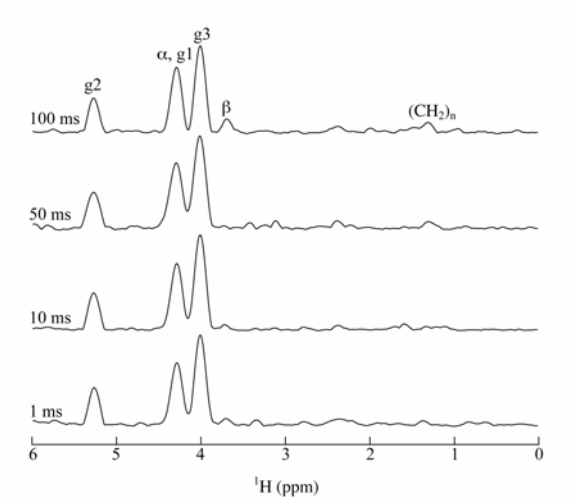

Figure 6.5 The ^{1}H projections from the 2D ^{1}H-^{31}P CP dipolar HETCOR MAS NMR spectra for DOPC (Figure 4) at increasing mixing periods τ_m.

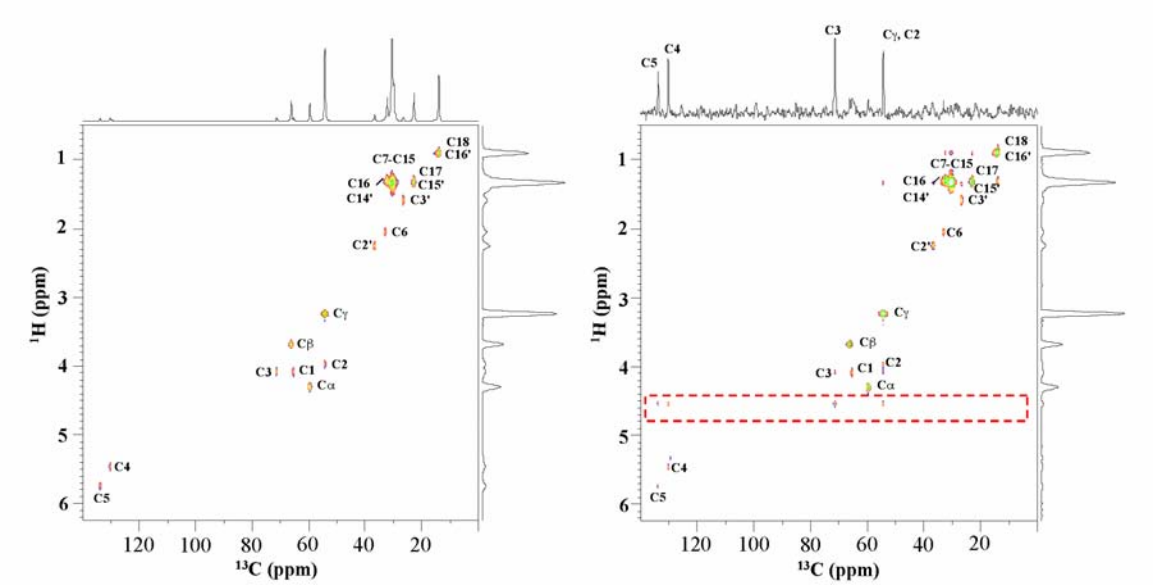

Figure 6.6 The 2D ^{1}H-^{13}C INEPT HETCOR MAS NMR spectra for SM with A) τ_m = 10 μs ^{1}H-^{1}H NOE mixing period and a B) τ_m = 50 ms mixing period. The SM ^{1}H/^{13}C assignments are shown. The top ^{13}C projection in (B) is the slice along the H_2O $\delta(^{1}H)$ = +4.8 ppm chemical shift.

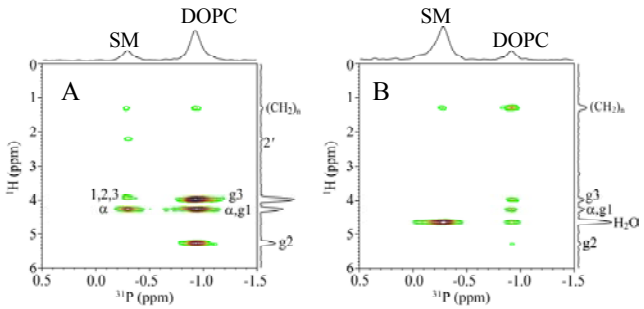

Figure 6.7 The 2D ^{1}H-^{31}P CP dipolar HETCOR MAS NMR spectra for a 1:1 SM/DOPC mixture recorded at a sample temperature of 318 K with two different ^{1}H-^{1}H NOE mixing periods; A) τ_m = 20 μs and B) τ_m = 500 ms.

Page Left Intentionally Blank

Chapter 7

Simulation of Sphingomyelin Bilayers

7.1 Simulation Introduction

In synthetic lipid mixtures the mixing of distinct domains is quite clear. The underlying mechanism is thought to be a microphase separation, which is based on the different interactions among the constituent lipids and sterols. The two key phases are the liquid ordered and liquid disordered phases. The distinction is primarily that the diffusion in the liquid ordered phase is slower than in the disordered phase. While the name implies a structural difference, measurement of such a difference has not been done. Understanding the interactions between the different lipids as well as within the same lipid type is important to understand the connection between the different lipid types and the possible domain or phases. The structural differences between sphingomyelin and glycerolipids lies in the linkage between the tails and the phosphatidylcholine head groups, which are identical in both types. The sphingomyelin lipids have a ceramide linkage on one side and a hydroxyl group in the linkage to the other tail chain. The glycerolipids have glycerol linkages, which have carbonyl groups. A key difference is the hydrogen bond capability of these linkages. Sphingomyelin has both acceptor and donor sites, while the glycerolipids only have hydrogen bond acceptors. Thus, sphingomyelin can hydrogen bond to itself and to other sphingomyelin molecules.

Many simulations of sphingomyelin containing lipid bilayers have already been performed.[127, 159, 173, 198, 212-220] performed simulations of a single sphingomyelin lipid in water and found intramolecular hydrogen bonds. Chiu et al. [159] did large scale simulations of a sphingomyelin bilayer and found both inter- and intra-molecular hydrogen bonds in the bilayer. More recent works have studied mixtures of sphingomyelin with a glycerolipid and cholesterol [215, 216, 220].

In this chapter, we present simulations of sphingomyelin bilayer as a function of temperature, since kT defines the basic energy scale of soft matter. Temperature dependent studies provide insight into the fundamental interactions. For example, the density of water is quite constant in the liquid range in comparison to other liquids such as alkanes that do not hydrogen bond. This difference between polar and nonpolar

liquids is often not relevant, but in the context of lipid bilayer, which involve amphiphile containing polar and nonpolar parts, the competition of such interactions is fundamental to their properties. With respect to the difference between sphingomyelin and glyerolipids, the importance of hydrogen bond interactions is foremost and knowing their effect on structure and physical properties is essential to understand the properties of lipid bilayers.

7.2 Simulation Methods

Atomistic simulations of sphingomyelin (SM) bilayers were performed. We used the GROMACS code to perform the simulations {Lindahl, 2001 #100}. The force-field is the same as the previous work by Chiu *et al.*{Chiu, 2003 #96}. **Figure 7.1** shows the structure of 16:0 SM and the labeling scheme. We will use this labeling scheme in our discussion of the simulation results. The starting state was formed using a single sphingomyelin conformation which is replicated in a 10x10 lattice to build 100 molecules per layer. The *z*-direction is taken to be perpendicular to the bilayer. Water is added to volume outside the lipid molecules. A short energy minimization is applied to remove bad contacts. Simulation runs of about 100 ns were performed. Within the initial part of the simulation the molecules equilibrate. The initial setup had all the molecules with the same orientation. This results in a correlated chain of lipids forming through hydrogen bonding. In order to prevent the starting state dependence, initial configuration were created with each replicated molecule in the lattice being randomly rotated. A 2 fs time step is used. Temperature is controlled by using the Nose-Hoover thermostat. The simulations were performed between the range of 320 K to 345 K. Semi-isotropic Parrinello-Rahman constant pressure algorithm was used with a pressure of 1 atm, i.e., pressure coupling which is isotropic in the *x*- and *y*-directions, but different in the *z*-direction. The SETTLE algorithm was used to constrain the bond lengths in the water molecules.

7.3 Simulation Results

The area per lipid (*A*) is a key quantity for characterizing lipid bilayers and furthermore plays an important role in domains. If different lipid types have sufficiently different *A*, then the likelihood increases for domain formation and even phase separation. In **Table 7.1** we list the values of *A* for the SM lipid bilayers as a function of

temperature. The values of A for SM are much smaller than for DPPC or DOPC. At 323 K, A = 53 Å for the large scale simulations of sphingomyelin**.** The rise in A for SM as a function of temperature is small. Only an increase of 2 $Å^2$ occurs, which is about 4% change.

Table 7.1 Simulated area per lipid for SM bilayers as a function of temperature.

T (K)	A ($Å^2$)
320	46.9
325	47.9
330	47.5
335	48.0
340	48.4
345	49.1

We now consider the hydrogen bonding within the lipid bilayer. Previous work of Chiu et al. showed strong hydrogen bonding. This includes both intramolecular hydrogen bonds within SM lipids and intermolecular hydrogen bonds between lipids or a lipid and water. The key H atoms that participate in such hydrogen bonds are H15 and H35. Chiu et al. found that H35 forms intramolecular hydrogen bonds, while H15 participates in intermolecular hydrogen bonds. We find the same behavior, which is expected given that we are using the same force-field. We describe the temperature dependence of the hydrogen bonding. The hydrogen bonding is determined from calculations of the radial distribution functions (rdfs). In rdfs involving a H atom and an acceptor atom, there is a peak near r = 1.7Å, which corresponds to the hydrogen bond. The average number of hydrogen bonds per H atom (n_{HB}) is equal to the number of acceptor atoms in the hydrogen bond peak. The peak heights have to be large to have one hydrogen bond on average, because n_{HB} is the integral of g(r) over the volume of the peak times the number density of the acceptor atoms and the volume and density are small numbers. The value of n_{HB} scales with the peak heights for atoms in the lipid head group; thus peak height differing by a factor of 100 imply a very large difference in the number of hydrogen bonds between the respective pairs under consideration.

We first consider the radial distribution functions for the H15. There are large hydrogen bond peaks in the rdfs with OA34 (**Figure 7.2**) and O17 (**Figure 7.3**). The peak height for OA34 ranges from 29 to 41 and for O17 ranges from 71 to 84. At T = 345

K, n_{HB} = 0.49 for O17 and 0.26 for OA34. Thus, three-quarters of the H15 atoms are hydrogen bonded to either O17 or OA34. The other possible acceptor atoms in the head group do not form an appreciable number of hydrogen bonds. **Figure 7.4** shows the rdf for H15 and water oxygens. The largest peak at r = 1.7Å is about 1.1, but with the larger water number density, n_{HB} = 0.19 at T = 345 K. Overall, 94% of the H15 atoms are hydrogen bonded to either O17, OA34 or OW and 1 or 2% are bonded to other O atoms in the head group.

We now consider the temperature dependence in **Figures 7.2** – **7.4**. For the H15-OA34 there is some T dependence. The peak height grows from the smallest at T = 320 K to T = 330 K in between. For $T \geq 330$ K, the peak heights are the same. The larger peaks at higher temperatures are not what would be expected. Low temperatures are normally associated with higher order and larger peaks in rdfs, but in this case there is more order occurring at higher temperatures. Examination of the T dependence for H15-OW in **Figure 7.4** shows the opposite behavior. The T = 320 K and 325 K have the largest peaks. The peaks heights at T = 330 K, 335 K and 340 K are about equal, and T = 345 K has the smallest peak height. Thus, there appears to be a shift in the hydrogen bond partner as a function of temperature from OA34 to OW, the water O atom. In terms of n_{HB} this amounts to a small (~4%) shift. The hydrogen bonding to O17 does not have a discernable T dependence. While the peaks are not equal in the plot, the largest peak occurs for T = 345K and the second largest is the lowest T = 320K. The smallest peak occurs for T = 340K. It appears that the differences indicate the intrinsic uncertainty in the data more than a trend in temperature.

We now consider the other H atom H35 in the sphingomyelin linkage between the tails and the head groups. H35 was previously shown to form a substantial number of intramolecular hydrogen bonds to the phosphate O atoms. **Figures 7.5** and **7.6** show the rdfs for H35-OA34 and H35-O17, respectively. Unlike for H15, the peaks are small indicating few hydrogen bonds. Similarly the peaks for hydrogen bonds with water shown in **Figure 7.7** is about 10 times smaller than for H15. **Figure 7.8** shows the H35-OS11 rdf which has a substantial hydrogen bond peak. At T = 320 K, n_{HB} = 0.67. The peaks for OS7, OM9, and OM10 are much smaller giving values of n_{HB} = 0.01 to 0.02. The temperature dependence of the H35 hydrogen bonding is tiny at most. The hydrogen bonding is dominated by the OS11, which has almost no T dependence. Only the T = 320 K peak is distinct from the rest.

The O atoms in the sphingomyelin head group can hydrogen bond to water besides the H15 and H35 atoms within sphingomyelin. **Figure 7.9** shows the rdf for OA34 and the water hydrogens. The number of H atoms pairing with OA34 varies from 0.74 per atom at T = 345 K to 0.84 per atom at T = 320 K. This temperature variation corresponds to that seen in the H15-OA34 hydrogen bonding. We can now see that the increase with temperature in the hydrogen bond peak in **Figure 7.2** is due to a switch in hydrogen bonding of OA34 to H15 from the water hydrogens and fewer water oxygens hydrogen bonding to H15. The other O atoms in the head group do have significant hydrogen bonding to water hydrogens, but there is little to no T dependence. **Figure 7.10** shows the O17-HW hydrogen bond peaks which is similar in magnitude to the OA34-HW peaks, but the O17 peaks are all the same except for T = 345 K which is a bit smaller. **Figure 7.11** shows the OM9-HW rdf. There is no T dependence. The value of n_{HB} is 1.00 or half of the possible 2 hydrogen bonds occur and are with water hydrogens. As expected by symmetry the data for OM10 is very similar to the OM9 data. The OS7 hydrogen bonding to water is half that of OM9 and OM10 with n_{HB} = 54. Because of the large amount of intramolecular hydrogen bonding to H35, OS11 has only a small amount of hydrogen bonding to water; n_{HB} = 0.14, and there is negligible T dependence.

7. 4 Simulation Conclusions

We explicitly calculated the temperature dependence of the sphingomyelin bilayer structure. The simulations of sphingomyelin lipid bilayers show that both intermolecular and intramolecular hydrogen bonding occur, and that the most of the acceptors and donors are close to fully bonded on average. For the most part, there is little temperature dependence of the hydrogen bonding. There is a small exchange of hydrogen bonding between the amide hydrogen (H15) to the carbonyl O (OA34) and water oxygens. As the temperature increases more hydrogen bonds are formed between H15 and OA34 and fewer bonds occur to the water oxygens. Otherwise, in the range of temperatures studied, 320-345 K the hydrogen bond network does not significantly change. This is consistent with the behavior of pure water whose structure varies little with temperature in the liquid regime. The density of water varies much less as a function of temperature in comparison to alkane liquids, for example. We find similar behavior in the area/lipid in the sphingomyelin bilayers. First, the strong hydrogen bonding results in a lower area per lipid in comparison to the glycerolipids, which do not form intermolecular hydrogen bonds. Second, the area/lipid does not increase much with

temperature. There is only an increase of about 2 $Å^2$ over the temperature range studied.

These results have implications for organization of mixed lipid bilayers. The strong hydrogen bonding tendencies of sphingomyelin can be a molecular mechanism that leads to domain formation. In a mixture of sphingomyelin and glycerolipids, the sphingomyelin lipids will have a smaller area/lipid and a more rigid elastic behavior that is constant over a wide range of biologically relevant temperatures. These characteristics will also influence the preferential interactions with proteins. The interactions of the sphingomyelin head groups with proteins will involve hydrogen bonding of the carbonyl and amide H atoms, which does not occur for glycerolipids. The sphingolipids form a tighter packed structure and their domains will prefer proteins that can accommodate such packing.

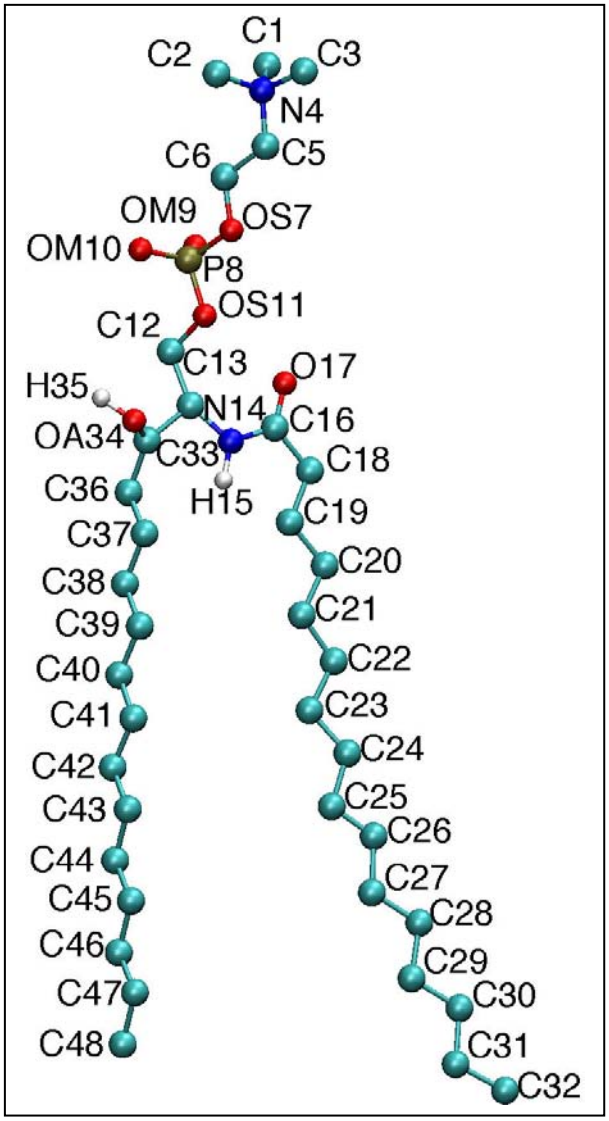

Figure 7.1 Sphingomyelin molecule used in simulations showing labels of each atom.

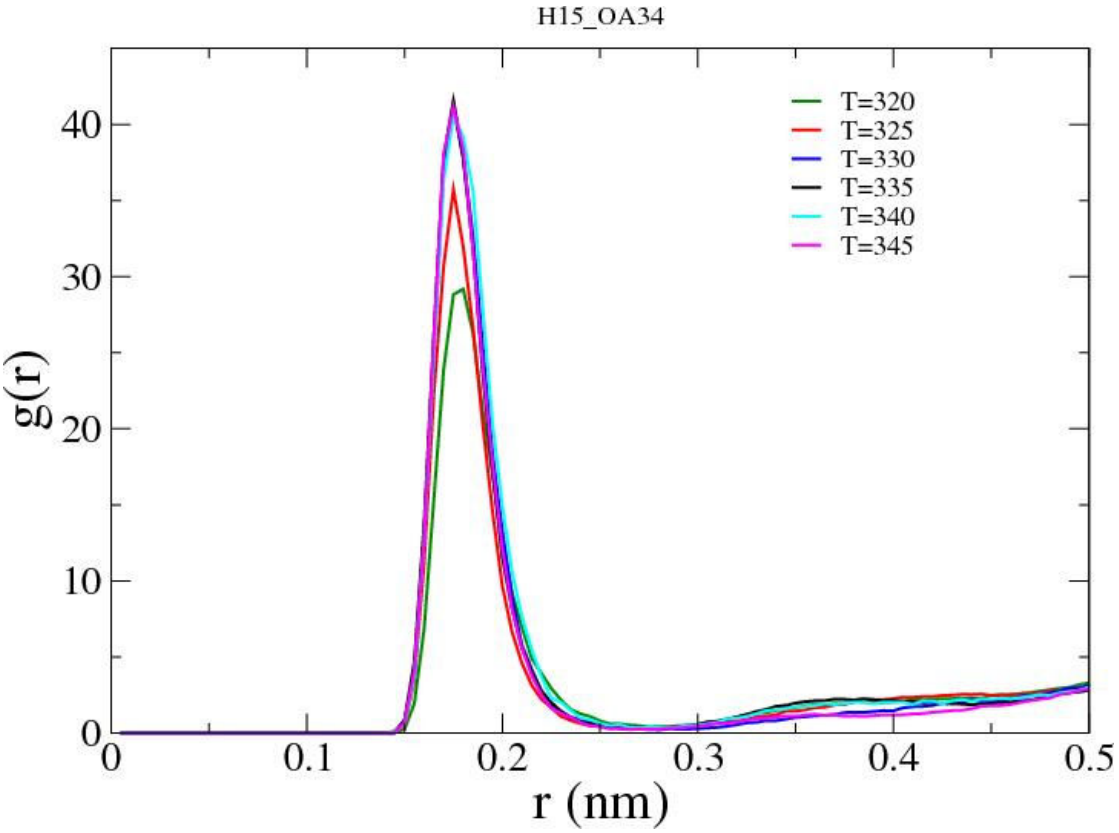

Figure 7.2 Radial distribution function for H15 and OA34 for temperatures shown in legend. The peak near r = 0.17 nm corresponds to hydrogen bonds.

.

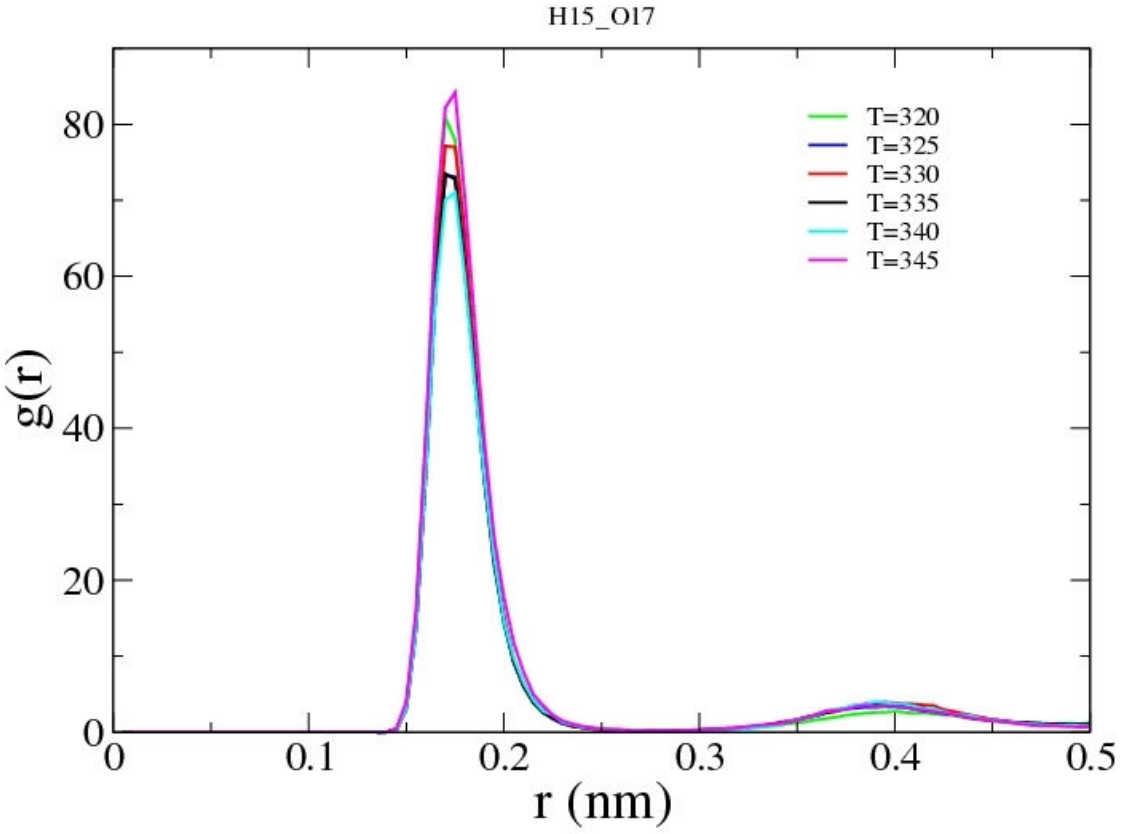

Figure 7.3 Radial distribution function for H15 and O17 for temperatures shown in legend. The peak near r = 0.17 nm corresponds to hydrogen bonds.

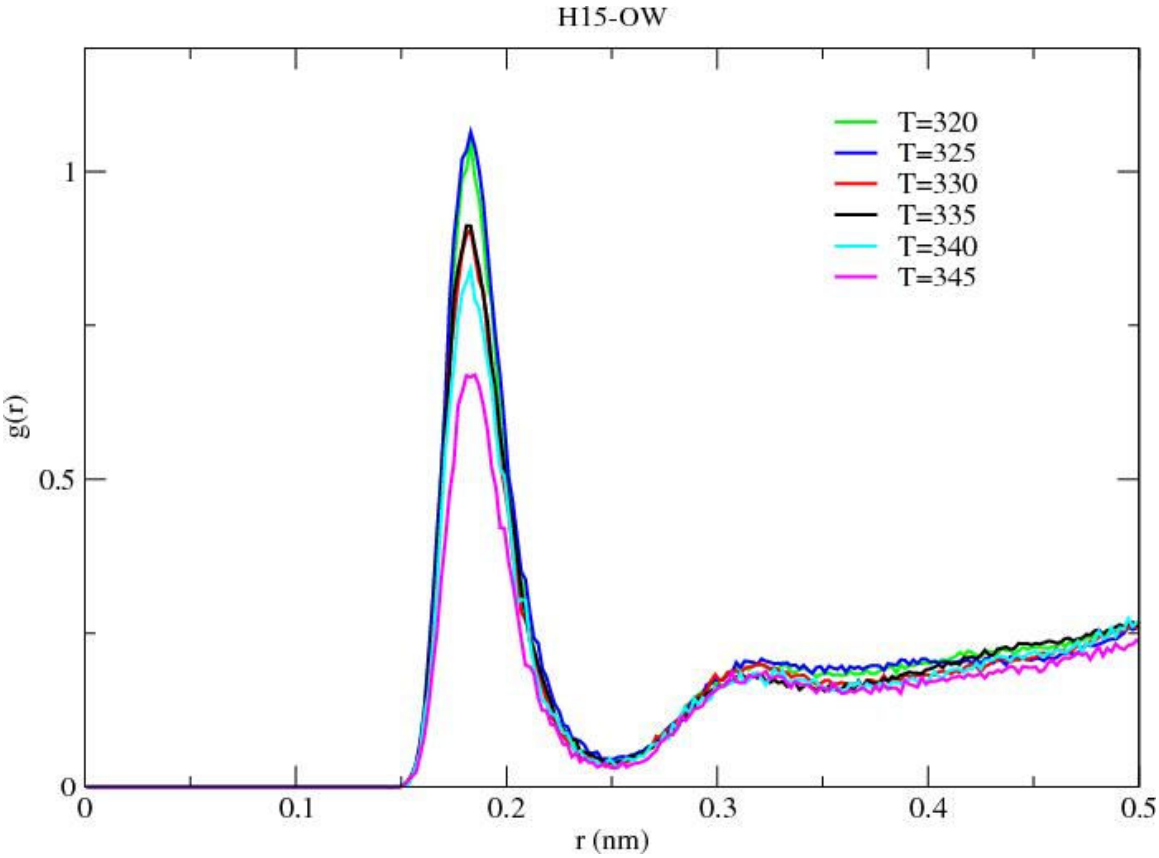

Figure 7.4 Radial distribution function for H15 and OW for temperatures shown in legend. The peak near r = 0.17 nm corresponds to hydrogen bonds.

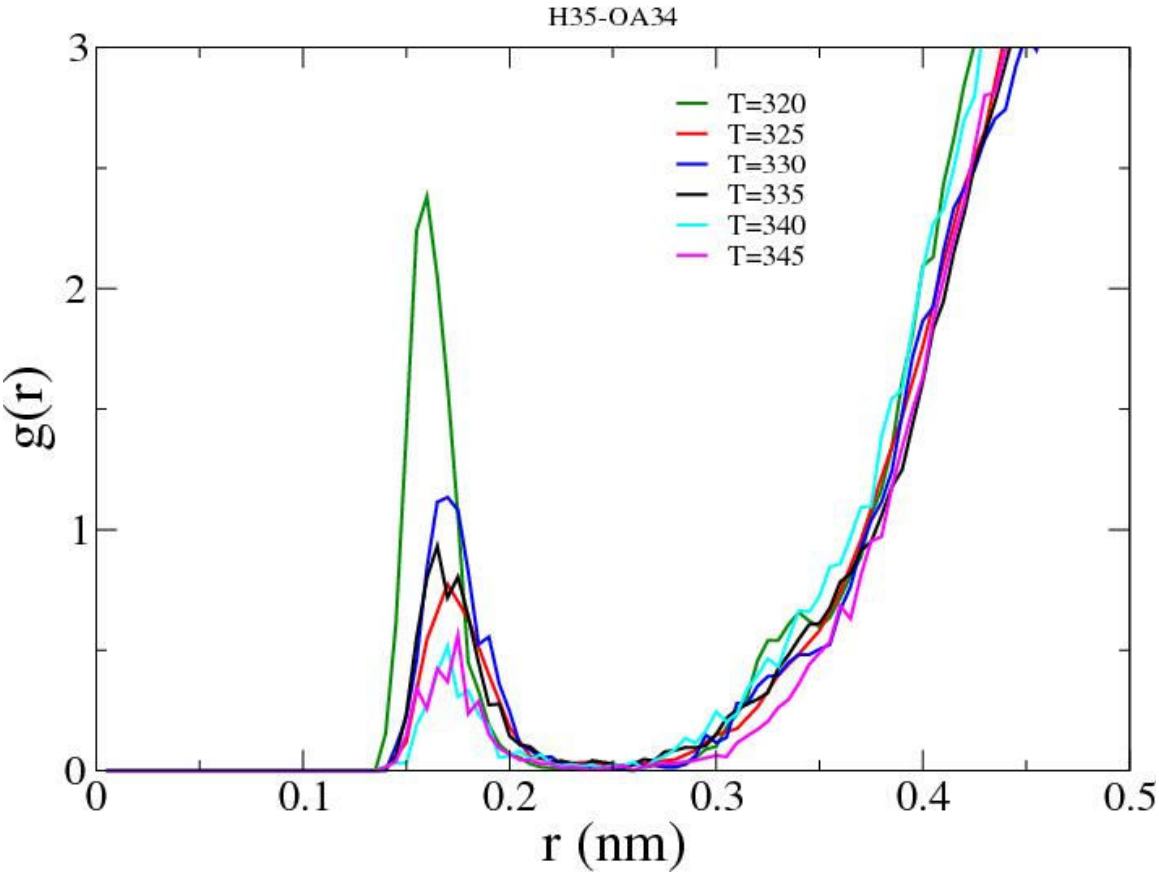

Figure 7.5 Radial distribution function for H35 and OA34 for temperatures shown in legend. The peak near r = 0.17 nm corresponds to hydrogen bonds.

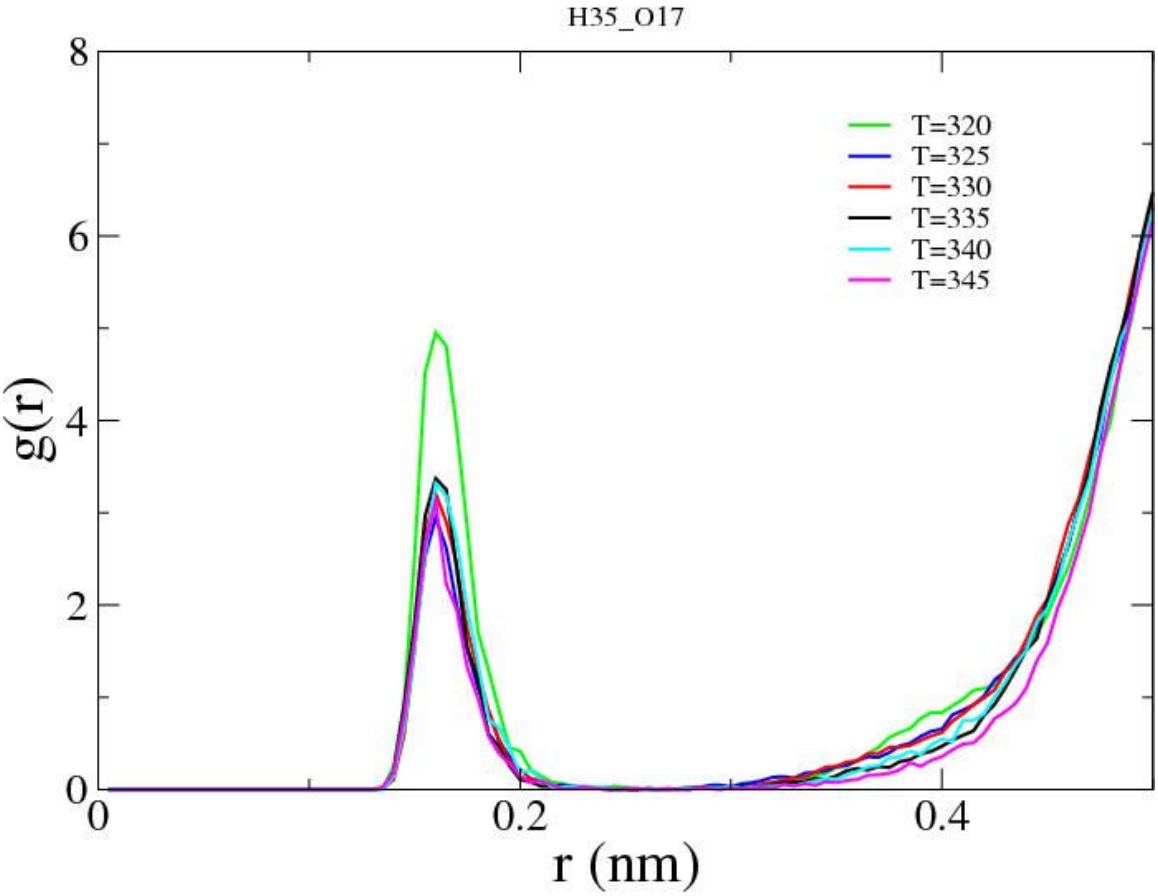

Figure 7.6 Radial distribution function for H35 and O17 for temperatures shown in legend. The peak near r = 0.17 nm corresponds to hydrogen bonds.

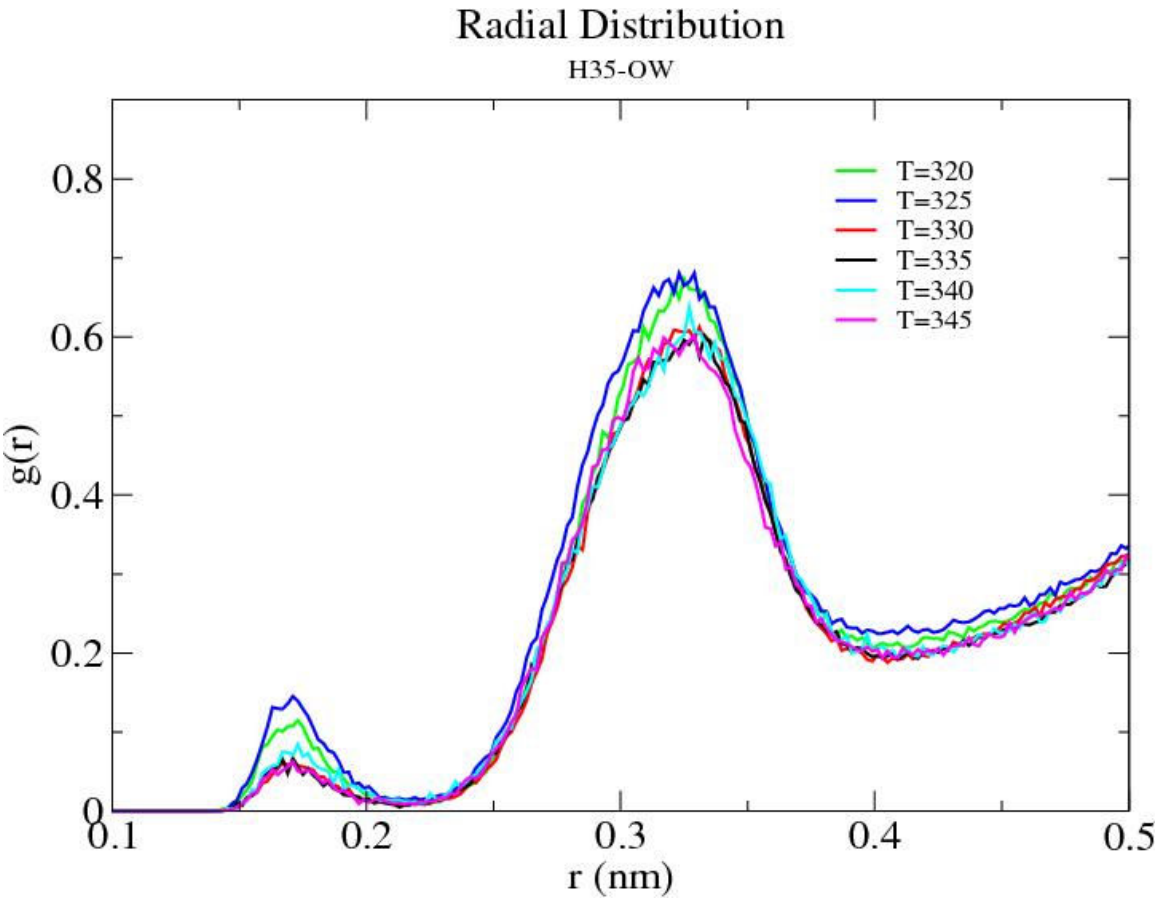

Figure 7.7 Radial distribution function for H35 and OW for temperatures shown in legend. The peak near r = 0.17 nm corresponds to hydrogen bonds.

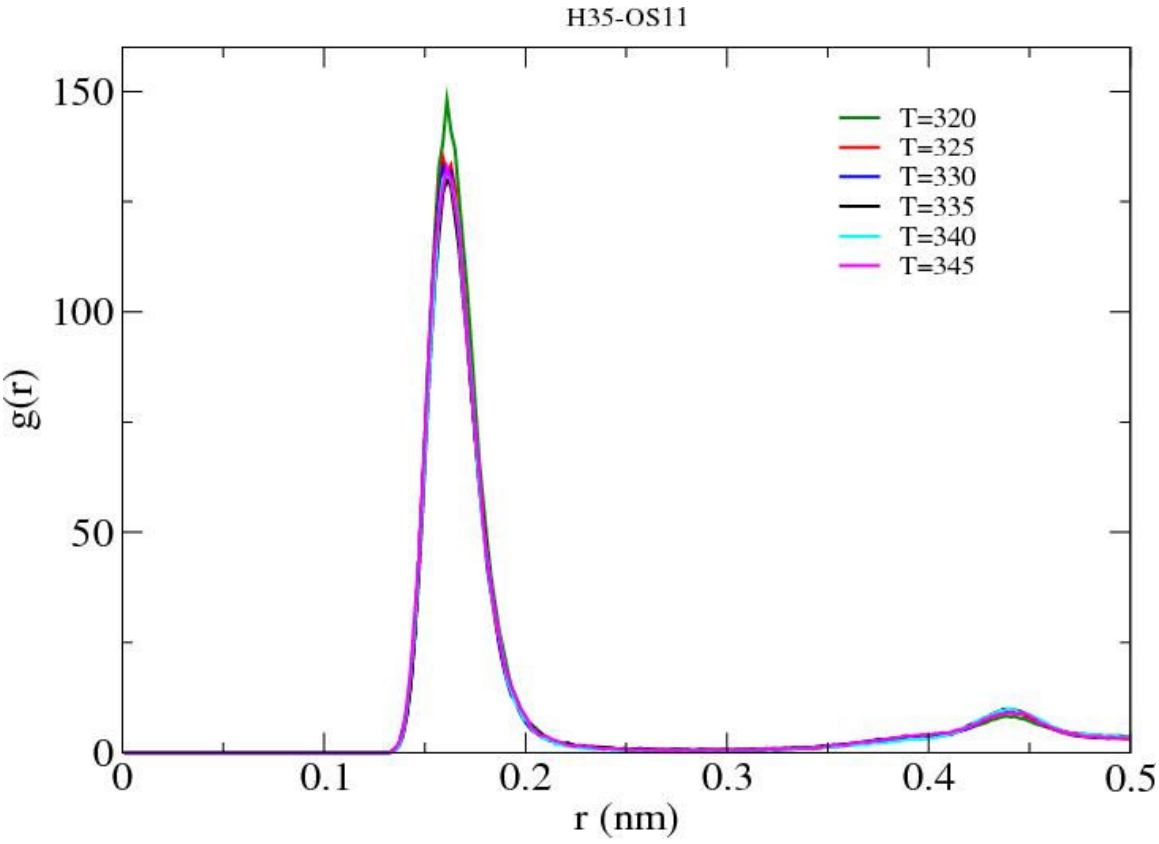

Figure 7.8 Radial distribution function for H35 and OS11 for temperatures shown in legend. The peak near r = 0.17 nm corresponds to intramolecular hydrogen bonds.

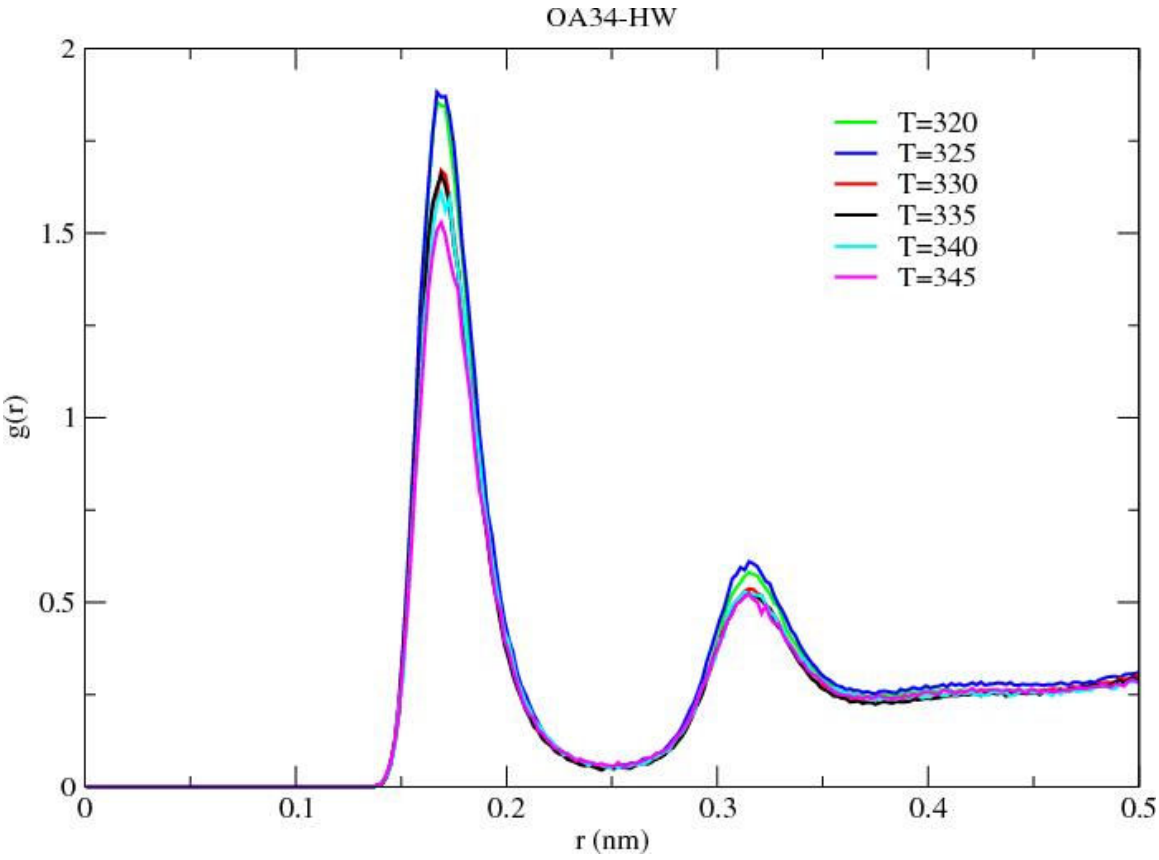

Figure 7.9 Radial distribution function for HW and OA34 for temperatures shown in legend. The peak near r = 0.17 nm corresponds to hydrogen bonds.

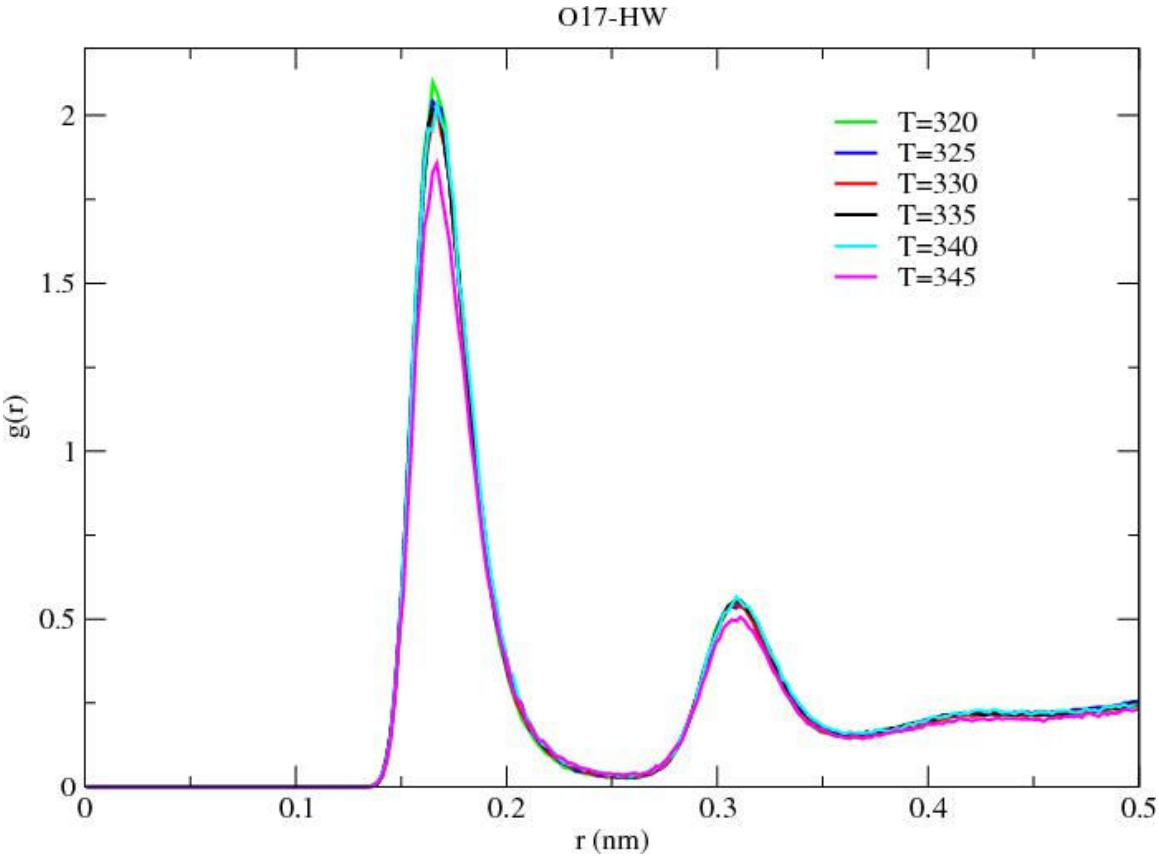

Figure 7.10 Radial distribution function for HW and O17 for temperatures shown in legend. The peak near r = 0.17 nm corresponds to hydrogen bonds.

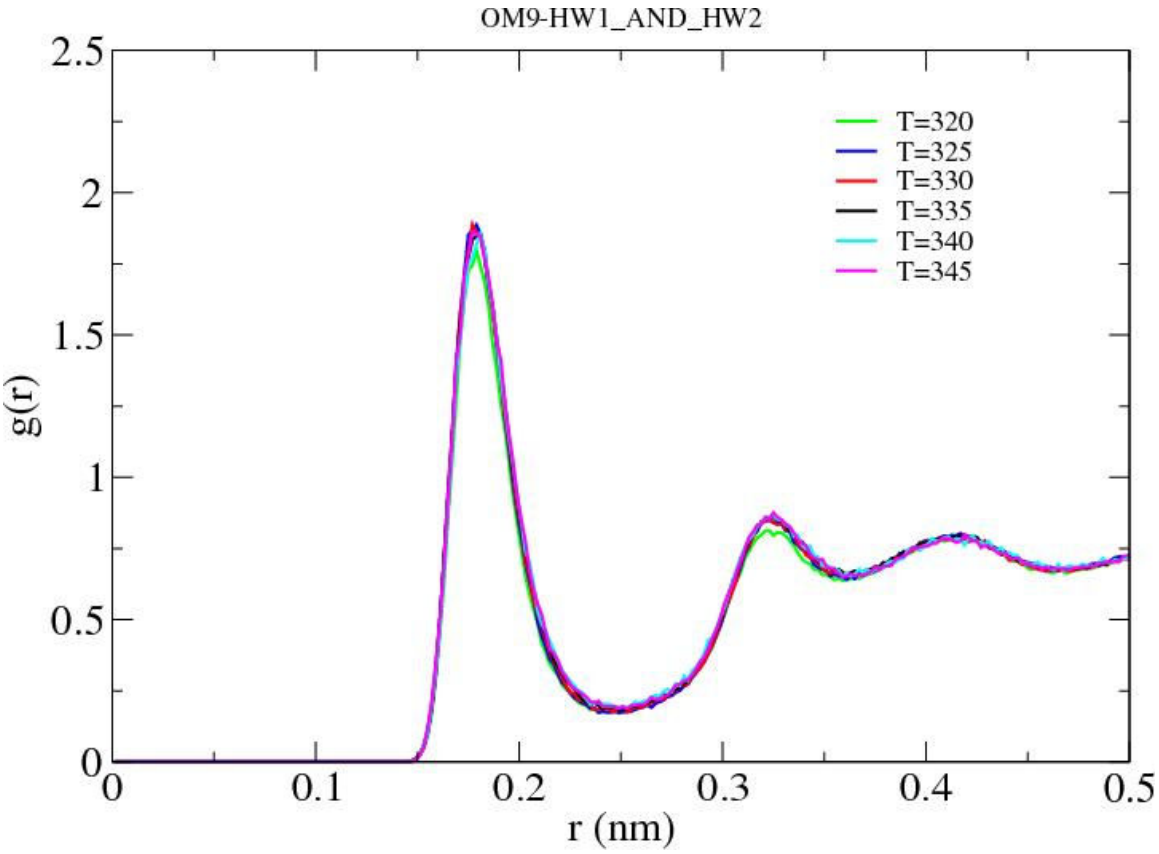

Figure 7.11 Radial distribution function for the water hydrogens HW and OM9 for temperatures shown in legend. The peak near r = 0.17 nm corresponds to hydrogen bonds.

References

[1]. Singer, S. J.; Nicolson, G. L., The Fluid mosaic Model of the Structure of Cell Membranes. *Science* **1972,** 175, (4023), 720-731.

[2]. Fantini, J.; Garmy, N.; Mahfoud, R.; Yahi, N. Lipid Rafts: Structure, Function and Role in Hiv, Alzheimer's and Prion Disease. http://www.expertreviews.org/02005392h.htm (20 December),

[3]. Pike, L. J., Lipid Rafts: Bringing Order to Chaos. *Journal of Lipid Research* **2003,** 44, 655-667.

[4]. Pike, L. J., Lipid Rafts: Heterogeneity on the High Seas. *Biochem. J.* **2004,** 378, 281-292.

[5]. Simons, K.; Ikonen, E., Functional Rafts in Cell Membranes. *Nature* **1997,** 387, (6633), 569-572.

[6]. Anderson, R. G. W.; Jacobson, K., A role for lipid shells in targeting proteins to caveolae, rafts, and other lipid domains. *Science* **2002,** 296, 1821-1825.

[7]. Binder, W. H.; Barragan, V.; Menger, F. M., Domains and rafts in lipid membranes. *Angew. Chem. Int. Ed.* **2003,** 42, 5802-5827.

[8]. Simons, K.; Vaz, W. L. C., Model Systems, Lipid Rafts, and Cell Membranes. *Annual Review of Biophysics and Biomolecular Structure* **2004,** 33, 269-295.

[9]. Ikonen, E., Roles of lipid rafts in membrane transport. *Curr. Opin. Cell Biol.* **2001,** 13, 470-477.

[10]. Brown, D. A.; London, E., Functions of Lipid Rafts in Biological Membranes. *Annual Review of Cell and Developmental Biology* **1998,** 14, 111-136.

[11]. Simons, K.; Ehehalt, R., Cholesterol, Lipid Rafts and Disease. *The Journal of Clinical Investigation* **2002,** 110, (5), 597-603.

[12]. Baron, G. S.; Wehrly, K.; Dorward, D. W.; Chesebro, B.; Caughey, B., Conversion of raft associated prion protein to the protease-resistant state requires insertion of PrP-res (PrP^{Sc}) into contiguous membranes. *EMBO J.* **2002,** 21, 1031-1040.

[13]. Kakio, A.; Nishimoto, S.; Yanagisawa, K.; Kozutsumi, Y.; Matsuzaki, K., Interactions of amyloid β-protein with various gangliosides in raft-like membranes: Importance of GM1 ganglioside-bound form as an endogenous seed for Alzheimer amyloid. *Biochemistry* **2002,** 41, 7385-7390.

[14]. van der Goot, F. G.; Harder, T., Raft Membrane Domains: From a Liquid-Ordered Membrane Phase to a Site of Pathogen Attack. *Seminars in Immunology* **2001,** 13, (2), 89-97.

[15]. Herreros, J.; Ng, T.; Schiavo, G., Lipid Rafts Act as Specialized Domains for tetanus Toxin Binding and Intenalization into Neurons. *Molecular Biology of the Cell* **2001,** 12, 2947-2960.

[16]. Mañes, S.; del Real, G.; Lacalle, R. A.; Lucas, P.; Gómez-Moutón, C., Membrane raft microdomains mediate lateral assemblies required for HIV-1 infection. *EMBO Rep 1* **2000**, 190-196.

[17]. Liao, Z.; Cimakasky, L. M.; Hampton, R.; Nguyen, D. H.; Hildreth, J. E. K., Lipid rafts and HIV pathogenesis: host membrane cholesterol is required for infection by HIV type 1. *AIDS Res. Hum. Retroviruses* **2001,** 17, 1009-1019.

[18]. Puri, A.; Hug, P.; Jernigan, K.; Barchi, J.; Kim, H.-J.; Hamilton, J.; Wiels, J.; Murray, G. J.; Brady, R. O.; Blumenthal, R., The neutral glycosphingolipid

globotriaosylceramide promotes fusion mediated by a CD4-dependent CXCR4-utilizing HIV type 1 envelope glycoprotein. *Proc. Natl. Acad. Sci. USA* **1998,** 95, 14435-14440.
[19]. Brown, D. A.; London, E., Structure of Detergent-Resistant Membrane Domains: Does Phase Separation Occur in Biological Membranes? *Biochemical and Biophysical Research Communications* **1997,** 240, (1), 1-7.
[20]. Vist, M. R.; Davis, J. H., Phase Equilibria of Cholesterol/Dipalmitoylphosphatidylcholine Mixtures: ^{2}H Nuclear Magnetic Resonance and Differential Scanning Calorimetry. *Biochemistry* **1990,** 29, (2), 451-464.
[21]. Veatch, S. L.; Keller, S. L., Organization in Lipid Membranes Containing Cholesterol. *Physical Review Letters* **2002,** 89, (26), 268101-1 - 268101-4.
[22]. Veatch, S. L.; Keller, S. L., Separation of Liquid Phases in Giant Vesicles of Ternary Mixtures of Phospholipids and Cholesterol. *Biophysical Journal* **2003,** 85, (5), 3074-3083.
[23]. Veatch, S. L.; Keller, S. L., Miscibility Phase Diagrams of Giant Vesicles Containing Sphingomyelin. *Physical Review Letters* **2005,** 94, 148101 (1-4).
[24]. Veatch, S. L.; Polozov, I. V.; Gawrisch, K.; Keller, S. L., Liquid Domains in Vesicles Investigated by NMR and Fluorescence Microscopy. *Biophysical Journal* **2004,** 86, (5), 2910-2922.
[25]. de Almeida, R. F. M.; Fedorov, A.; Prieto, M., Sphingomyelin/Phosphatidylcholine/Cholesterol Phase Diagram: Boundaries and Composition of Lipid Rafts. *Biophysical Journal* **2003,** 85, (4), 2406-2416.
[26]. Dietrich, C.; Bagatolli, L. A.; Volovyk, Z. N.; Thompson, N. L.; Levi, M.; Jacobson, K.; Gratton, E., Lipid Rafts Reconstituted in Model Membranes. *Biophysical Journal* **2001,** 80, (3), 1417-1428.
[27]. Nicolini, C.; Thiyagarajan, P.; Winter, R., Small-Scale Composition Fluctuations and Microdomain Formation in Lipid Raft Models as Revealed by Small-Angle Neutron Scattering. *Physical Chemistry Chemical Physics* **2004,** 6, 5531-5534.
[28]. Rinia, H. A.; Snel, M. M. E.; van der Eerden, J. P. J. M.; de Kruijff, B., Visualizing detergent resistant domains in model membranes with atomic force microscopy. *FEBS Lett.* **2001,** 501, 92-96.
[29]. Jacobson, K.; Mouritsen, O. G.; Anderson, R. G. W., Lipid Rafts, at a Crossroad Between Cell Biology and Physics. *Nature Cell Biology* **2007,** 9, 7-14.
[30]. Barenholz, Y.; Thompson, T. E., Sphingomyelins in Bilayers and Biological Membranes. *Biochimica et Biophysica Acta* **1980,** 604, 129-158.
[31]. Barenholz, Y.; Thompson, T. E., Sphingomyelin: Biophysical Aspects. *Chemistry and Physics of Lipids* **1999,** 102, 29-34.
[32]. Parton, R. G.; Simons, K., Digging into caveolae. *Science* **1995,** 269, 1398-1399.
[33]. van Duyl, B. Y.; Ganchev, D.; Chupin, V.; de Kruijff, B.; Killian, J. A., Sphingomyelin is Much More Effective than Saturated Phosphatidylcholine in Excluding Unsaturated Phosphatidylcholine from Domains Formed with Cholesterol. *FEBS Letters* **2003,** 547, 101-106.
[34]. Baumgart, T.; Hess, S. T.; Webb, W. W., Imaging Coexisting Fluid Domains in Biomemebrane Models Coupling Curvature and Line Tension. *Nature* **2003,** 425, 821-824.
[35]. Filippov, A.; Oradd, G.; Lindblom, G., Lipid Lateral Diffusion in Ordered and Disordered Phases in Raft Mixtures. *Biophysical Journal* **2004,** 86, (2), 891-896.

[36]. Collado, M. I.; Goni, F. M.; Alonso, A.; Marsh, D., Domain Formation in Sphingomyelin/Cholesterol Mixed Membranes Studied by Spin-Label Electron Spin Resonance Spectroscopy. *Biochemistry* **2005,** 44, (12), 4911-4918.
[37]. Chachaty, C.; Rainteau, D.; Tessier, C.; Quinn, P. J.; Wolf, C., Building Up of the Liquid-Ordered Phase Formed by Sphingomyelin and Cholesterol. *Biophysical Journal* **2005,** 88, (6), 4032-4044.
[38]. Radhakrishnan, A.; McConnell, H., Condensed complexes in vesicles containing cholesterol and phospholipids. *Proc. Natl. Acad. Sci. USA* **2005,** 102, 12662-12666.
[39]. Gawrisch, K.; Eldho, N. V.; Polozov, I. V., Novel NMR Tools to Study Structure and Dynamics of Biomembranes. *Chemistry and Physics of Lipids* **2002,** 116, 135-151.
[40]. Gaede, H. C.; Gawrisch, K., Multi-dimensional pulsed field gradient magic angle spinning NMR experiments on membranes. *Magnetic Resonance in Chemistry* **2004,** 42, 115-122.
[41]. Lindström, F.; Williamson, P. T. F.; Gröbner, G., Molecular Insight into the Electrostatic Membrane Surface Potential by $^{14}N/^{31}P$ MAS NMR Spectroscopy: Nociceptin-Lipid Association. *J. Amer. Chem. Soc.* **2005,** 127, 6610-6616.
[42]. Glaubitz, C.; Watts, A., Magic Angle-Oriented Sample Spinning (MAOSS): A New Approach Towards Biomembrane Studies. *J. Magn. Reson.* **1998,** 130, 305-316.
[43]. Urbina, J. A.; Oldfield, E., Solid State Nuclear Magnetic Resonance Spectrscopic Approaches to the Study of Molecular Organization of Biological Membranes. In *Biomembrane Structures*, Harris, P. I.; Chapman, D., Eds. IOS Press: Washington, D. C., 1998; Vol. 20, pp 113-133.
[44]. Warschawski, D. E.; Devaux, P. F., Polarization Transfer in Lipid Membranes. *J. Magn. Reson.* **2000,** 145, 367-372.
[45]. Soubias, O.; Réat, V.; Saurel, O.; Milon, A., High Resolution 2D $^{1}H-^{13}C$ Correlation of Cholesterol in Model membrane. *J. Magn. Reson.* **2002,** 158, 143-148.
[46]. Hong, M.; Schmidt-Rohr, K.; Nanz, D., Study of phospholipid Structure by ^{1}H, ^{13}C and ^{31}P Dipolar Couplings from Two-Dimensional NMR. *Biophysical Journal* **1995,** 69, 1939-1950.
[47]. Forbes, J.; Husted, C.; Oldfield, E., High-Field, High Resolution Proton "Magic-Angle" Sample-Spinning Nuclear Magnetic Resonance Spectroscopic Studies of Gel and Liquid Crystalline Lipid Bilayers and the Effects of Cholesterol. *J. Amer. Chem. Soc.* **1988,** 110, 1059-1065.
[48]. Forbes, J.; Bowers, J.; Shan, X.; Moran, L.; Oldfield, E.; Moscarello, M. A., Some Recent Developments in Solid-State Nuclear Magnetic Resonance Spectroscopic Studies of Lipids and Biological Membranes, Including the Effects of Cholesterol in Model and Natural Systems. *J. Chem. Soc. Faraday Trans.1,* **1988,** 84, (11), 3821-3849.
[49]. Oldfield, E.; Bowers, J.; Forbes, J., High-Resolution Proton and Carbon-13 NMR of Membranes: Why Sonicate. *Biochemistry* **1987,** 26, 6919-6923.
[50]. Warschawski, D. E.; Devaux, P. F., $^{1}H-^{13}C$ Polarization Transfer in Membranes: A Tool for Probing Lipid Dynamics and the Effect of Cholesterol. *J. Magn. Reson.* **2005,** 177, 166-171.
[51]. Huster, D.; Gawrisch, K., NOESY NMR Crosspeaks Between Lipid Headgroups and Hydrocarbon Chains: Spin Diffusion or Molecular Disorder? *J. Amer. Chem. Soc.* **1999,** 121, 1992-1993.

[52]. Huster, D.; Arnold, K.; Gawrisch, K., Investigation of Lipid Organization in Biological Membranes by Two-Dimensional Nuclear Overhauser Enhancement Spectroscopy. *J. Phys. Chem. B.* **1999,** 103, 243-251.
[53]. Holte, L. L.; Gawrisch, K., Determining Ethanol Distribution in Phospholipid Multilayers with MAS-NOESY Spectra. *Biochemistry* **1997,** 36, 4669-4674.
[54]. Huster, D.; Arnold, K.; Gawrisch, K., Influence of Docosahexaenoic Acid and Cholesterol on Lateral Lipid Organization in Phospholipid Mixtures. *Biochemistry* **1998,** 37, 17299-17308.
[55]. Yau, W.-M.; Gawrisch, K., Later Lipid Diffusion Dominates NOESY Cross-Relaxation in Membranes. *J. Amer. Chem. Soc.* **2000,** 122, 3971-3972.
[56]. Feller, S. E.; Brown, C. A.; Nizza, D. T.; Gawrisch, K., Nuclear Overhauser Enhancement Spectroscopy Cross-Relaxation Rates and Ethanol Distribution Across Membranes. *Biophysical Journal* **2002,** 82, 1396-1404.
[57]. Chen, Z.-j.; Stark, R. E., Evaluation Spin Diffusion in MAS-NOESY Spectra of Phospholipid Mulitbilayers. *Solid State Nuclear Magnetic Resonance* **1996,** 7, 239-246.
[58]. Gabriel, N. E.; Roberts, M. F., Short-Chain Lecithin/Long-Chain Phospholipid Unilamellar Vesicles: Asymmetry, Dynamics and Enzymatic Hydrolysis of the Short-Chain Component. *Biochemistry* **1987,** 26, 2432-2440.
[59]. Orädd, G.; Westerman, P. W.; Lindblom, G., Lateral Diffusion Coefficients of Separate Lipid Species in a Ternary Raft-Forming Bilayer: A PFG-NMR Multinuclesr Study. *Biophysical Journal* **2005,** 89, 315-320.
[60]. Polozov, I. V.; Gawrisch, K., Domains in Binary SOPC/POPE Lipid Mixtures Studied by Pulse Field Gradient ^{1}H MAS NMR. *Biophysical Journal* **2004,** 87, 1741-1751.
[61]. Pampel, A.; Zick, K.; Glauner, H.; Engelke, F., Studying Lateral Diffusion in Lipid Layers by Combining a Magic Angle Spinning NMR Probe with a Microimaging Gradient System. *J. Amer. Chem. Soc.* **2004,** 126, 9534-9535.
[62]. Soubias, O.; Gawrisch, K., Probing Specific Lipid-Protein Interaction by Saturation Transfer Difference NMR Spectroscopy. *J. Amer. Chem. Soc.* **2005,** 127, 13110-13111.
[63]. Hong, M.; Schmidt-Rohr, K.; Zimmermann, H., Conformational Constraints on the Headgroup and sn-2 Chain of Bilayer DMPC from NMR Dipolar Couplings. *Biochemistry* **1996,** 35, 8335-8341.
[64]. Everts, S.; H., D. J., ^{1}H and ^{13}C NMR of Multilamellar Dispersions of Polyunsaturated (22;6) Phospholipids. *Biophysical Journal* **2000,** 79, 885-897.
[65]. Lee, C. W. B.; Griffin, R. G., Two-dimensional ^{1}H/^{13}C Heteronuclear Chemical Shift Correlation Spectrscopy of Lipid Bilayers. *Biophysical Journal* **1989,** 55, 355-358.
[66]. Gross, J. D.; Warschawski, D. E.; Griffin, R. G., Dipolar Recoupling in MAS NMR: A Probe for Segmental Order in Lipid Bilayers. *J. Amer. Chem. Soc.* **1997,** 119, 796-802.
[67]. Dvinskikh, S. V.; Castro, V.; Sandström, D., Efficient Solid-State NMR Methods For Measuring Heteronuclear Dipolar Couplings in Unoriented Lipid Membrane Systems. *Phys. Chem. Chem. Phys.* **2005,** 7, 607-613.
[68]. Urbina, J. A.; Moreno, B.; Arnold, W.; Taron, C. H.; Orlean, P.; Oldfield, E., A Carbon-13 Nuclear Magnetic Resonance Spectroscopic Study of Inter-Proton Order

Parameters: A New Approach to Study Order and Dynamics in Phospholipid Membrane Systems. *Biophysical Journal* **1998,** 75, 1372-1383.
[69]. Gross, J. D.; Costa, P. R.; Dubacq, J.-P.; Warschawaski, D. E.; Lirsac, P.-N.; Devaux, P. F.; Griffin, R. G., Multidimensional NMR in Lipid Systems. Coherence Transfer Through J Couplings Under MAS. *J. Magn. Reson. B* **1995,** 106, 187-190.
[70]. Soubias, O.; Piotto, M.; Saurel, O.; Assemat, O.; Réat, V.; Milon, A., Detection of Natural Abundance ^{1}H-^{13}C Correlations of Cholesterol in its Membrane Environment Using a Gradient Enhanced HSQC Experiment Under High Resolution Magic Angle Spinning. *J. Magn. Reson.* **2003,** 165, 303-308.
[71]. Soubias, O.; Jolibois, F.; Réat, V.; Milon, A., Understanding Sterol-Membrane Interactions, Part II: Complete ^{1}H and ^{13}C Assignments by Solid-State Spectroscopy and Determination of the Hydrogen-Bonding Partners of Cholesterol in a Lipid Bilayer. *Chem. Eur. J.* **2004,** 10, 6005-6014.
[72]. Alonso, B.; Massiot, D., Multi-scale NMR Characterization of Mesostructured Materials Using ^{1}H-^{13}C Through-Bond Polarization Transfer, Fast MAS, and ^{1}H Spin Diffusion. *J. Magn. Reson.* **2003,** 163, 347-352.
[73]. Dvinskikh, S. V.; Castro, V.; Sandström, D., Heating Caused by Radiofrequency Irradiation and Sample Rotation in ^{13}C Magic Angle Spinning NMR Studies of Lipid Membranes. *Magnetic Resonance in Chemistry* **2004,** 42, 875-881.
[74]. States, D. J.; Haberkorn, R. A.; Ruben, D. J., A Two-Dimensional Nuclear Overhauser Experiment with Pure Adsorption Phase in Four Quadrants. *J. Magn. Reson.* **1982,** 48, 286-292.
[75]. Sodickson, D. K.; Levitt, M. H.; Vega, S.; Griffin, R. G., Broad band dipolar recoupling in the nuclear magnetic resonance of rotating solids. *Journal of Chemical Physics* **1993,** 98, (9), 6742-8.
[76]. Bennett, A. E.; Ok, J. H.; Griffin, R. G.; Vega, S., Chemical shift correlation spectroscopy in rotating solids: radio frequency-driven dipolar recoupling and longitudinal exchange. *Journal of Chemical Physics* **1992,** 96, (11), 8624-7.
[77]. Jäger, C.; Feike, M.; Born, R.; Spiess, H. W., Direct detection of connectivities in glasses by 2D NMR. *Journal of Non-Crystalline Solids* **1994,** 180, (1), 91-5.
[78]. Bennett, A. E.; Rienstra, C. M.; Auger, M.; Lakshmi, K. V.; Griffin, R. G., *J. Chem. Phys.* **1995,** 103, 6951-6958.
[79]. Guo, W.; Hamilton, J. A., A Multinuclear Solid-State NMR Study of Phospholipid-Cholesterol Interactions. Dipalmitoylphosphatidylcholine-Cholesterol Binary System. *Biochemistry* **1995,** 34, 14174-14184.
[80]. Ipsen, J. H.; Karlström, G.; Mouritsen, O. G.; Wennerström, H.; Zuckermann, M. J., Phase Equilibrium in the Phosphatidyl-Cholesterol System. *Biochimica Biophysica Acta* **1987,** 905, 162-172.
[81]. Trouard, T. P.; Nevzorov, A. A.; Alam, T. M.; Job, C.; Zajicek, J.; Brown, M. F., Influence of Cholesterol on Dynamics of Dimyristoylphosphatidylcholine Bilayers as Studied by Deuterium NMR Relaxation. *J. Chem. Phys.* **1999,** 110, (17), 8802-8818.
[82]. Schenker, K. V.; Philipsborn, v., Optimization of INEPT and DEPT Experiments for Spin Systems with Hetero- and Homonuclear Couplings. *J. Magn. Reson.* **1985,** 61, 294-305.

[83]. Huster, D.; Yao, X.; Hong, M., Membrane Protein Topology Probed by ^{1}H Spin Diffusiion From Lipids Using Solid State NMR Spectroscopy. *J. Amer. Chem. Soc.* **2002,** 124, (5), 874-883.
[84]. Bennett, A. E.; Rienstra, C. M.; Griffiths, J. M.; Zhen, W.; Lansbury, P. T.; Griffin, R. G., Homonuclear radio frequency-driven recoupling in rotating solids. *J. Chem. Phys.* **1998,** 108, (22), 9463-9479.
[85]. Geen, H.; Gottwald, J.; Graf, R.; Schnell, I.; Spiess, H. W.; Titman, J. J., Elucidation of Dipolar Coupling Networks Under Magic-Angle Spinning. *J. Magn. Reson.* **1997,** 125, 224-227.
[86]. Raya, J.; Bianco, A.; Furrer, J.; Briand, J.-P.; Piotto, M.; Elbayed, K., Proton Dipolar Recoupling in Resin-Bound Peptides under High-Resolution Magic Angle Spinning. *J. Magn. Reson.* **2002,** 157, 43-51.
[87]. Lange, A.; Luca, S.; Baldus, M., Structural Constraints from proton Mediated Rare-Spin Correlation Spectroscopy in Rotating Solids. *J. Amer. Chem. Soc.* **2002,** 2002, 9704-9705.
[88]. Matsuki, Y.; Akutsu, H.; Fujiwara, T., Precision ^{1}H-^{1}H distance measurement via ^{13}C NMR signals: utilization of ^{1}H-^{1}H double quantum dipolar interactions recoupled under magic angle spinning conditions. *Magnetic Resonance in Chemistry* **2004,** 42, 291-300.
[89]. Reif, B.; Jaroniec, C. P.; Tienstra, C. M.; Hohwy, M.; Griffin, R. G., ^{1}H-^{1}H MAS Correlation Spectroscopy and Distance Measurements in a Deuterated Peptide. *J. Magn. Reson.* **2001,** 151, 320-327.
[90]. Reif, B.; Griffin, R. G., ^{1}H Detected ^{1}H,^{15}N Correlation Spectroscopy in Rotating Solids. *J. Magn. Reson.* **2003,** 160, 78-83.
[91]. Gullion, T.; Baker, D. B.; Conradi, M. S., New, Compensated Carr-Purcell Sequences. *J. Magn. Reson.* **1990,** 89, 479-484.
[92]. Fujiwara, T.; Khandelwal, P.; Akutsu, H., Compound Radio-Frequency-Driven Recoupling Pulse Sequences for Efficient Magnetization Transfer by Homonuclear Dipolar Interactions under Magic-Angle Spinning Conditions. *J. Magn. Reson.* **2000,** 145, 73-83.
[93]. Robyr, P.; Meier, B. H.; Ernst, R. R., Radio-Frequency-Driven Nuclear Spin Diffusion in Solids. *Chem. Phys. Lett.* **1989,** 162, (6), 417.
[94]. Colombo, M. G.; Meier, B. H.; Ernst, R. R., Rotor-Driven Spin Diffusion in Natural Abundance ^{13}C Spin Systems. *Chem. Phys. Lett.* **1988,** 146, (3,4), 189-196.
[95]. Brinlmann, A.; Edén, M.; Levitt, M. H., Synchronous helical pulse sequences in magic-angle spinning nuclear magnetic resonance: Double quantum recoupling of multiple-spin systems. *J. Chem. Phys.* **2000,** 112, (19), 8539-8554.
[96]. Thieme, K.; Zech, G.; Kunz, H.; Spiess, H. W.; Schnell, I., Dipolar Recoupling in NOESY-Type ^{1}H-^{1}H NMR Experiments Under HRMAS Conditions. *Org. Lett.* **2002,** 4, (9), 1559-1562.
[97]. Schnell, I., Merging Concepts from Liquid-State and Solid-State NMR Spectroscopy for the Investigation of Supra- and Biomolecular Systems. *Current Analytical Chemistry* **2005,** 1, 3-27.
[98]. Urbina, J. A.; Pekerar, S.; Le, H.; Patterson, J.; Montez, B.; Oldfield, E., Molecular order and dynamics of phophatidylcholine bilayer membranes in the presence

of cholesterol, ergosterol and lanosterol: a comparative study using ^{2}H-, ^{13}C-, and ^{31}P-NMR spectroscopy. *Biochim. Biophys. Acta* **1995,** 1238, 163-176.
[99]. Leguerneve, C.; Auger, M., New approach to study fast and slow motions in lipid bilayers: Application to dimyristoylphophatidylcholine-cholesterol interactions. *Biophys. J.* **1995,** 68, 1952-1959.
[100]. Guo, W.; Hamilton, J. A., C-13 MAS NMR studies of crystalline cholesterol and lipid mixtures modeling atherosclerotic plaques. *Biophys. J.* **1996,** 71, 2857-2868.
[101]. Epand, R. M.; Epand, R. F.; Bain, A. D.; Sayer, B. G.; Hughes, D. W., Properties of Polyunsaturated Phosphatidylcholine Membranes in the presence and Absence of Cholesterol. *Magnetic Resonance in Chemistry* **2004,** 42, 139-147.
[102]. Bruzik, K. S.; Sobon, B.; Salamonczyk, G. M., Nuclear Magnetic Resonance Study of Sphingomyelin Bilayers. *Biochemistry* **1990,** 29, (16), 4017-4021.
[103]. Chi, L.-M.; Hsieh, C.-H.; Wu, W.-G., Probing the double bond and phase properties of natural lipid dispersions by cross polarization/magic angle spinning ^{13}C NMR. *J. Chin. Chem. Soc.* **1992,** 39, 35-42.
[104]. Guo, W.; Kurze, V.; Huber, T.; Afdhal, N. H.; Beyer, K.; Hamilton, J. A., A Solid-State NMR Study of Phospholipid-Cholesterol Interactions: Sphingomyelin-Cholesterol Binary Systems. *Biophysical Journal* **2002,** 83, (3), 1465-1478.
[105]. Epand, R. M., Cholesterol in Bilayers of Sphingomyelin or Dihydrosphingomyelin at Concentrations Found in Ocular Lens Membranes. *Biophysical Journal* **2003,** 84, (5), 3102-3110.
[106]. Epand, R. M.; Epand, R. F., Non-raft Forming Sphingomyelin-Cholesterol Mixtures. *Chemistry and Physics of Lipids* **2004,** 132, (1), 37-46.
[107]. Warschawski, D. E.; Fellmann, P.; Devaux, P. F., High-resolution ^{31}P-^{1}H two-dimensional nuclear magnetic resonance spectra of unsonicated lipid mixtures spinning at the magic-angle. *Eur. Biophys. J.* **1996,** 25, 131-137.
[108]. Lee, M.; Goldburg, W. I., Nuclear-magnetic-resonance line narrowing by a rotating rf field. *Phys. Rev. A.* **1965,** 140, 1261-1271.
[109]. van Rossum, B.-J.; Förster, H.; de Groot, H. J. M., High-Field and High-Speed CP-MAS 13C NMR Heteronuclear Dipolar-Correlation Spectrscopy of Solids with Frequency-Switched Lee-Goldberg Homonuclear Decoupling. *J. Magn. Reson.* **1997,** 124, 516-519.
[110]. Metz, G.; Wu, X. L.; Smith, S. O., Ramped-amplitude cross polarization in magic-angle-spinning NMR. *J. Magn. Reson. A* **1994,** 110, 219-227.
[111]. Schmidt-Rohr, K.; Clauss, J.; Spiess, H. W., Correlation of structure, mobility, and morphological information in heterogeneous polymer materials by two-dimensional wideline-spearation NMR spectroscopy. *Macrmolecules* **1992,** 25, 3273-3277.
[112]. van Rossum, B.-J.; Boender, G. J., High magnetic field for enhanced proton resolution in high-speed CP/MAS heteronuclear ^{1}H-^{13}C dipolar correlation spectroscopy. **1996**.
[113]. van Rossum, B.-J.; de Groot, C. P.; Ladizhansky, V.; Vega, S.; de Groot, H. J. M., A method for measuring heteronuclear (^{1}H-^{13}C) distances in high speed MAS NMR. *J. Amer. Chem. Soc.* **2000,** 122, 3465-3472.
[114]. Bennett, A. E.; Rienstra, C. M.; Auger, M.; Lakshmi, K. V.; Griffin, R. G., Hetereonuclear Decoupling in Rotating Solids. *Journal of Chemical Physics* **1995,** 103, (16), 6951-6958.

[115]. Bruzik, K. S., Conformation of the Polar Headgroup of Sphingomyelin and Its Analogues. *Biochimica et Biophysica Acta* **1988,** 939, 315-326.
[116]. Bruzik, K. S., Synthesis and spectral properties of chemically and stereochemically homogeneous sphingomyelin and its analogues. *J. Chem. Soc., Perkin Trans. I* **1988**, 423-431.
[117]. Massiot, D.; Fayon, F.; Capron, M.; King, I.; Le Calve, S.; Alonso, B.; Durand, J.-O.; Bujoli, B.; Gan, Z.; Hoatson, G., Modeling One- and Two-Dimensional Solid-State NMR Spectra. *Magnetic Resonance in Chemistry* **2002,** 40, 70-76.
[118]. Barenholz, Y.; Suurkuusk, J.; Mountcastle, D.; Thompson, T. E.; Biltonen, R. L., A Calorimetric Study of the Thermotropic Behavior of Aqueous Dispersions of Natural and Synthetic Sphingomyelins. *Biochemistry* **1976,** 15, (11), 2441-2447.
[119]. Oldfield, E.; Chapman, D., Effects of cholesterol and cholesterol derivatives on hydrocarbon chain mobility in lipids. *Biochem. Biophys. Res. Commun.* **1971,** 43, 610-616.
[120]. Brown, M. F.; Seelig, J., Influence of cholesterol on the polar region of phosphatidylcholine and phosphatidylethanolamine bilayers. *Biochemistry* **1978,** 17, 381-384.
[121]. Davis, J. H., The description of membrane lipid conformation, order and dynamics by ^{2}H-NMR. *Biochim. Biophys. Acta* **1983,** 737, 117-171.
[122]. Holland, G. P.; McIntyre, S. K.; Alam, T. M., Distinguishing Individual Lipid Headgroup Mobility and Phase Transitions in Raft-Forming Lipid Mixtures with ^{31}P MAS NMR. *Biophysical Journal* **2006,** 90, (11), 4248-4260.
[123]. Nagle, J. F.; Liu, Y.; Tristram-Nagle, S.; Epand, R. M.; Stark, R. E., Re-Analysis of Magic Angle Spinning Nuclear Magnetic Resonance Determination of Interlamellar Waters in Lipid Bilayer Dispersions. *Biophysical Journal* **1999,** 77, 2062-2065.
[124]. McIntosh, T. J.; Simon, S. A.; Needham, D.; Huang, C., Structure and Cohesive Properties of Sphingomyelin/Cholesterol Bilayers. *Biochemistry* **1992,** 31, (7), 2012-2020.
[125]. Oldfield, E.; Chapman, D., Molecular dynamics of cerebroside-cholesterol and sphingomyelin-cholesterol interactions: implications for myelin membrane structure. *FEBS Lett.* **1972,** 21, 303-306.
[126]. Cullis, P. R.; Hope, M. J., The Bilayer Stabilizing Role of Sphingomyelin in the Presence of Cholesterol. *Biochimica et Biophysica Acta* **1980,** 597, 533-542.
[127]. Niemelä, P.; Hyvönen, M. T.; Vattulainen, I., Structure and dynamics of sphingomyelin bilayer: insight gained through systematic comparison to phosphatidylcholine. *Biophys. J.* **2004,** 87, 2976-2989.
[128]. Talbott, C. M.; Vorobyov, I.; Borchman, D.; Taylor, K. G.; DuPre, D. B.; Yappert, M. C., Conformational Studies of Sphingolipids by NMR Spectroscopy. II. Sphingomyelin. *Biochimica et Biophysica Acta* **2000,** 1467, 326-337.
[129]. Maulik, P. R.; Shipley, G. G., *N*-Palmitoyl Sphingomyelin Bilayers: Structure and Interactions with Cholesterol and Dipalmitoylphosphatidylcholine. *Biochemistry* **1996,** 35, (24), 8025-8034.
[130]. Maulik, P. R.; Shipley, G. G., Interactions of N-Stearoyl Sphingomyelin with Cholesterol and Dipalmitoylphosphatidylcholine in Bilayer Membranes. *Biophysical Journal* **1996,** 70, 2256-2265.

[131]. Ladizhansky, V.; Vega, S., Polarization transfer dynamics in Lee-Goldburg cross polarization nuclear magnetic resonance experiments on rotating solids. *J. Chem. Phys.* **2000,** 112, 7158-7168.
[132]. Jolibois, F.; Soubias, O.; Réat, V.; Milon, A., Understanding Sterol-Membrane Interactions Part I: Hartree-Fock versus DFT Calculations of 13C and 1H NMR Isotropic Chemical Shifts of Sterols in Solution and Analysis of Hydrogen Bonding Effects. *Chem. Eur. J.* **2004,** 10, 5996-6004.
[133]. Seelig, J.; Gally, H., Investigation of Phosphatidylethanolamine Bilayers by Deuterium and Phosphorus-31 Nuclear Magnetic Resonance. *Biochemistry* **1976,** 15, (24), 5199-5204.
[134]. Seelig, J., ^{31}P Nuclear Magnetic Resonance and the Head Group Structure of Phospholipids in Membranes. *Biochimica et Biophysica Acta* **1978,** 515, 105-140.
[135]. Niederberger, W.; Seelig, J., Phosphorous-31 chemical shift anisotropy in unsonicated phospholipid bilayers. *J. Amer. Chem. Soc.* **1976,** 98, 3704-3706.
[136]. Griffin, R. G.; Powers, L.; Pershan, P. S., Head-group conformation in phospholipids: A phosphorous-31 nuclear magnetic resonance study of oriented monodomain dipalmitoylphosphatidylcholine bilayers. *Biochemistry* **1978,** 17, 2718-2722.
[137]. Campbell, R. F.; Melrovitch, E.; Freed, J. H., Slow-motional NMR line shapes for very anisotropic rotational diffusion. Phosphorous-31 NMR in phospholipids. *J. Phys. Chem.* **1979,** 83, 525-533.
[138]. Dufourc, E. J.; Mayer, C.; Stohrer, j.; Althoff, G.; Kothe, G., Dynamics of Phosphate Head Groups in Biomembranes: Comprehensive Analysis Using Phosphorus-31 Nuclear Magnetic Resonance Lineshape and Relaxation Time Measurements. *Biophysical Journal* **1992,** 61, 42-57.
[139]. Malcolm, I. C.; Ross, J. C.; Higinbotham, J., A Study of the Headgroup Motion of Sphingomyelin Using 31P NMR and an Analytical Soluble Model. *Solid State Nuclear Magnetic Resonance* **2005,** 27, 247-256.
[140]. Shaikh, S. R.; Brzustowicz, M. R.; Gustafson, N.; Stillwell, W.; Wassall, S. R., Monosaturated PE Dopes Not Phase Seperate From the LIPID Raft Molecules Sphingomyelin and Cholesterol: Role of Polyunsaturation? *Biochemistry* **2002,** 41, 10593-10602.
[141]. Hao, Y.-H.; Chen, J.-W., Influence of cholesterol on the biophysical properties of the sphingomyelin/DOPC binary system. *J. Membrane Biol.* **2001,** 183, 85-92.
[142]. Heerklotz, H., Triton promotes domain formation in lipid raft mixtures. *Biophys. J.* **2002,** 83, 2693-2701.
[143]. Aussenac, F.; Tavares, M.; Dufourc, E. J., Cholesterol Dynamics in Membranes of Raft Composition: A Molecular View from ^{2}H and ^{31}P Solid-State NMR. *Biochemistry* **2003,** 42, (6), 1383-1390.
[144]. Spooner, P. J. R.; Watts, A., Cytochrome *c* interactions with cardiolipin in bilayers: a multinuclear magic-angle spinning NMR study. *Biochemistry* **1992,** 31, 10129-10138.
[145]. Pinheiro, T. J. T.; Watts, A., Resolution of individual lipids in mixed phospholipid membranes and specific lipid-cytochrome c interactions by magic-angle spinning solid-state phosphorous-31 NMR. *Biochemistry* **1994,** 33, 2459-2467.

[146]. Bonev, B.; Watts, A.; Bokvist, M.; Gröbner, G., Electrostatic peptide-lipid interactions of amyloid-β peptide pentalysine with membrane surfaces monitored by ^{31}P MAS NMR. *Phys. Chem. Chem. Phys.* **2001,** 3, 2904-2910.
[147]. Bonev, B. B.; Chan, W. C.; Bycroft, B. W.; Roberts, G. C. K.; Watts, A., Interaction of the lantibiotic nisin with mixed lipid bilayers: A ^{31}P and ^{2}H NMR study. *Biochemistry* **2000,** 39, 11425-11433.
[148]. Bokvist, M.; Lindström, F.; Watts, A.; Gröbner, G., Two types of Alzheimer's β-amyloid (1-40) peptide membrane interactions: aggregation preventing transmembrane anchoring *versus* accelerated surface fibril formation. *J. Mol. Biol.* **2004,** 335, 1039-1049.
[149]. Traïkia, M.; Warschawski, D. E.; Recouvreur, M.; Cartaud, J.; Devaux, P. F., Formation of unilamellar vesicles by repitive freeze-thaw cycles: characterization by electron microscopy and ^{31}P-nuclear magnetic resonance. *Eur. Biophys. J.* **2000,** 29, 184-195.
[150]. Griffin, R. G., Observation of the effect of water on the ^{31}P nuclear magnetic resonance spectra of dipalmitoyllecithin. *J. Amer. Chem. Soc.* **1976,** 98, 851-853.
[151]. Tenchov, B., On the reversibility of the phase transitions in lipid water systems. *Chem. Phys. Lipids* **1991,** 57, 165-177.
[152]. Ruiz-Arguello, M. B.; Veiga, M. P.; Arrondo, J. L. R.; Goni, F. M.; Alonso, A., Sphingomyelinase Cleavage of Sphingomyelin in Pure and Mixed Lipid Membranes. Influence of the Physical State of the Sphingolipid. *Chemistry and Physics of Lipids* **2002,** 114, (1), 11-20.
[153]. Calhoun, W. I.; Shipley, G. G., Sphingomyelin-Lecithin Bilayers and Their Interaction with Cholesterol. *Biochemistry* **1979,** 18, (9), 1717-1722.
[154]. Smith, I. C. P.; Ekiel, I. H., *Phosphorous-31 NMR of Phospholipids in Membranes. Phosphorous-31 NMR: Principles and Applications*. Academic Press, Inc.: London, 1984.
[155]. Cullis, P. R.; de Kruyff, B.; Richards, R. E., Factors Affecting the Motion of the Polar Headgroup in Phospholipid Bilayers: A ^{31}P NMR Study of Unsonicated Phosphatidylcholine Liposomes. *Biochimica et Biophysica Acta* **1976,** 426, 433-446.
[156]. Dubinnyi, M. A.; Lesovoy, D. M.; Dubovskii, P. V.; Chupin, V. V.; Arseniev, A. S., Modeling of ^{31}P-NMR spectra of magnetically oriented phospholipid liposomes: A new analytical solution. *Solid State Nucl. Magn. Reson.* **2006,** 29, 305-311.
[157]. Schäfer, H.; Mädler, B.; Sternin, E., Determination of orientational order parameters from ^{2}H NMR spectra of magnetically partially oriented lipid bilayers. *Biophys. J.* **1998,** 74, 1007-1014.
[158]. Hodgkinson, P.; Emsley, L., The reliability of the determination of tensor parameters by solid-state nuclear magnetic resonance. *J. Chem. Phys.* **1997,** 107, 4808-4816.
[159]. Chiu, S. W.; Vasudevan, S.; Jakobsson, E.; Mashl, R. J.; Scott, H. L., Structure of sphingomyelin bilayers: A simulation study. *Biophysical Journal* **2003,** 85, (6), 3624-3635.
[160]. Schmidt, C. F.; Barenholz, Y.; Thompson, T. E., A Nuclear Magnetic Resonance Study of Sphingomyelin in Bilayer Systems. *Biochemistry* **1977,** 16, (12), 2649-2656.
[161]. Bruzik, K. S.; Tsai, M., A Calorimetric Study of the Thermotropic Behavior of Pure Sphingomyelin Diastereomers. *Biochemistry* **1987,** 26, (17), 5364-5368.

[162]. Meyer, H. W.; Bunjes, H.; Ulrich, A. S., Morphological Transitions of Brain Sphingomyelin are Determined by the Hydration Protocol: Ripples Re-Arrange in Plane, and Sponge-Like Networks Disintegrate into Small Vesicles. *Chemistry and Physics of Lipids* **1999,** 99, 111-123.
[163]. Sparrman, T.; Westlund, P., An NMR Line Shape and Relaxation Analysis of Heavy Water Powder Spectra of the L_{α}, L_{β} and $P_{\beta'}$ Phases in the DPPC/Water System. *Physical Chemistry Chemical Physics* **2003,** 5, (10), 2114-2121.
[164]. Hui, S. W.; Stewart, T. P.; Yeagle, P. L., Temperature-Dependent Morphological and Phase Behavior of Sphingomyelin. *Biochimica et Biophysica Acta* **1980,** 601, 271-281.
[165]. Koynova, R. D.; Boyanov, A. I.; Tenchov, B. G., On the Phase Diagram of an L-Dipalmitoylphosphatidylcholine/Cholesterol Mixture. *FEBS Letters* **1985,** 187, (1), 65-68.
[166]. Mortensen, K.; Pfeiffer, W.; Sackmann, E.; Knoll, W., Structural properties of a phophatidylcholine-cholesterol system as studied by small-angle neutron scattering:ripple structure and phase diagram. *Biochim. Biophys. Acta* **1988,** 945, 221-245.
[167]. Meyer, H. W.; Semmier, K.; Quinn, P. J., The effect of sterols on structures formed in the gel/subgel phase state of dipalmitoylphosphatidycholine bilayers. *Mol. Membr. Biol.* **1997,** 14, 187-193.
[168]. Meyer, H. W.; Richter, W.; Brezesinski, G., Convex-concave curvatures in bilayers of dipalmitoylphophatidylcholine and cholesterol induced by amphotericin B/deoxycholate after prolonged storage. *Biochim. Biophys. Acta* **1994,** 1190, 9-19.
[169]. Orädd, G.; Lindblom, G., Lateral Diffusion Studied by Pulse Filed Gradient NMR on Oriented Lipid Membranes. *Magnetic Resonance in Chemistry* **2004,** 42, 123-131.
[170]. Fenske, D. B.; Jarrell, H. C., Phosphorous-31 Two-Dimensional Solid-State Echange NMR. *Biophysical Journal* **1991,** 59, 55-69.
[171]. Picard, F.; Paquet, M.-J.; DuFourc, E. K.; Auger, M., Measurement of the Lateral Diffusion of Dipalmitoylphosphatidylcholine Adsorbed on Silica beads in the Absence and Presence of Melittin: A 31P Two-Dimensional Exchnage Solid State NMR Study. *Biophysical Journal* **1998,** 74, 857-868.
[172]. Nyholm, T. K. M.; Nylund, M.; Slotte, J. P., A Calorimetric Study of Binary Mixtures of Dihydrosphingomyelin and Sterols, Sphingomyelin, or Phosphatidylcholine. *Biophysical Journal* **2003,** 84, (5), 3138-3146.
[173]. Rog, T.; Pasenkiewica-Gierula, M., Cholesterol-Sphingomyelin Interactions: A Molecular Dynamics Simulation Study. *Biophysical Journal* **2006,** 91, (10), 3756-3767.
[174]. Khelashvilli, G. A.; Scott, H. L., Combined Monte Carlo and Molecular Dynamics Simulation of Hydrated 18:0 Sphingomyelin-Cholesterol Lipid Bilayers. *Journal of Chemical Physics* **2004,** 120, (20), 9841-9847.
[175]. Maulik, P. R.; Shipley, G. G., X-Ray Diffraction and Calorimetric Study of N-Lignoceryl Sphingomyelin Membranes. *Biophysical Journal* **1995,** 69, 1909-1916.
[176]. Sankaram, M. B.; Thompson, T. E., Interaction of Cholesterol with Various Glycerophospholipids and Sphingomyelin. *Biochemistry* **1990,** 29, (47), 10670-10675.
[177]. Filippov, A.; Oradd, G.; Lindblom, G., The Effect of Cholesterol on the Lateral Diffusion of Phospholipids in Oriented Bilayers. *Biophysical Journal* **2003,** 84, (5), 3079-3086.

[178]. Filippov, A.; Oradd, G.; Lindblom, G., Sphingomyelin Structure Influences the Lateral Diffusion and Raft Formation in Lipid Bilayers. *Biophysical Journal* **2006,** 90, (6), 2086-2092.
[179]. Demel, R. A.; Jansen, J. W. C. M.; van Dijck, P. W. M.; van Deenen, L. L. M., The Preferential Interaction of Cholesterol with Different Classes of Phospholipids. *Biochimica et Biophysica Acta* **1977,** 465, (1), 1-10.
[180]. Ramstedt, B.; Slotte, J. P., Interaction of Cholesterol with Sphingomyelins and Acyl-Chain-Matched Phosphatidylcholines: A Comparative Study of the Effect of the Chain Length. *Biophysical Journal* **1999,** 76, 908-915.
[181]. Niu, S.; Litman, B. J., Determination of Membrane Cholesterol Partition Coefficient Using a Lipid Vesicle-Cyclodextrin Binary System: Effect of Phospholipid Acyl Chain Unsaturation and Headgroup Composition. *Biophysical Journal* **2002,** 83, (6), 3408-3415.
[182]. Terova, B.; Heczko, R.; Slotte, J. P., On the Importance of the Phosphocholine Methyl Groups for Sphingomyelin/Cholesterol Interactions in Membranes: A Study with Ceramide Phosphoethanolamine. *Biophysical Journal* **2005,** 88, (4), 2661-2669.
[183]. Silvius, J. R., Role of Cholesterol in Lipid Raft Formation: Lessons from Lipid Model Systems. *Biochimica et Biophysica Acta* **2003,** 1610, 174-183.
[184]. van Dijck, P. W. M.; de Kruijff, B.; van Deenen, L. L. M.; de Geir, J.; Demel, R. A., The Preference of Cholesterol for Phosphatidylcholine in Mixed Phosphatidylcholine-Phosphatidylethanolamine Bilayers. *Biochimica et Biophysica Acta* **1976,** 455, (2), 576-587.
[185]. Yeagle, P. L.; Young, J. E., Factors Contributing to the Distribution of Cholesterol Among Phospholipid Vesicles. *Journal of Biological Chemistry* **1986,** 261, (18), 8175-8181.
[186]. Ramstedt, B.; Slotte, J. P., Sphingolipids and the Formation of Sterol-Enriched Ordered Membrane Domains. *Biochimica et Biophysica Acta* **2006,** 1758, 1945-1956.
[187]. Huang, J.; Buboltz, J. T.; Feigenson, G. W., Maximum Solubility of Cholesterol in Phosphatidylcholine and Phosphatidylethanolamine Bilayers. *Biochimica et Biophysica Acta* **1999,** 1417, 89-100.
[188]. Kan, C.; Ruan, Z.; Bittman, R., Interaction of Cholesterol with Sphingomyelin in Bilayer Membranes: Evidence that the Hydroxy Group of Sphingomyelin Does Not Modulate the Rate of Cholesterol Exchange Between Vesicles. *Biochemistry* **1991,** 30, (31), 7759-7766.
[189]. Bittman, R.; Kasireddy, C. R.; Mattjus, P.; Slotte, J. P., Interaction of Cholesterol with Sphingomyelin in Monolayers and Vesicles. *Biochemistry* **1994,** 33, (39), 11776-11781.
[190]. Veiga, M. P.; Arrondo, J. L. R.; Goni, F. M.; Alonso, A.; Marsh, D., Interaction of Cholesterol with Sphingomyelin in Mixed Membranes Containing Phosphatidylcholine, Studied by Spin-Label ESR and IR Spectroscopies. A Possible Stabilization of Gel-Phase Sphingolipid Domains by Cholesterol. *Biochemistry* **2001,** 40, (8), 2614-2622.
[191]. Heimburg, T., A Model for the Lipid Pretransition: Coupling of Ripple Formation with the Chain-Melting Transition. *Biophysical Journal* **2000,** 78, (3), 1154-1165.
[192]. Kranenburg, M.; Smit, B., Phase Behavior of Model Lipid Bilayers. *Journal of Physical Chemistry B* **2005,** 109, (14), 6553-6563.

[193]. Ramstedt, B.; Slotte, J. P., Comparison of the Biophysical Properties of Racemic and D-*erythro*-*N*-acyl Sphingomyelins. *Biophysical Journal* **1999,** 77, 1498-1506.
[194]. Cohen, R.; Barenholz, y.; Gatt, S.; Dagan, A., Preparation and Characterization of Well Defined D-*erythro* Sphingomyelins. *Chemistry and Physics of Lipids* **1984,** 35, (4), 371-384.
[195]. Bar, L. K.; Barenholz, Y.; Thompson, T. E., Effect of Sphingomyelin Composition on the Phase Structure of Phoshatidylcholine-Sphingomyelin Bilayers. *Biochemistry* **1997,** 36, (9), 2507-2516.
[196]. Kuikka, M.; Ramstedt, B.; Ohvo-Rekila, H.; Tuuf, J.; Slotte, J. P., Membrane Properties of D-*erythro*-*N*-acyl Sphingomyelins and Their Corresponding Dihyro Species. *Biophysical Journal* **2001,** 80, 2327-2337.
[197]. Malcolm, I. C.; Ross, J. C.; Higinbotham, J., A Study of the Headgroup Motion of Sphingomyelin using ^{31}P NMR and an Analytically Soluble Model. *Solid State Nuclear Magnetic Resonance* **2005,** 27, 247-256.
[198]. Mombelli, E.; Morris, R.; Taylor, W.; Fraternali, F., Hydrogen-Bonding Propensities of Sphingomyelin in Solution and in a Bilayer Assembly: A Molecular Dynamics Study. *Biophysical Journal* **2003,** 84, (3), 1507-1517.
[199]. Niemela, P.; Hyvonen, M. T.; Vattulainen, I., Structure and Dynamics of Sphingomyelin Bilayer: Insight Gained through Systematic Comparison to Phosphatidylcholine. *Biophysical Journal* **2004,** 87, (5), 2976-2989.
[200]. Alam, T. M.; Holland, G. P., ^{1}H-^{13}C INEPT MAS NMR Correlation Experients with ^{1}H-^{1}H Mediated Magnetization Exchange to Probe Organization in Lipid Biomembranes. *Journal of Magnetic Resonance* **2006,** 180, 210-221.
[201]. Mannock, D. A.; McIntosh, T. J.; Jiang, X.; Covey, D. F.; McElhaney, R. N., Effects of Natural and Enantiomeric Cholesterol on the Thermotropic Phase Behavior and Structure of Egg Sphingomyelin Bilayer Membranes. *Biophysical Journal* **2003,** 84, (2), 1038-1046.
[202]. Maulik, P. R.; Sripada, P. K.; Shipley, G. G., Structure and Thermotropic Properties of Hydrated *N*-Stearoyl Sphingomyelin Bilayer Membranes. *Biochimica et Biophysica Acta* **1991,** 1062, 211-219.
[203]. Milburn, M. P.; Jeffrey, K. R., Dynamics of the Phosphate Group in Phospholipid Bilayers. *Biophysical Journal* **1987,** 52, 791-799.
[204]. Adolphi, N. L.; Badola, S.; Browder, L. A.; Bowman, J., R.C., Magic-Angle Spinning NMR Study of Deuterium Site Occupancy and Dynamics in $ZrNiD_{1.0}$ and $ZrNiD_{3.0}$. *Physical Review B* **2001,** 65, 024301-1 - 024301-9.
[205]. Suwelack, D.; Rothwell, W. P.; Waugh, J. S., Slow Molecular Motion Detected in the NMR Spectra of Rotating Solids. *Journal of Chemical Physics* **1980,** 73, (6), 2559-2569.
[206]. Mehnert, T.; Jacob, K.; Bittman, R.; Beyer, K., Structure and Lipid Interaction of *N*-Palmitoylsphingomyelin in Bilayer Membranes as Revealed by ^{2}H-NMR Spectroscopy. *Biophysical Journal* **2006,** 90, (3), 939-946.
[207]. Huang, J.; Feigenson, G. W., A Microscopic Interaction Model of Maximum Solubility of Cholesterol in Lipid Bilayers. *Biophysical Journal* **1999,** 76, 2142-2157.
[208]. Steinbauer, B.; Mehnert, T.; Beyer, K., Hydration and Lateral Organization in Phospholipid Bilayers Containing Sphingomyelin: A ^{2}H-NMR Study. *Biophysical Journal* **2003,** 85, (2), 1013-1024.

[209]. Zhou, Z.; Sayer, B. G.; Hughes, D. W.; Stark, R. E.; Epand, R. M., Studies of Phospholipid Hydration by High-Resolution Magic-Angle Spinning Nuclear Magnetic Resonance. *Biophysical Journal* **1999,** 76, 387-399.
[210]. Yeagle, P. L.; Hutton, W. C.; Martin, R. B., Sphingomyelin Multiple Phase Behavior as Revealed by Multinuclear Magnetic Resonance Spectroscopy. *Biochemistry* **1978,** 17, (26), 5745-5750.
[211]. Gawrisch, K.; Gaede, H. C.; Mihailescu, M.; White, S. H., Hydration of POPC Bilayers Studies by ^{1}H-PFG-MAS-NOESY and Neutron Diffraction. *Eur. Biophys. J.* **2007,** 36, 281-291.
[212]. Hyvonen, M. T.; Kovanen, P. T., Molecular dynamics simulation of sphingomyelin bilayer. *Journal of Physical Chemistry B* **2003,** 107, (34), 9102-9108.
[213]. Khelashvili, G. A.; Scott, H. L., Combined Monte Carlo and molecular dynamics simulation of hydrated 18 : 0 sphingomyelin-cholesterol lipid bilayers. *Journal of Chemical Physics* **2004,** 120, (20), 9841-9847.
[214]. Pandit, S. A.; Jakobsson, E.; Scott, H. L., Simulation of the Early Stages of Nano-Domain Formaiton in Mixed Bilayers of Sphingomyelin, Cholesterol, and Dioleylphosphatidylcholine. *Biophysical Journal* **2004,** 87, (5), 3312-3322.
[215]. Pandit, S. A.; Scott, H. L., Molecular-dynamics simulation of a ceramide bilayer. *Journal of Chemical Physics* **2006,** 124, (1).
[216]. Pandit, S. A.; Vasudevan, S.; Chiu, S. W.; Mashl, R. J.; Jakobsson, E.; Scott, H. L., Sphingomyelin-cholesterol domains in phospholipid membranes: Atomistic simulation. *Biophysical Journal* **2004,** 87, (2), 1092-1100.
[217]. Niemela, P.; Hyvonen, M. T.; Vattulainen, I., Effect of chain length and saturation on sphingomyelin bilayers - A molecular dynamics simulation study. *Biophysical Journal* **2005,** 88, (1), 70A-70A.
[218]. Rog, T.; Pasenkiewica-Gierula, M., Cholesterol Effects on the Phosphatidylcholine Bilayer Nonpolar Region: A Molecular Simulation Study. *Biophysical Journal* **2001,** 81, (4), 2190-2202.
[219]. Bhide, S. Y.; Zhang, Z. C.; Berkowitz, M. L., Molecular dynamics simulations of SOPS and sphingomyelin bilayers containing cholesterol. *Biophysical Journal* **2007,** 92, (4), 1284-1295.
[220]. Aittoniemi, J.; Niemela, P. S.; Hyvonen, M. T.; Karttunen, M.; Vattulainen, I., Insight into the putative specific interactions between cholesterol, sphingomyelin, and palmitoyl-oleoyl phosphatidylcholine. *Biophysical Journal* **2007,** 92, (4), 1125-1137.

Appendix 1. ^{1}H NOESY of DMPC and SM - Supplemental Material

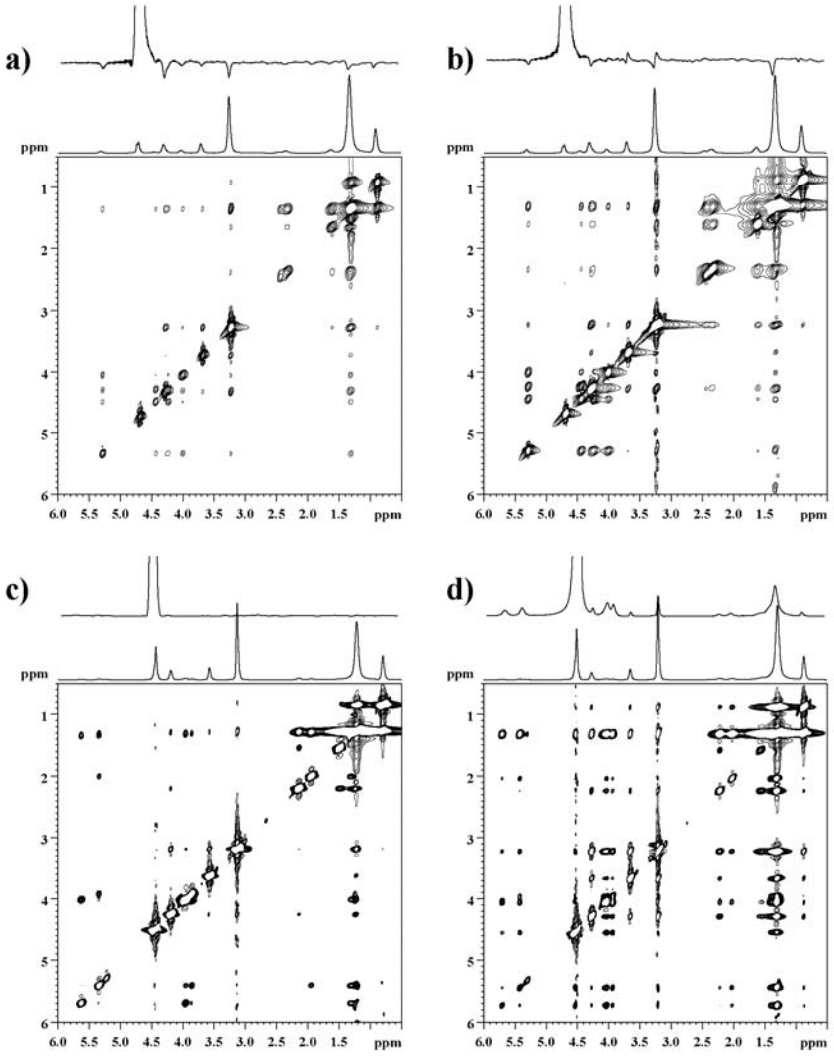

Figure 1S: The 2D phase sensitive NOESY for a) DMPC in D_2O (ν_r = 7500 Hz) at 303 K with a 50 ms and b) 200 ms mixing period, c) SM in D_2O (ν_r = 7500 Hz) at 312 K with a 50 ms and d) 250 ms mixing period. The F_2 projection shows the corresponding 1D ^{1}H MAS NMR spectrum, while the upper insert is the 1D ^{1}H slice through the water resonance. Note that for DMPC the water resonance does not reveal strong positive cross peaks even at longer mixing times, but instead reveals small negative NOE cross peaks consistent with the rapid tumbling of the small water molecule. Similar results have been reported for POPC. This observation is in contrast to the NOESY results for SM mixtures in which the water resonance reveals positive cross peaks to lipid resonances for mixing times greater than 50 ms, with numerous positive cross peaks observed at the longer (250 ms) mixing times. The appearance of positive cross peaks (same phase of the auto correlation peaks) is consistent with tightly bound water or cross peaks arising from exchange. See text for additional discussion. These 2D ^{1}H MAS NOESY NMR results are consistent with the positive ^{31}P and ^{13}C detected NOESY MAS NMR experiments reported in the paper.

Distribution

10	MS0886	Todd M. Alam, 1816
1	MS 0886	Sarah K. McIntyre, 1816
1	MS 0885	Justine Johannes, 1810
1	MS 1411	Jim Voigt, 1816
1	MS 1315	Mark Stevens, 8332
1		Prof. Greg Holland Dept. of Chemistry/Biochemistry Magnetic Resonance Research Center Arizona State University Tempe, AZ 85287-1604
1	MS-0123	D. L. Chavez, LDRD Office
1	MS 9018	Central Technical Files, 8944 (electronic copy)
1	MS 0899	Technical Library, 9536 (electronic copy)

Sandia National Laboratories